NANOCARRIER MEDIATED THERAPIES FOR THE GLIOMAS OF THE BRAIN

A Dissertation
Presented to
The Academic Faculty

by

Abhiruchi Agarwal

In Partial Fulfillment
of the Requirements for the Degree
Doctor of Philosophy in the
School of Biomedical Engineering

Georgia Institute of Technology
May, 2011

NANOCARRIER MEDIATED THERAPIES FOR THE GLIOMAS OF THE BRAIN

Approved by:

Dr. Ravi V. Bellamkonda, Advisor
School of Biomedical Engineering
Georgia Institute of Technology

Dr. Julia Babensee
School of Biomedical Engineering
Georgia Institute of Technology

Dr. Niren Murthy
School of Biomedical Engineering
Georgia Institute of Technology

Dr. Mostafa El-Sayed
School of Chemistry & Biochemistry
Georgia Institute of Technology

Dr. Ananth Annapragada
School of Health Information Sciences
University of Texas-Houston Health Science Center

Date Approved: [January 4, 2011]

|| *Om Shri Ganeshaya Namah* ||

Na hi jñānēna sadr̥śaṁ pavitramiha vidyatē

Here (in this world), there is nothing as pure (sublime) as knowledge

ACKNOWLEDGEMENTS

I was always inclined towards biological sciences. In fact, after high school, I wanted to be a medical doctor. Somehow, I managed to obtain bachelors in Electrical Engineering. At this point I realized, I would still like to go back to biological sciences. I joined Dr. Bellamkonda's lab. I was a young and excited graduate student with no idea even how to hold a pipette. They were quite challenging first two years. Needless to say, I was not very productive in those years. Dr. Bellamkonda's lab was very focused on biomaterials. I was again clueless in this area, but was determined to learn. I decided to gain masters in material science and engineering while preparing myself to work in a 'wet' lab. Having said that, the first person I want to thank is my advisor Dr. Ravi Bellamkonda. Without his immense patience, guidance, and most importantly financial support, this journey would not have been possible. Dr. Bellamkonda's advising style quite perturbed me initially. I needed an advisor who would stand next to me at the bench and guide me. Quite contrary to my expectations, he expected me to 'figure things out'. I now realize and thank his style because he prepared me to take on any challenge and execute it without being fearful.

This journey would not have been possible without the unconditional love, and moral support throughout these intense years I have received from my parents. My primary inspiration to undertaking this journey is my mother who herself holds a PhD in chemistry. I want to thank my dad Vijai Krishna and my mom Dr. Kamlesh Agarwal for standing by my side at all times. They have sacrificed their own enjoyments to give me and my brother the best education and life. I can never thank them enough in a lifetime. They have encouraged and led us both to pursue a good education. I am very fortunate to

have them and I thank Lord Krishna for their presence in my life. I want to thank my brother Abhishek Agarwal for being there by my side over the years. He has patiently born a lot of my temper resultant of a lot of bad days at lab. I, also, want to thank my mother-in-law Alka Shah for her encouragement and support in my pursuit.

My desire to attain a PhD was further manifested by my undergraduate mentor in the department of ECE, Dr. Thomas Gaylord. I thank Dr. Gaylord for giving me the opportunity to conduct undergraduate research in his lab. His guidance and support helped me attain my first publication and my way into graduate school.

The lab that you are a part of and the people you are with make a huge difference in the person you turn out to be in the end. I want to acknowledge the lab members during the earlier years of my graduate school who have been an important part in my professional development. My earliest mentors were Mahesh Dodla and Justin Saul. I was lucky to have Mahesh as my first mentor because Mahesh was the kind of person who never lost patience. Under his guidance, I learnt many techniques in the lab including cell harvest, cell culturing, animal surgeries and histological techniques. Justin was my doorway to the world of cancer nano-therapeutics. He taught me how to fabricate, characterize, and use liposomes. His mentorship helped me decide my thesis path to cancer therapeutics instead of neural tissue engineering. After Justin left, I found a new mentor in Efstathios Karathanasis who joined us as a post doc after finishing his PhD from Dr. Annapragada's lab. Stathis made research look like a piece of cake. Every day he made me feel like I can graduate tomorrow. He instilled enthusiasm in me and encouraged me whenever I felt like quitting. He was always available for discussion and provided me a lot of guidance throughout my pursuit. He also brought immense comical

relief to the lab. I also want to thank Kathleen McNeeley. Katie was a graduate student on the cancer therapeutics side before me. All animal models and related techniques were already established by her in our lab. She transferred all her knowledge to me and made my journey relatively easy. Having suffered the atrocities of *in vivo* work, she was my database to what is possible and more importantly 'what not to do'. She has been an invaluable resource for me in the lab.

I want to mention a few other names in the lab that were not involved in my research but made my time in the lab very enjoyable and whose friendships I endear. I want to acknowledge Ananta Laxmi Ayyagari, Chenyu Kao, Wei He, Mary Millner, Anjana Jain and Vivek Mukhtyar. Laxmi was a post doc in the lab. She was a true Indian at heart. She never enjoyed eating out and so always brought her own food. In fact, she brought enough to share with all of us. I loved her cooking, although, I could barely endure her spice level. Chenyu was a graduate student who earned his master's from our lab. His jovial and teasing nature lifted the spirits in the lab. He was always smiling and had a very helping nature. Wei He was the quite one but a very pleasant person to talk to. Laxmi, Chenyu, and Wei together were my break time mates and relief from lab work during my earlier years. Mary Millner started as a graduate student at the same time as me. I was very amused by Mary initially because she was the first white person that I came across who was vegetarian. Together we shared times of our accomplishments and dissatisfactions. We have much in common including the fact that we started dating and married our husbands in the same years.

Anjana Jain and Vivek Mukhtyar are two people in the lab that became my very good friends. Anjana was a graduate student when I started in the lab. The more I

interacted with her, the more I realized that we were rather alike. We are so alike that sometime we think and say the same words at the exact moment in time. It can be scary. Anjana is a very caring person. She has become one of my closest friend with whom I can share and talk about everything. Vivek started as a graduate student in our lab after me. He is a very friendly person and loves making new friends. He is constantly smiling and loves cooking. He has hosted us in his apartment on several occasions and cooked delicious Indian food. The annoying long years of my graduate school became pleasant with their friendships by my side. I am very thankful to them for the great deal of help they provided me planning and during my wedding. They are and will remain like my brother and sister. I also want to acknowledge Chandra Valmikinathan, a post doc in our lab. He has only been in our lab for a year, but he has become a very good friend over the past year. After Stathis left to take on a position as an assistant professor in Case Western Reserve, Chandra has earned the title of the official comedian of the lab.

I am thankful to my committee members Dr. Ananth Annapragada, Dr. Mostafa El-Sayed Dr. Julia Babensee, and Dr Niren Murthy for their guidance, feedback, and support on my thesis. Dr. Annapragada has been a collaborator, a tremendous source of knowledge, and expertise on liposomes over the years. His guidance has been very valuable to me over the years. I want to thank Dr. El-Sayed for providing me the knowledge of gold nanorods and his support in my thesis. His graduate students Megan Mackey, Erik Dreaden, and Lauren Austin have helped a lot with fabricating the gold rods, insights into theory of the gold nanorods, and use of the NIR laser. I, also, want to acknowledge Dr. David Jaye and Cissy Geigerman at Emory for their help with my studies on the peptide targeted liposome project.

I would like to acknowledge our past and present lab managers Douglas Swehla and Alex Ortiz respectively. I want to thank them for putting up with my rush orders and for promptly ordering all the supplies I needed in my research. I want to thank my undergraduate mentees; Lynn Replogle and Rohan Trivedi who put in hours of their time in my experiments and helped me hone my mentoring capabilities. I also cannot forget all the present and past lab members for all their help and support.

I also want to mention Dr. Thomas Krucker who hosted me at the Novartis Institute of Biomedical Research in Cambridge, Massachusetts. Thomas taught me and introduced me to the world of molecular imaging. His guidance reinforced my desire to finish my PhD.

During my years as a graduate student, I have found many good friends in the BME department who helped me get away from the lab. Their friendships made the adversities of graduate school a breeze. Amongst these are Kartik Sundereswaran, Udita Adurkar, Michael Heffernan, and Kartik Sundar. I especially want to acknowledge Kartik Sundareswaran. Kartik and I started our journeys in the PhD program at the same time. He, however, was clearer about his goals and needless to say finished a lot faster. Kartik has been a good listener to all my ramblings and ventings.

I am also thankful to my roommate Rupa Bhaumik, with whom I have continued to be good friends, who has always extended warmth and good advice, and who has welcomed me in her house at any hour. Her new daughter Shayna and her husband Sudipto are now an integral part of my life and I am grateful to them for their friendship. I also cannot forget all my friends from undergrad who stayed in Atlanta and made my weekends fun and my days in school lighter.

Lastly and most importantly, I want to thank my husband Ankit Shah. He has so patiently supported and motivated me over the years. His companionship and love helped me continue my journey and finish what I started. He has always been very mindful of my odd hours in the lab. He would even accompany me during the late hours in the lab and sit by my side while I finish my work. He has been extremely encouraging during times of frustration and has enabled me get through the long and tedious years of graduate school. I have neglected him at times because I was trying to finish an experiment. He has worked so hard over the years to keep us financially happy. Now, I hope to make up for the lost time with him and continue the rest of our journey together.

This thesis would not have been possible without the financial contributions received from the, Georgia Cancer Coalition, Nora Redman Foundation, National Science Foundation, President's Undergraduate Research Scholarship (PURA), Undergraduate Research Scholarship (URS), and Center for Drug Design, and Delivery (GAANN fellowship).

TABLE OF CONTENTS

Page

LIST OF TABLES

Page

LIST OF FIGURES

Page

SUMMARY

Existing methods of treating glioma are not effective for eradicating the disease. Therefore, new and innovative methods of treatment alone or in combination with existing therapies are necessary. Delivery of therapeutic agents through delivery carriers such as liposomes diminishes the harmful effects of the agent in healthy tissues and allows increased accumulation in the tumor. In addition, targeted chemotherapy using liposomes provides the opportunity for further increase in drug accumulation in tumor. However, the current targeting strategies suffer accelerated plasma clearance and are not advantageous in improving efficacy. The search for new tumor targets, novel ligands, new strategies for targeting, and particle stabilization will advance our ability to improve delivery at the tumor level while decreasing toxicity to normal tissues.

The global objective of this thesis was to improve the status of current liposomal therapy to achieve higher efficacy in tumors. Here, we show a novel mechanism to increase targeting to tumor while uncompromising on the long circulation of stealth liposomes. Long circulation is essential for passive accumulation of the nanocarriers due to EPR effect, in order to see benefits of targeting. Using phage display technique, a variety of tumor specific peptides were identified for use as targeting moieties. One potential advantage of the approach proposed here is the rapid identification of patient tumor specific peptide that evades the RES. This could lead to the development of a nanocarrier system with high avidity and selectivity for tumors. Therefore, tumor accumulation of the targeted formulations will be higher than that of non-targeted liposomes due to increased drug retention at the tumor site and uncompromised blood residence time.

In addition, it has been shown that the distribution of nanocarriers, spatially within the tumor, is limited that might further hinder the distribution of the encapsulated drug, thereby limiting efficacy. It is necessary to release the drug from within the nanocarrier to promote increased efficacy. Here, we were able to address the problem of drug diffusion within the tumor interstitium using a combination therapy employing a remotely triggered thermosensitive liposomal chemotherapeutic. We fabricated a thermosensitive liposomal nanocarrier that maintained its stability at physiological temperature to minimize toxicity to healthy cells. We, then, showed a remote triggering mechanism mediated by gold nanorods heated via NIR can help in achieving precise control over the desired site for drug release. These strategies enabled increased drug availability at the tumor site and contributed to tumor retardation. Additionally, we show that the synergistic therapy employing gold nanorods and thermosensitive liposomes may have great potential to be translated to the clinic.

CHAPTER 1

INTRODUCTION

1.1 Statement of the problem

Malignant tumors of the central nervous system like meningiomas, astrocytomas, glioblastoma multiforme (GBM) are the leading cause of death from solid tumors in children and third leading cause of death in adolescents and adults. Brain tumor incidence is about 14.8 per 100,000 person-years. About 12,760 patients of benign and malignant tumors die each year [1]. An inability to control the local growth of these solid tumors leads to significant morbidity and mortality. About 60% of the therapies fail eventually with local recurrence in the United States alone [2]. Clinical use of most conventional chemotherapeutics is often limited due to inadequate delivery of therapeutic drug concentrations to the tumor target tissue or severe and harmful toxic effects on normal organs.

It is important to develop novel technologies that can be used for targeted drug delivery to tumors thereby improving the therapeutic index of cytotoxic, anti-tumor drugs. After their discovery in 1965, liposomes became a promising tool for drug delivery. Much research has been conducted on stabilizing liposomes and increasing their plasma half life. Polyethylene glycol coated long circulating liposomes [3-4] accumulate significantly in tumors due to a leaky vasculature and the lack of an effective lymphatic drainage system [5]. This effect is often referred to as the enhanced permeability and retention effect (EPR) [6-7]. The pore sizes in solid tumor vasculature vary from 100 to 780 nm, and are generally much larger than in normal vasculature where the gaps between endothelial cells are usually less than 6 nm [5]. This results in selective *passive*

targeting of liposomes in tumors through passive diffusion while sparing healthy tissue. It was demonstrated in patients with brain glioblastomas and metastatic brain tumors that long circulating liposomal nanocarriers overcome the blood brain barrier (BBB) in the tumor lesions resulting in 13-19 times higher accumulation in the glioblastoma as compared to the normal brain [8].

Liposomal anthracyclines were the first nanotherapeutics to be approved for clinical use as the first line for treatment of AIDS-related Kaposi's sarcoma and relapsed ovarian cancer and are under numerous clinical trials (128 active studies) for treatment of other types of cancer. However, in the past 20 years even after significant development and improvement in nanoparticle drug delivery only 2 nanoparticle loaded drugs have been approved till date for clinical use (Doxil and Abraxane) [5, 9]. When tested *in vitro*, nanoparticle loaded drugs show excellent cytotoxicity and specificity. The question that emerged then, is why these drugs, ostensibly carried by a particle that *should*, by the EPR effect localize itself with high specificity in solid tumors, not show an immediate and significant improvement in efficacy. Failure in efficacy could be attributed to sequential barriers following the systemic administration of a nanoparticle drug that can be outlined as follows: 1) Organ distribution and clearance. 2) Inability to diffuse uniformly in the tumor due to nanocarrier size. 3) Resistance to release of drug from the nanoparticles localized into tumors, effectively neutralizing the drug.

1.2 Hypothesis

We have hypotheses to increase the efficacy and specificity. Currently, liposomal nanocarriers can potentially be tagged with high affinity targeting ligands that bind to tumor cells. However, the principal shortcoming of existing targeting ligands, such as

folate and antibodies, is that they significantly compromise circulation time when presented on nanocarriers [10-13]. Long circulation is critical for increasing passive accumulation of liposomal nanocarriers in the tumors to reap the benefits of targeted nanocarriers. We hypothesize that improving the specificity by identification of small peptide ligands that afford selective tumor targeting without compromising circulation time would be greatly advantageous. To overcome the non-uniform distribution of the encapsulated drug and resistance to release of drug from nanoparticles, we believe the use of stably circulating thermosensitive liposomes that can be triggered remotely using nano-antennas to release its contents. Therefore, due to its small size, the drug will have a greater opportunity to diffuse further into the tumor lesion away from the blood vasculature.

1.3 Objectives

The goal of this thesis is to achieve enhanced tumor efficacy with liposomal nanocarriers in comparison to existing drug encapsulating nanocarriers. To achieve this goal, we employed active and passive targeting, and destabilization of nanocarriers at target site while preventing normal tissue uptake.

The objectives to achieve these goals were:

1) Identify new targeting moieties and design a targeted nanocarrier that has comparable blood plasma half life to non-targeted nanocarriers, and characterize nanocarrier *in vivo* performance in a glioma animal model.
2) Fabricate a stable, long circulating, thermo-sensitive nanocarrier that can be triggered remotely using gold nanorods and near-infrared radiation to release

its contents and demonstrate the success of such a system in increasing efficacy *in vivo*.

a. Fabricate a liposome and evaluate the stability of such a liposomes in retaining the drug at physiological temperature
b. Determine the effectiveness of gold nanorods in triggering the drug release and evaluate the efficacy of this system, thereby, in increasing tumor cytotoxicity.

The search for tumor targets, novel ligands, new strategies for targeting, and particle stabilization will advance our ability to improve delivery at the tumor level while decreasing toxicity to normal tissues. Here, we propose a novel mechanism to increase tumor targeting while uncompromising on the long circulation of stealth liposomes. Long circulation is essential for passive accumulation of the nanocarriers due to EPR effect, in order to see benefits of targeting. Identifying several non-immunogenic motifs specific to the tumor type can greatly enhance nanocarrier accumulation at the tumor site. To address the problem of drug diffusion within the tumor interstitium, it is necessary to release the drug from within the nanocarrier. It is important to fabricate such nanocarriers without compromising their stability in circulation to minimize toxicity to healthy cells. Using a remote triggering mechanism can help in achieving precise control over the desired site for drug release. Eventually, these strategies should enable increased drug retention and availability at the tumor site and contribute to enhanced tumor retardation.

1.4 References

1. Buckner, J.C., et al., *Central nervous system tumors.* Mayo Clin Proc, 2007. **82**(10): p. 1271-86.
2. Ponce, A.M., et al., *Hyperthermia mediated liposomal drug delivery.* Int J Hyperthermia, 2006. **22**(3): p. 205-13.
3. Allen, T.M., et al., *Liposomes containing synthetic lipid derivatives of poly(ethylene glycol) show prolonged circulation half-lives in vivo.* Biochim Biophys Acta, 1991. **1066**(1): p. 29-36.
4. Woodle, M.C. and D.D. Lasic, *Sterically stabilized liposomes.* Biochim Biophys Acta, 1992. **1113**(2): p. 171-99.
5. Haley, B. and E. Frenkel, *Nanoparticles for drug delivery in cancer treatment.* Urol Oncol, 2008. **26**(1): p. 57-64.
6. Torchilin, V.P., *Targeted pharmaceutical nanocarriers for cancer therapy and imaging.* AAPS J, 2007. **9**(2): p. E128-47.
7. Greish, K., et al., *Macromolecular therapeutics: advantages and prospects with special emphasis on solid tumour targeting.* Clin Pharmacokinet, 2003. **42**(13): p. 1089-105.
8. Koukourakis, M.I., et al., *High intratumoural accumulation of stealth liposomal doxorubicin (Caelyx) in glioblastomas and in metastatic brain tumours.* Br J Cancer, 2000. **83**(10): p. 1281-6.
9. Tiwari, S.B. and M.M. Amiji, *A review of nanocarrier-based CNS delivery systems.* Curr Drug Deliv, 2006. **3**(2): p. 219-32.

10. Gabizon, A., et al., *In vivo fate of folate-targeted polyethylene-glycol liposomes in tumor-bearing mice.* Clin Cancer Res, 2003. **9**(17): p. 6551-9.

11. Pan, X.Q., H. Wang, and R.J. Lee, *Antitumor activity of folate receptor-targeted liposomal doxorubicin in a KB oral carcinoma murine xenograft model.* Pharm Res, 2003. **20**(3): p. 417-22.

12. Wu, J., Q. Liu, and R.J. Lee, *A folate receptor-targeted liposomal formulation for paclitaxel.* Int J Pharm, 2006. **316**(1-2): p. 148-53.

13. Huwyler, J., D. Wu, and W.M. Pardridge, *Brain drug delivery of small molecules using immunoliposomes.* Proc Natl Acad Sci U S A, 1996. **93**(24): p. 14164-9.

CHAPTER 2

BACKGROUND AND RELEVANT LITERATURE REVIEW

2.1 Brain Tumor Prevalence

Brain tumors continue to be a challenge to treat because they are inherently diffuse, highly invasive, and non-localized. Instead of completely and permanently eliminating a malignant brain tumor, current treatments have been shown to merely prolong patient survival [1-3]. Radiation therapy and surgical resection are often incapable of completely removing deeply penetrated and diffuse brain tumors. The penetration of radiation therapy is limited by the energy of the incident photons, and increasing the energy to allow for deeper penetration invariably results in irradiation of healthy tissue. Recurrence of tumors is common following surgical resection since it is often difficult to completely eradicate both the tumor and the invading tumor front without harming any adjacent healthy brain tissue. As a result, median survival duration is merely 12 months following the combination of surgical resection and focal radiotherapy [1].

Currently, chemotherapy is not the primary treatment of choice for malignant brain tumors due to the exposure of non-target organs to chemotherapeutic resulting from systemic administration as well as due to the presence of the highly impermeable BBB, which limits transport to lipophilic or low molecular weight, uncharged compounds. In an effort to prevent exposure of healthy organs to the toxic side effects of chemotherapeutics, implantable biodegradable drug depots within a brain tumor are currently being used in clinical practice to localize a chemotherapeutic and allow for

prolonged and controlled drug delivery [4]. Gliadel® is an intracranial implantable polyanhydride polymer loaded with BCNU. BCNU and carmustine have been widely used as systemic agents due to their lipophilicity but effectiveness is restricted by the dose-limited side effects [5-6]. On the other hand, Gliadel® has produced better results for patients with grade IV glioma extending the median survival by 13.4 weeks compared to placebo [7-8]. However, this method relies on drug diffusion from a central core. As a result, drug usually cannot reach the tumor periphery where the most aggressive cells persist. Chemotherapy via systemic intravascular administration utilizes the tumor's own blood supply for transport allowing for drug delivery throughout the tumor and is minimally non-invasive. Therefore, new strategies to improve systemic delivery of chemotherapeutics will be an additional beneficial tool for treatment of gliomas.

2.2 Nanocarriers in Drug Delivery to Solid Tumors

Nanoparticles are systems that are constructed to be in nanometer (nm) size and range from a few nm to several hundred nm depending on their intended use. The particle size is purposely constructed for the nanoparticle to pass through the fenestrations of the leaky cancer endothelium. In addition, lack of tumor lymphatics enables the preferential accumulation of nanoparticulate drug at tumor site. This phenomenon is called the enhanced permeation and retention effect (EPR). The result of the EPR effect is an altered biodistribution for the nanocarrier-associated drug, with a notably higher concentration of the drug accumulating at the site of disease, and a lower concentration accumulating in healthy tissues.

Particle size also determines if the circulating nanoparticle is opsonized and rapidly cleared by the reticulo-endothelial system (RES), which is predominantly

distributed in liver, lungs, spleen, and bone marrow. The surface of the nanoparticle must be modified to escape the RES. One such approach has been the alteration of the polymeric composition of the particle. An example is the addition of polyethylene glycol (PEG) over the surface of the nanoparticle. Pegylating enables shielding of the nanoparticles from macrophages and imparts it to be “STEALTH” particle. Hydrophilic polymers like PEG coating the nanoparticle surface repel plasma proteins and escape opsonization and clearance. This has been described as a “cloud” effect [9-10].

A variety of materials are used to construct nanoparticles including ceramic, polymers, lipids, and metals. Nanoparticle structures may contain predominantly organic molecules or have inorganic elements usually incorporating a metal as a core. Nanoparticles have a variety of sizes and shapes, which include spheres, branched structures, shells, tubes, fullerenes, emulsions, and liposomes. Therapeutic drugs can be incorporated into the nanoparticle by entrapment, surface attachment, or encapsulation. The characteristics of each particle differ in terms of drug loading capacity, particle and drug stability, drug release rates, and targeted delivery ability. Each class of nanoparticles encompasses different characteristics; however, the following essential conditions are universal [11]: biodegradability, biocompatibility, non-immunogenicity, physical stability in the blood. A few of the nanoparticles being researched for drug delivery are discussed here.

Table 2.1. Nanocarrier based drugs on the market

Compound	Commercial name	Nanocarrier	Indications
Styrene maleic anhydride-neocarzinostatin	Zinostatin/Stimalmer	Polymer–protein conjugate	Hepatocellular carcinoma
Peg-l-asparaginase	Oncaspar	Polymer–protein conjugate	Acute lymphoblastic leukemia
Peg-granulocyte colony-stimulating factor (G-CSF)	Neulasta/Pegfilgrastim	Polymer–protein conjugate	Prevention of chemotherapy-associated neutropenia
IL2 fused to diphtheria toxin	Ontak (Denilelukin diftitox)	Immunotoxin (fusion protein)	Cutaneous t-cell lymphoma
Anti-CD33 antibody conjugated to calicheamicin	Mylotarg	Chemo-immunoconjugate	Acute myelogenous leukemia
Anti-CD20 conjugated to yttrium-90 or indium-111	Zevalin	Radio-immunoconjugate	Relapsed or refractory, low-grade, follicular, or transformed non-Hodgkin's lymphoma
Anti-CD20 conjugated to iodine-131	Bexxar	Radio-immunoconjugate	Relapsed or refractory, low-grade, follicular, or transformed non-Hodgkin's lymphoma
Daunorubicin	DaunoXome	Liposomes	Kaposi's sarcoma
Doxorubicin	Myocet	Liposomes	Combinational therapy of recurrent breast cancer, ovarian cancer, Kaposi's sarcoma
Doxorubicin	Doxil/Caelyx	Peg-liposomes	Refractory Kaposi's sarcoma, recurrent breast cancer, ovarian cancer
Vincristine	Onco TCS	Liposomes	Relapsed aggressive non-Hodgkin's lymphoma (nHl)
Paclitaxel	Abraxane	Albumin-bound paclitaxel nanoparticles	Metastatic breast cancer

2.2.1 Dendrimers

A dendrimer is characterized by its highly branched 3D structure that provides a high degree of surface functionality and versatility. Due to their multivalent and monodisperse character, dendrimers have stimulated wide interest in the field of chemistry and biology, especially in applications like drug delivery, gene therapy and

chemotherapy. Dendrimers' well defined three-dimensional structure, the availability of many functional surface groups, their low polydispersity and their ability to mimic make them attractive drug delivery vehicles. Drug molecules can be loaded both in the interior of the dendrimers as well as attached to the surface groups. Dendrimers can function as drug carriers either by encapsulating drugs within the dendritic structure, or by inter-acting with drugs at their terminal functional groups via electrostatic or covalent bonds (prodrug).

The versatile nature of dendrimers allows them to deliver either hydrophobic or hydrophilic agents to a target site. Drugs may be covalently attached to functional groups on the dendrimer or simply associated with the internal core of the sphere by electrostatic interactions, hydrogen bonding, or hydrophobic interactions [12]. The anticancer drug doxorubicin was covalently bound to this carrier via an acid-labile hydrazone linkage. The cytotoxicity of doxorubicin was significantly reduced (80–98%), and the drug was successfully taken up by several cancer cell lines. The encapsulation behavior of these compounds for the anticancer drugs adriamycin and methotrexate was studied. The highest encapsulation efficiency, with on average 6.5 adriamycin molecules and 26 methotrexate molecules per dendrimer, was found for the generation number = 4 (G, the number of focal points when going from the core towards the dendrimer surface) Polyamidoamines (PAMAM) polymer terminated with PEG2000 chains. The anticancer drug 5-fluorouracil encapsulated into G = 4 PAMAM dendrimers with PEG5000 surface chains revealed reasonable drug loading, and reduced release rate and hemolytic toxicity compared to the non-PEGylated dendrimer [13]. In contrast, up to 24 drug molecules were encapsulated into the hyper branched polyol. The drug was successfully transported

into lung epithelial carcinoma cells by the dendrimers. Dendrimers are promising in various pharmaceutical applications in the coming years as they possess unique properties, such as high degree of branching, multivalency, globular architecture and well-defined molecular weight, thereby offering new scaffolds for drug delivery.

2.2.2 Polymeric Micelles

Polymeric micelles are nano-sized particles, made up of polymer chains, and are usually spontaneously formed by self-assembly in a liquid as a result of hydrophobic or ion pair interactions between polymer segments. Micelles are useful for delivery of water insoluble drugs carried in the hydrophobic central core [14-15]. The core of the micelles, which is either the hydrophobic part or the ionic part of the nanoparticles, can contain molecules such as therapeutic drugs, while the shell provides interactions with the solvent and make the nanoparticles stable in the liquid.

Polymeric micelles are composed of block or graft copolymers. Block copolymers are generally linear polymers that are composed of a sequence of at least two polymer segments that differ in physico-chemical properties, e.g. charge and/or polarity. In graft copolymers, side chain segments are grafted to a main polymer chain. Fully hydrophilic block or graft copolymers in which one of the segments carry a charge may form stable complexes in water together with oppositely charged (macro) molecules, resulting in polyion complex micelles or polyelectrolyte micelles. On the other hand, amphiphilic block copolymers are capable to self-assemble, when placed in a solvent that is selective for one of the polymeric segments, to form micelles. Many important characteristics of a micelle (critical micelle concentration CMC, association number Z, core radius R_c, shell thickness L, hydrodynamic radius R_h) are determined by the copolymer characteristics,

e.g. its molecular weight and composition. Micellization of amphiphilic block copolymers in water is an entropy-driven process as a consequence of hydrophobic interactions and changes of the water structure in vicinity of the polymer chains.

Intravenous injection of a polymeric micellar drug formulation prevents the breakdown of the micelles due to biological barriers encountered, for example, by oral administration. The biggest challenge, although, is the prevention of a-specific interactions of the drug-containing micelles with blood components (e.g. with proteins, which can eventually cause premature excretion by the body) and non-target cells or tissues. Another problem is the stable retention of the drug by the micelles during circulation. Micelles are also prone to dilution. Micelles maintain a dynamic equilibrium with free unimers that can be absorbed by blood proteins, which will cause an adverse shift of this equilibrium. If diluted below the CMC, however, individual copolymers are rapidly removed by the kidneys [16]. Also, the drug molecules may gradually diffuse out of the micelles and bind to proteins or cells before they reach the target site. In the case of polyion complex micelles, the relatively high physiological salt concentration or exchange with charged biomolecules may cause premature dissociation of the polymer-drug complexes. There are several efforts to overcome the above mentioned problems are ongoing.

2.2.3 Polymeric Nanoparticles

These nanoparticles are composed of a matrix system in which drug is distributed by entrapment, attachment, or encapsulation or vesicular systems with a central cavity or core to which a drug is confined. The surface of the nanoparticle may be modified by the

addition of polymers and biological materials like ligands or antibodies may also be attached for targeting purposes.

Polymers are the most commonly explored materials for constructing nanoparticle-based drug carriers. One of the earliest reports of their use for cancer therapy dates back to 1979 [17] when adsorption of anticancer drugs to polyalkylcyanoacrylate nanoparticles was described. Couvreur et al. revealed the release mechanism of the drugs from the polymer in calf serum, followed by tissue distribution and efficacy studies in a tumor model [18]. Polymeric nanoparticles can be made from synthetic polymers, including poly(lactic acid) (PLA) and poly(lactic co-glycolic acid), or from natural polymers such as chitosan [19] and collagen [20] and may be used to encapsulate drugs without chemical modification. The drugs can be released in a controlled manner through surface or bulk erosion, diffusion through the polymer matrix, swelling followed by diffusion, or in response to the local environment. Several multifunctional polymeric nanoparticles are now in various stages of pre-clinical and clinical development [21-23]. Concerns arising from the use of polymer-based nanocarriers include the inherent structural heterogeneity of polymers, reflected, for example, in a high polydispersity index (the ratio of the weight-and-number-average molecular weight (M_w/M_n)). There are, however, a few examples of polymeric nanoparticles that show near-homogenous size distribution [24].

At least 12 polymer–drug conjugates have entered Phase I and II clinical trials and are especially useful for targeting blood vessels in tumors. Examples include anti-endothelial immunoconjugates, fusion proteins [25-27], and caplostatin, the first polymer-angiogenesis inhibitor conjugates [28]. Polymers that are chemically conjugated

with drugs are often considered new chemical entities (NCEs) owing to a distinct pharmacokinetic profile from that of the parent drug. Despite the variety of novel drug targets and sophisticated chemistries available, only four drugs (doxorubicin, camptothecin, paclitaxel, and platinate) and four polymers (N-(2-hydroxylpropyl) methacrylamide (HPMA) copolymer, poly-*L*-glutamic acid, PEG, and dextran) have been repeatedly used to develop polymer–drug conjugates [29-30].

2.2.4 Carbon Nanotubes

Carbon nanotubes are a family of fullerenes composed of carbon in the form of a hollow ellipsoid tube. Nanotubes self assemble as either single- or multi-walled with a hollow cage like architecture. One popular form of nanotubes is the soluble derivatives of fullerene such as C60 which has promise as a pharmaceutical. The C_{60} variant resembles a black and white soccer ball. Atoms may be trapped inside fullerenes and tubes and antibodies or ligands bound to the surface for targeting [15]. Tolerability is largely unknown.

Carbon nanotubes (CNT) range from 1 to 10s of nanometers in diameter, and their length can range from several to hundreds of microns. Drugs can be covalently attached to functional groups on the external surface of the nanotubes [31]. Soluble derivatives of fullerenes have good biocompatibility and low toxicity and are under investigation as antiviral agents [32], antibacterial agents [33], anticancer therapies [34], antioxidants and anti-apoptosis agents for potentially treating amyotrophic lateral sclerosis and Parkinson's disease [35].

The ability of functionalized CNT (*f*-CNT) to penetrate into the cells offers the potential of using *f*-CNT as vehicles for the delivery of small drug molecules [36-37]The

development of delivery systems able to carry one or more therapeutic agents with recognition capacity, optical signals for imaging and/or specific targeting is of fundamental advantage, for example in the treatment of cancer and different types of infectious diseases [38]. Water-soluble CNT functionalized with substituted carborane cages was developed as a delivery system for an efficient boron neutron capture therapy [39] aimed at the treatment of cancer cells. These studies showed that some specific tissues contained carborane following intravenous administration of the CNT conjugate and carborane was concentrated mainly at the tumour site. Another class of carbon nanomaterial similar to CNT, Single-walled carbon nanohorns (nanostructured spherical aggregates of graphitic tubes), has also been used for drug delivery [40]. Murakami *et al*. loaded these tubes with dexamethasone and found that dexamethasone could be adsorbed in large amounts onto oxidized nanohorns and maintains its biological integrity after being liberated. This was confirmed by activation of glucocorticoid response in mouse bone marrow cells and induction of alkaline phosphatase in mouse osteoblasts. In view of these results, *f*-CNT represents a new, emerging class of delivery systems for the transport and translocation of drug molecules into different types of mammalian cells. Although these CNT conjugates displayed no cytotoxicity *in vitro*, for further development, it will be important to assess their metabolism, biodistribution and clearance from the body.

2.2.5 Liposomes are Ideal Candidates for Chemotherapy

Liposomes constitute a class of nanoparticulate drug carriers generally characterized by the presence of one or more amphiphile bilayers enclosing an interior aqueous space. Liposomes have been used to increase the therapeutic index of a wide

range of antineoplastic agents. This has primarily been accomplished by improving the pharmacokinetic profile or allowing for site-specific drug delivery to solid tumors. Liposomes are self-assembled colloidal particles resembling tiny cells that occur naturally and can be prepared artificially [41]. Phospholipids can self-organize and form ordered structures in solvents due to hydrophilic and lipophilic interactions. The orientation of these self-assembled lipid structures is such that the polar portion of the molecule is in contact with the polar media and shields the nonpolar part, and vice versa. When they are at high concentrations, liquid-crystalline phases are formed with the most common being lamellar and lesser common being hexagonal and cubic phases. Upon suspension in water, they disperse into colloidal suspensions such as liposomes, and hexasomes. The shape of the phospholipid is of great importance for the symmetry of lipid self-assembly and liquid- crystalline-phase formation (see fig 2.1). Based on the cross-sectional area of the hydrophilic part (S_{hydro}) relative to the one of the lipophilic part (S_{lipo}), micelles (high surface curvature) are formed when $S_{hydro}>S_{lipo}$ while inverse micelles (negative surface curvature) are formed $S_{hydro}<S_{lipo}$. In the case that the two areas are similar, a bilayered configuration (liposome) is the most stable form. The high surface tension forces a flat lamellar sheet to bend resulting in a decrease of the "edge" energy as well as an increase of the energy for the induced curvature. In order to further minimize the energy, the bending is complete forming a sphere which results in zero "edge" energy. At low temperatures, the bilayer is in a gel state in which the lipid chains have a close packing. At high temperatures or in the presence of unsaturated acyl chains, the bilayer is in a liquid-crystalline state. The temperature (T_m) where the gel-to-liquid crystalline transition occurs depends on the acyl chains. Unsaturated lipids have lower T_m

since double bonds introduce kinks prohibiting close packing. Therefore, liposomes are lipid vesicular sacs with a thin lipid bilayer membrane separating the internal aqueous compartment from the external aqueous media. Since S_{hydro} and S_{lipo} depend on temperature or ionization (pH), phase transitions between various phases can be induced.

Steric stabilization tackled the problems associated with colloidal and biological

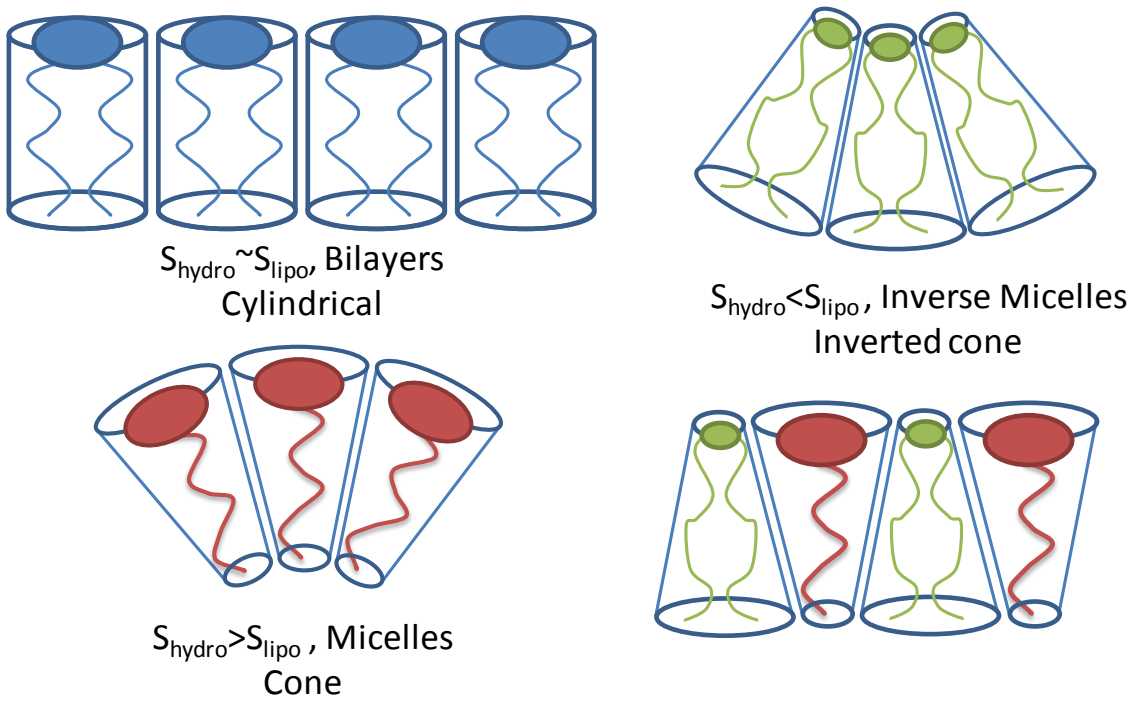

Figure 2.1. Three typical lipid shapes: cylindrical leading to lamellar arrangement, cone leading to micellar structures (positive membrane curvature) and inverted cone leading to inverted phases (negative membrane curvature). The association between cone and inverted cone shaped molecules leads to a lamellar assembly.

instability of liposomes. Coating of liposomes with the inert hydrophilic polymers methoxypolyethylene glycol (mPEG) allowed prolonged liposome circulation in blood and stability by reducing interactions with blood proteins. For example, pegylated liposomal doxorubicin (Doxil®, Alza/Johnson & Johnson, Mountain View, CA), a stable and long-circulating liposome formulation of doxorubicin, has become a widely used

anticancer agent. Doxil has been approved for the treatment of Kaposi's sarcoma, ovarian cancer, metastatic breast cancer, and has shown activity in other tumor types as well [15].

Drugs retained in long circulating liposomes benefit from site-specific accumulation in the pathological areas such as tumors due to a discontinuous or otherwise more permeable microvasculature and nonfunctioning lymphatics [15, 42]. Liposomes of approximately 100 nm in size readily distribute into solid tumors with an efficiency that depends partially on the anatomical location. Long circulating liposomal accumulation maximizes around 48-65 h at the tumor [15]. The liver and spleen, two major organs of the reticulo-endothelial system (RES) are major sites of liposome clearance due to the presence of macrophages that efficiently phagocytose liposomes.

Achieving site specific drug targeting is the key to increased therapeutic efficacy and reduced side-effects. Strategies that enable intracellular delivery of drugs that exert their effects in cytoplasmic compartments are hallmarks in the development of successful drug delivery vehicles. Many physical and chemical properties of various phospholipids can be employed to gain site-specific drug delivery from liposomes.

Liposomes can also act as rapid release formulations of the active drug, providing rapid exposure of the targeted tissue to the drug thereby increasing toxicity. When optimally designed with appropriate lipids, liposomes can remain impermeable at body temperature and allow rapid release of their aqueous content to occur following their accumulation in the tumor. Various studies have explored the use of pH, temperature, and light to trigger drug release at the targeted site. The lipids comprising the bilayer can be sensitive to temperature or pH changes. These studies have suggested that pH, temperature, and light can be used to cause phase transition of the phospholipids

(lamellar-to-hexagonal or gel-to-liquid crystalline transition) that in turn, enables the release of drugs from liposomal bilayers. The combination of prolonged circulation, drug encapsulation, and their susceptibility to triggered release of the drug at tumor site makes liposomes ideal candidates for drug delivery to tumors.

2.2.5.1 Use of Targeting Ligands on Liposomes can Increase Tumor Specificity and Drug Availability

Receptor-mediated molecular targeting is one approach to promote specific localization. Targeting of chemotherapeutic drugs to receptors over-expressed by gliomas cells decrease the side effects associate with traditional chemotherapy and enable the administration of lower drug dosages to achieve the same therapeutic effect. Incorporating targeting ligands over-expressed by tumor cells, not only facilitates targeting to the tumor cell but also drug retention at the target site by preventing retrograde movement of liposomes into the bloodstream. Targeting ligands can be chosen to bind receptors that undergo receptor-mediated endocytosis to facilitate drug uptake by cells [43-44]. High affinity tumor targeting ligands can be readily coupled covalently to the distal ends of nanocarrier PEG chains. In fact, one or more ligands may be coupled to the same nanocarrier, potentially conferring added selectivity. A number of the ligand-presenting liposomal systems targeting differentially expressed receptors on tumor cells (relative to normal tissue) have been reported and shown to promote increased drug uptake [43, 45].

The folate receptor (FR) is one of the numerous transmembrane receptors known to be over-expressed by gliomas [46]. Several in vitro liposomal studies utilizing FR as a target have demonstrated significantly higher cytotoxicities from FR-targeted

formulations compared to non-targeted formulations resulting from increased uptake of drug by target cells [47-51]. Survival studies, however, have demonstrated mixed results. No therapeutic advantage was observed between non-targeted and FR-targeted formulations administered to mice bearing subcutaneous carcinomas. Highly specific antibodies that bind target antigens with high affinities have also been used to target tumor. However, attachment of antibodies to liposomes has been shown to stimulate uptake by the RES. More recent studies have focused on preventing premature clearance by Fc-receptor mediated uptake by the RES by the use of antibody fragments as an alternative [52-53]. Liposomes targeting with antibodies or antibody fragments has been examined previously for HER2 [44, 54-55], disialoganglioside (GD2) [56], CD19 [57-58], prostate-specific membrane antigen (PSMA) [59-60], transferrin receptor [61-63], and epidermal growth factor receptor (EGFR) [64-65]. The incorporation of small peptides into liposomes has been investigated to target aminopeptidase N [66-67], matrix metalloproteinase (MMP) [68], and integrin [69-70] on or around tumor cells.

Numerous studies have also shown that targeting ligand attachment to PEG chains anchored in liposomal membranes results in accelerated plasma clearance [63, 66, 71-75]. Decreased plasma concentrations of targeted formulations have been reported regardless of the targeting moiety to be an antibody [63] or a receptor ligand [76]. It is believed that targeting moieties anchored with similar length or longer PEG on the liposome surface retains the ability to interact with plasma proteins responsible for RES clearance. Prolonged circulation is critical to passive accumulation of the targeted nanocarrier. Accelerated plasma clearance could be responsible for the inability of targeted nanocarriers to increase survival *in vivo*. Therefore, the major design goal of this project

was to identify small peptide-based targeting ligands for nanocarriers that are selective to gliomas and do not compromise circulation time.

2.2.5.2 Triggered Release of Drugs from Liposomes can Increase Drug Distribution and Cellular Toxicity

The use of site-specific targeting has not yet been sufficient to obtain a significantly increased efficacy in the treatment of cancer when compared to passively accumulating liposomes. This can very well be due to destructive uptake of the liposomes by the target cells, possibly due to lysosomal degradation [77]. Liposomes, therefore, have to be designed either to escape the endosomes after cell internalization or to release the drugs outside the cell, which may be in conflict with site-specific targeting. Several strategies have been proposed to accomplish site-specific triggered drug release in tumor tissue. Liposomes triggered by acid [78-83], enzymes [84-85], small changes in temperature [86-90] and light [91-92] have all been shown to be useful concepts for releasing encapsulated drugs. However, liposomes designed with these specific trigger mechanisms have not yet reached the pharmaceutical market.

Acid triggered release

The original strategy of using the acidic microenvironment characterizing tumors for triggered release [78] has not been very successful as the highest acidity in tumors is distant from the tumor vasculature. As a result, liposomes often fail to reach this tissue [93-94]. In addition, the pH of the tumor interstitium rarely declines below pH 6.5, making it technically difficult to design liposomes that are stable in the blood but become

disrupted in the tumor tissue [82]. A more viable strategy has been to exploit the very acidic environment in endosomes and lysosomes where the pH is below 5.0 [95-96].

Triggered release of pH-sensitive liposomes is the most biocompatible method for releasing drugs directly in the cytoplasm of cells. Research in acid triggered drug delivery has resulted in the use of fusogenic liposomes [97-98]. After cell internalization, the pH change triggers a liposome morphology change where a lipid bilayer, L_{α}, to hexagonal, H_{II}, phase transition occurs [77]. The main lipid diacylphosphatidylethanolamine (DOPE) when mixed with that with micellar forming lipids such as PEG-coated lipids can form stable liposomes. After acid catalyzed cleavage or removal of the PEG-lipids from the liposomes, they become fusogenic and are expected to fuse with the endosome membrane leading to drug release into the cytoplasm of the cell.

Several groups have presented the idea of using mildly acidic amphiphiles that become protonated when entering an acidic environment. This leads to a decrease in hydration of the headgroup followed by destabilization of the liposome as non-bilayer fusogenic structures are formed [99]. Diacylsuccinylglycerols have been shown to stabilize DOPE, are pH-sensitive and effective drug carriers *in vitro* [81]. Cholesterol hemisuccinate (CHEMS) has been shown as an attractive constituent in pH-triggered liposomes. Oleic acid (OA) lipids are used in OA: PE liposomes and they are considerably more sensitive to pH than the former two, releasing their content below pH 6.5 [83, 101]. The use of acid sensitive liposomes has been one of the most extensively studied active triggering strategies. Since Yatvin et al. [78] reported this strategy in 1980 there have been many new ideas and reports of new chemical entities in the literature, yet

the liposome drug delivery field has still not been able to provide convincing clinical results.

Light triggered release

The employment of lipids that either isomerize, fragment or polymerize upon photoexcitation [77, 102] give rise to the principle of light triggered release liposomes. Bondurant et al. [91, 103] reported a PEG-liposome formulation containing 1,2-bis[10-(2′,4′-hexadienoyloxy)-decanoyl]-*sn*-glycero-3-phosphocholine (bis-SorbPC), a photosensitive lipid that forms a cross-linked lipid network upon exposure to UV-light. The polymerization causes leakage during the polymerization process due to the formation of defects in the bilayer. However, the use of UV-light is not very suitable for biological applications due to the potential damage to healthy tissue and it is therefore desirable to use light with a longer wavelength. The incorporation of a cyanine dye into the PEG-liposomes made them sensitive to visible light [102]. Thompson and co-workers [92, 104-106] have reported the use of plasmalogen photooxidation for triggered release. Many sensitizing agents like zinc phthalocyanine, tin octabutoxyphthalocyanine and bacteriochlorophyll *a* have been investigated. Bacteriochlorophyll *a* that has an absorption maximum at 820 nm was found to produce the fastest release [104]. An extension of the concept was made by encapsulating Ca^{2+} in diplasmalogen liposomes that upon photooxidative release activated phospholipase A_2 (PLA_2), which is a calcium dependent enzyme [105]. PLA_2 then contributes to the drug release by hydrolyzing acyl-phospholipids in the liposome. Thompson and co-workers [106] have also showed that calcium-dependent transglutaminase can be activated by this principle. Another example

of photofragmentation was reported by Zhang and Smith [107]. They used a lipid called NVOC-DOPE, which could be fragmented upon excitation at 345 nm to produce DOPE resulting in destabilization of the liposomes. Liposomes containing photoisomerizable lipids can also be used for light triggered drug release. The well-known *trans–cis* isomerization of azobenzenes was exploited by Bisby et al. [108-109]. An azobenzene-glycero-phosphocholine isomerization was shown to result in fast release from liposomes in the gel phase upon UV-light activation. It is however important to underline that the principle of light triggered activation has not yet been proven to be a viable method for obtaining drug release from liposomes *in vivo*.

Enzyme triggered release

The uses of enzymes that are upregulated in tumor tissue have been used for site-specific drug release. Cell associated proteases have been suggested as possible candidates for enzymatically triggered drug release from liposomes [84]. Davis and Szoka [110] have designed liposomes that are sensitive to alkaline phosphatase and upon cleavage of the lipid conjugate results in the generation of fusogenic lipids that destabilize the liposome. They showed that liposomes consisting of cholesterol phosphate derivatives and DOPE could be induced to collapse upon phosphatase-catalyzed removal of the phosphate group. Thompson and co-workers have also employed enzymes as part of a trigger mechanism. They proposed the use of phospholipase A_2 (PLA_2) [105] and transglutaminase [106] for site-specific drug release. Alonso and co-workers [111-112] have used sphingomyelinase and phospholipase C as enzymatic triggers of liposome mixtures of sphingomyelin, phosphatidylcholine, phosphatidylethanolamine and

cholesterol to create fusogenic liposomes. Villar et al. [113-114] have furthermore suggested that phosphatidylinositol-specific phospholipase C can be employed for triggered drug release by promoting the site-specific formation of fusogenic liposomes.

Heat triggered release

In 1978, Yatvin et al. [86] proposed the use of mild local hyperthermia for tumor-specific drug release. Their basic strategy was to design liposomes with the main phase transition just above physiological temperature. The objective of this principle is to design liposomes with a narrow phase transition region with respect to temperature, as this will result in selective and controlled drug release due to a narrow temperature range with lipid membrane heterogeneity and leaky interfacial membrane regions [90, 115]. Yatvin and co-workers [86-87] used DPPC as the main lipid component and added small amounts of DSPC to adjust the main phase transition temperature. Several other formulations based on this composition have been designed [116-117], including long circulating thermosensitive liposomes that released more than 60% of their contents when heated at 42 °C for 30 min *in vitro* [88, 118]. The use of hyperthermia allows for increased liposome tumor accumulation as a consequence of increased tumor blood flow [119] and increased microvascular permeability [118, 120], and therefore, has a significant advantage over other triggering concepts. In addition, hyperthermia itself has been shown to be cytotoxic [121].

The strategy of using microenvironment-sensitive polymers as described for pH-sensitive liposomes has also been employed for temperature-sensitive liposomes. Many synthetic and natural polymers are known to become water insoluble above a lower

critical solution temperature (LCST) while being soluble below this temperature [89]. The physical behavior of temperature-sensitive polymers can be exploited as a trigger in liposomal drug delivery because of the significant difference in polymer hydration below and above the LCST. Among thermosensitive polymers, poly(*N*-isopropylacrylamide) is the most extensively studied [89, 122]. Many others have been synthesized to adjust the LCST to a desired temperature which can be achieved by copolymerization [123-124]. The anchoring of the polymers to the liposome has been performed in a variety of ways and appeared to be important for the destabilization of the liposomes [89, 125-126].

A new liposome formulation that was optimized for doxorubicin release at 39–40°C was introduced by Needham, Dewhirst and co-workers [90, 127]. They designed liposomes incorporated with lyso-phospholipids that were kinetically trapped in the liposomal membrane in the gel phase. When the liposomes were heated above the main phase transition, the lyso-phospholipids were shown to leave the bilayer, which drastically enhanced the permeability of the liposomal membrane at temperatures close to the gel-to-fluid phase transition [127].

The main shortcoming of the current state of the use of hyperthermia and liposomes is that it requires the location of the tumor is known and the tumor site is accessible to local hyperthermia [120]. However, this provides an exciting opportunity for remote triggering mechanism and will be discussed later in detail.

2.3 Limited Efficacy due to Inhomogeneous Liposome Distribution

The success of passive (and subsequent active) targeting of nanoscale chemotherapeutic agent therapy for intracranial tumors is critically dependent on the access that these agents have to tumors via the leaky vasculature across the BBB [42,

128-129]. Unfortunately, it is well-known that the degree of tumor vascular leakiness differs not only among similar type tumors but also spatially within the same tumor [130-132]. For instance, previous studies in our laboratory showed that the standard deviation of the intratumoral accumulation of liposomal doxorubicin in a rat brain tumor was 150% of the mean value [133]. Due to non-uniform distribution of tumor blood vessels, the distribution of nanocarrier drug is patchy and inhomogeneous. As the size of the nanocarrier further limits the diffusion of the drug deeper into the tumor tissue, the drug distribution is limited to the periphery of the tumor where most vascularization is seen [134]. A study evaluating localization of liposomal doxorubicin in solid lung tumors showed that 98% of the tumor-associated drug was not tumor-cell associated and a small proportion of the drug co-localized with the tumor-associated macrophages [135]. Therefore, bioavailability of the liposomal encapsulated drug may be required to promote increased tumor-cell drug uptake. Dewhirst et al. have shown that triggered release of the drug from thermosensitive liposomes can greatly enhance efficacy at the tumor site [90, 127, 136-138].

2.4 Gold Nanorods for Remote Thermal Destabilization of Liposomes

Triggered contents release from nanosized particulates has interesting potential applications in drug targeting and diagnostics. Heat sensitive liposome technology is a potential method to produce triggered systems for controlled contents delivery. The temperature required for gel-to-liquid crystalline phase transition in the liposomes can be adjusted by lipid composition. This property has been used in the cancer treatments, where a slightly higher temperature in the tumor triggers the drug release from the liposomes with a phase transition below 41 °C [90, 139].

Many external remote triggers have been explored to induce contents release from liposomes. For example, Huang and MacDonald studied ultrasound-triggered release from acoustically active liposomes [140]. Peyman et al. used laser light to release drugs from the liposomes [141], whereas Mueller et al. reported destabilization of liposomes using visible and ultraviolet light [142], although these methods are known to disturb cell membranes.

In recent years, tremendous development of nanotechnology has provided a variety of nanostructures with unique optical properties that are useful in biology and biomedical applications. Noble metal nanoparticles, like gold, absorb light strongly in the visible region due to the coherent oscillations of the metal conduction band electrons in strong resonance with visible frequencies of light. This phenomenon is called surface plasmon resonance (SPR). Gold nanoparticles, for this reason, are ideal in cancer diagnostics and therapy. SPR frequency is dependent upon the size and shape of the gold nanoparticles. Changing the shape of the gold nanoparticles from a sphere to a rod significantly redshifts the SPR absorption wavelength into the NIR region. NIR region of the light spectrum is optically transparent and minimally absorbed by tissue chromophores and water making it optimal for clinical applications. Therefore, NIR-resonant gold nanostructures are extremely useful for clinical therapy applications involving tumors that are located deep within bodily tissue [143-150].

In tumors of the brain, water bath mediated heat therapy poses several risks. Hyperthermia to a local region in the brain using a water bath is unattainable. Further, water bath mediated hyperthermia in the brain can trigger brain death. Gold nanorods can provide an opportunity to locally disrupt the liposomes in specific areas of the brain with

the help of NIR. By modulating the NIR power and gold nanorod dose, intratumoral temperature can be tightly controlled. Co-injecting gold nanorods and thermosensitive liposomes of similar sizes may cause co-accumulation at the tumor site due to EPR effect while sparing healthy brain tissue. In addition, tagging thermosensitive liposomes with gold nanorods can be further explored to this effect.

2.5 Conclusions

Existing methods of treating glioma are not effective for eradicating the disease. Therefore, new and innovative methods of treatment alone or in combination with existing therapies are necessary. Ideal glioma therapy requires minimally invasive administration and can be targeted to tumors thereby sparing non-target organs. Liposomes are ideal candidates for such delivery because they can be administered intravascularly. Delivery of therapeutic agents through delivery carriers such as liposomes diminishes the harmful effects of the agent in healthy tissues and allows increased accumulation in the tumor. In addition, targeted chemotherapy using liposomes provides the opportunity for further increase in drug accumulation in tumor. The use of antigens over-expressed by tumors as targeting ligands is an effective means of targeting. However, such unique antigens are rare and their receptors are usually expressed in small quantities on healthy cells causing even lower doses of chemotherapeutics reaching them to be toxic. The current targeting strategies, also, suffer accelerated plasma clearance and are not advantageous in improving efficacy. The search for new tumor targets, novel ligands, new strategies for targeting, and particle stabilization will advance our ability to improve delivery at the tumor level while decreasing toxicity to normal tissues. Here, we proposed a novel mechanism to increase targeting to tumor while uncompromising on the

long circulation of stealth liposomes. Long circulation is essential for passive accumulation of the nanocarriers due to EPR effect, in order to see benefits of targeting. Identifying several non-immunogenic motifs specific to the tumor type can greatly enhance nanocarrier accumulation at the tumor site.

It has been shown by us and elsewhere that the distribution of nanocarriers, spatially within the tumor, is limited that might further hinder the distribution of the encapsulated drug, thereby limiting efficacy. To address the problem of drug diffusion within the tumor interstitium, it is necessary to release the drug from within the nanocarrier. Currently used triggered systems suffer from loss of drug in the circulation due to leaky characteristics. It is important to fabricate nanocarriers without compromising their stability in circulation to minimize toxicity to healthy cells. Using a remote triggering mechanism can help in achieving precise control over the desired site for drug release. Eventually, these strategies should enable increased drug retention and availability at the tumor site and contribute to tumor retardation.

2.6 References

1. D.S. Mohan, et al., *Outcome in elderly patients undergoing definitive surgery and radiation therapy for supratentorial glioblastoma multiforme at a tertiary institution.* Int. J. Radiat. Biol. Phys., 1998. **42**: p. 981–987.
2. F.G. Barker, et al., *Survival and functional status after resection of recurrent glioblastoma multiforme.* Neurosurgery, 1998. **42**: p. 709–720.
3. K.L. Black and B.K. Pikul, *Gliomas--past, present, and future.* Clin Neurosurg, 1999. **45**: p. 160-3.

4. P.P. Wang, J. Frazier, and H. Brem, *Local drug delivery to the brain.* Advanced Drug Delivery Reviews, 2002. **54**: p. 987–1013

5. P.L. Kornblith and M. Walker, *Chemotherapy for malignant gliomas.* J. Neurosurg. , 1988. **68**: p. 1-17.

6. M.D. Walker, et al., *Randomized comparisons of radiotherapy and nitrosoureas for the treatment of malignant glioma after surgery.* N. Engl. J. Med., 1980. **303**: p. 1323-1329.

7. H. Brem, et al., *The safety of interstitial chemotherapy with BCNU-loaded polymer followed by radiation therapy in the treatment of newly diagnosed malignant gliomas: phase I trial.* J. Neurooncol., 1995. **26**: p. 111-123.

8. S. Valtonen, et al., *Interstitial chemotherapy with carmustine-loaded polymers for high-grade gliomas: a randomized double-blind study.* Neurosurgery 1997. **41**: p. 44-48.

9. Brigger, I., C. Dubernet, and P. Couvreur, *Nanoparticles in cancer therapy and diagnosis.* Adv Drug Deliv Rev, 2002. **54**(5): p. 631-51.

10. S. I. Jeona, et al., *Protein—surface interactions in the presence of polyethylene oxide: I. Simplified theory.* Journal of Colloid and Interface Science, 1991. **142**(1): p. 149-158

11. Lockman, P.R., et al., *Nanoparticle technology for drug delivery across the blood-brain barrier.* Drug Dev Ind Pharm, 2002. **28**(1): p. 1-13.

12. Gupta, U., et al., *Dendrimers: novel polymeric nanoarchitectures for solubility enhancement.* Biomacromolecules, 2006. **7**(3): p. 649-58.

13. Svenson, S. and D.A. Tomalia, *Dendrimers in biomedical applications--reflections on the field.* Adv Drug Deliv Rev, 2005. **57**(15): p. 2106-29.

14. Moghimi, S.M., A.C. Hunter, and J.C. Murray, *Nanomedicine: current status and future prospects.* Faseb Journal, 2005. **19**(3): p. 311-30.

15. Haley, B. and E. Frenkel, *Nanoparticles for drug delivery in cancer treatment.* Urol Oncol, 2008. **26**(1): p. 57-64.

16. Torchilin, V.P., *Self-assembling complexes for gene delivery: from laboratory to clinical trial*, ed. A.V. Kabanov, P.L. Felgner, and L.W. Seymour. 1998, New York: Wiley.

17. Couvreur, P., et al., *Adsorption of anti-neoplastic drugs to polyalkylcyanoacrylate nanoparticles and their release in calf serum.* J. Pharm. Sci., 1979. **68**: p. 1521-1524.

18. Couvreur, P., *Tissue distribution of anti-tumor drugs associated with polyalkylcyanoacrylate nanoparticles.* J. Pharm. Sci., 1980. **69**: p. 199-202.

19. Calvo, P., et al., *Chitosan and chitosan ethylene oxide propylene oxide block copolymer nanoparticles as novel carriers for proteins and vaccines.* Pharm. Res., 1997. **14**: p. 1431-1436.

20. Elsamaligy, M.S. and P. Rohdewald, *Reconstituted collagen nanoparticles, a novel drug carrier delivery system.* J. Pharm. Pharmacol., 1983. **35**: p. 537-539.

21. LaVan, D.A., T. McGuire, and R. Langer, *Small-scale systems for in vivo drug delivery.* Nat. Biotechnol., 2003. **21**: p. 1184-1191.

22. Farokhzad, O.C. and R. Langer, *Nanomedicine: Developing smarter therapeutic and diagnostic modalities.* Adv. Drug Deliv. Rev., 2006. **58**: p. 1456-1459.

23. Moses, M.A., H. Brem, and R. Langer, *Advancing the field of drug delivery: taking aim at cancer*. Cancer Cell, 2003. **4**: p. 337-341.

24. Guo, R., *Synthesis of alginic acid-poly[2-(diethylamino)ethyl methacrylate] monodispersed nanoparticles by a polymer-monomer pair reaction system.* Biomacromolecules, 2007. **8**: p. 843-850.

25. Arap, W., R. Pasqualini, and E. Ruoslahti, *Cancer treatment by targeted drug delivery to tumor vasculature in a mouse model.* Science, 1998. **279**: p. 377-380.

26. Halin, C., *Enhancement of the antitumor activity of interleukin-12 by targeted delivery to neovasculature.* Nat. Biotechnol., 2002. **20**: p. 264-269.

27. Schraa, A.J., *Targeting of RGD-modified proteins to tumor vasculature: A pharmacokinetic and cellular distribution study.* Int. J. Cancer, 2002. **102**: p. 469-475.

28. Satchi-Fainaro, R., *Targeting angiogenesis with a conjugate of HPMA copolymer and TNP-470.* Nat. Med., 2004. **10**: p. 255-261.

29. Duncan, R., *Polymer conjugates as anticancer nanomedicines.* Nat. Rev. Cancer, 2006. **6**: p. 688-701.

30. Satchi-Fainaro, R., R. Duncan, and C.M. Barnes, *Polymer Therapeutics II: Polymers as Drugs, Conjugates and Gene Delivery Systems*. 2006, Nature Publishing Group. p. 1-65.

31. Chen, Q.D., et al., *Plasma activation of carbon nanotubes for chemical modification.* Journal of Physical Chemistry B, 2001. **105**(3): p. 618-622.

32. Schinazi, R.F., et al., *Synthesis and Virucidal Activity of a Water-Soluble, Configurationally Stable, Derivatized C60 Fullerene.* Antimicrobial Agents and Chemotherapy, 1993. **37**(8): p. 1707-1710.

33. Tsao, N., et al., *Inhibition of group A streptococcus infection by carboxyfullerene.* Antimicrobial Agents and Chemotherapy, 2001. **45**(6): p. 1788-1793.

34. Tabata, Y., Y. Murakami, and Y. Ikada, *Antitumor effect of poly(ethylene glycol)modified fullerene.* Fullerene Science and Technology, 1997. **5**(5): p. 989-1007.

35. Dugan, L.L., et al., *Carboxyfullerenes as neuroprotective agents.* Proc Natl Acad Sci U S A, 1997. **94**(17): p. 9434-9.

36. Pantarotto, D., et al., *Translocation of bioactive peptides across cell membranes by carbon nanotubes.* Chem Commun (Camb), 2004(1): p. 16-7.

37. Kam, N.W.S., et al., *Nanotube molecular transporters: Internalization of carbon nanotube-protein conjugates into mammalian cells.* Journal of the American Chemical Society, 2004. **126**(22): p. 6850-6851.

38. Ferrari, M., *Cancer nanotechnology: Opportunities and challenges.* Nature Reviews Cancer, 2005. **5**(3): p. 161-171.

39. Yinghuai, Z., et al., *Substituted carborane-appended water-soluble single-wall carbon nanotubes: New approach to boron neutron capture therapy drug delivery*. Journal of the American Chemical Society, 2005. **127**(27): p. 9875-9880.

40. Muralkami, T., et al., *Drug-loaded carbon nanohorns: Adsorption and release of dexamethasone in vitro.* Molecular Pharmaceutics, 2004. **1**(6): p. 399-405.

41. Lasic, D.D. and D. Papahadjopoulos, *Medical applications of liposomes*. 1998, Amsterdam ; New York: Elsevier. xiv, 779 p.

42. Yuan, F., et al., *Microvascular permeability and interstitial penetration of sterically stabilized (stealth) liposomes in a human tumor xenograft.* Cancer Res, 1994. **54**(13): p. 3352-6.

43. Gabizon, A., et al., *Targeting folate receptor with folate linked to extremities of poly(ethylene glycol)-grafted liposomes: in vitro studies.* Bioconjug Chem, 1999. **10**(2): p. 289-98.

44. Kirpotin, D.B., et al., *Antibody targeting of long-circulating lipidic nanoparticles does not increase tumor localization but does increase internalization in animal models.* Cancer Res, 2006. **66**(13): p. 6732-40.

45. Wong, J.Y., et al., *Direct measurement of a tethered ligand-receptor interaction potential.* Science, 1997. **275**(5301): p. 820-2.

46. Garin-Chesa, P., et al., *Trophoblast and ovarian cancer antigen LK26. Sensitivity and specificity in immunopathology and molecular identification as a folate-binding protein.* Am J Pathol, 1993. **142**(2): p. 557-67.

47. Lee, R.J. and P.S. Low, *Folate-mediated tumor cell targeting of liposome-entrapped doxorubicin in vitro.* Biochim Biophys Acta, 1995. **1233**(2): p. 134-44.

48. Lee, R.J. and P.S. Low, *Delivery of liposomes into cultured KB cells via folate receptor-mediated endocytosis.* J Biol Chem, 1994. **269**(5): p. 3198-204.

49. Ni, S., S.M. Stephenson, and R.J. Lee, *Folate receptor targeted delivery of liposomal daunorubicin into tumor cells.* Anticancer Res, 2002. **22**(4): p. 2131-5.

50. Gaber, M.H., *Modulation of doxorubicin resistance in multidrug-resistance cells by targeted liposomes combined with hyperthermia.* J Biochem Mol Biol Biophys, 2002. **6**(5): p. 309-14.

51. Saul, J.M., et al., *Controlled targeting of liposomal doxorubicin via the folate receptor in vitro.* J Control Release, 2003. **92**(1-2): p. 49-67.

52. Park, J.W., et al., *Anti-HER2 immunoliposomes: enhanced efficacy attributable to targeted delivery.* Clin Cancer Res, 2002. **8**(4): p. 1172-81.

53. Maruyama, K., et al., *Immunoliposomes bearing polyethyleneglycol-coupled Fab' fragment show prolonged circulation time and high extravasation into targeted solid tumors in vivo.* FEBS Lett, 1997. **413**(1): p. 177-80.

54. Kirpotin, D., et al., *Sterically stabilized anti-HER2 immunoliposomes: design and targeting to human breast cancer cells in vitro.* Biochemistry, 1997. **36**(1): p. 66-75.

55. Park, J.W., et al., *Development of anti-p185HER2 immunoliposomes for cancer therapy.* Proc Natl Acad Sci U S A, 1995. **92**(5): p. 1327-31.

56. Brignole, C., et al., *Neuroblastoma targeting by c-myb-selective antisense oligonucleotides entrapped in anti-GD2 immunoliposome: immune cell-mediated anti-tumor activities.* Cancer Lett, 2005. **228**(1-2): p. 181-6.

57. Lopes de Menezes, D.E., et al., *Cellular trafficking and cytotoxicity of anti-cd19-targeted liposomal doxorubicin in B lymphoma cells.* Journal of Liposome Research, 1999. **9**(2): p. 199-228.

58. Sapra, P. and T.M. Allen, *Improved outcome when B-cell lymphoma is treated with combinations of immunoliposomal anticancer drugs targeted to both the CD19 and CD20 epitopes.* Clin Cancer Res, 2004. **10**(7): p. 2530-7.

59. Ikegami, S., et al., *Selective gene therapy for prostate cancer cells using liposomes conjugated with IgM type monoclonal antibody against prostate-specific membrane antigen.* Hum Cell, 2005. **18**(1): p. 17-23.

60. Ikegami, S., et al., *Targeting gene therapy for prostate cancer cells by liposomes complexed with anti-prostate-specific membrane antigen monoclonal antibody.* Hum Gene Ther, 2006. **17**(10): p. 997-1005.

61. Cerletti, A., et al., *Endocytosis and transcytosis of an immunoliposome-based brain drug delivery system.* J Drug Target, 2000. **8**(6): p. 435-46.

62. Gosk, S., et al., *Targeting anti-transferrin receptor antibody (OX26) and OX26-conjugated liposomes to brain capillary endothelial cells using in situ perfusion.* J Cereb Blood Flow Metab, 2004. **24**(11): p. 1193-204.

63. Huwyler, J., D. Wu, and W.M. Pardridge, *Brain drug delivery of small molecules using immunoliposomes.* Proc Natl Acad Sci U S A, 1996. **93**(24): p. 14164-9.

64. Mamot, C., et al., *Epidermal growth factor receptor (EGFR)-targeted immunoliposomes mediate specific and efficient drug delivery to EGFR- and EGFRvIII-overexpressing tumor cells.* Cancer Res, 2003. **63**(12): p. 3154-61.

65. Saul, J.M., A.V. Annapragada, and R.V. Bellamkonda, *A dual-ligand approach for enhancing targeting selectivity of therapeutic nanocarriers.* J Control Release, 2006. **114**(3): p. 277-87.

66. Pastorino, F., et al., *Vascular damage and anti-angiogenic effects of tumor vessel-targeted liposomal chemotherapy.* Cancer Res., 2003. **63**(21): p. 7400-7409.

67. Pastorino, F., et al., *Targeting liposomal chemotherapy via both tumor cell-specific and tumor vasculature-specific ligands potentiates therapeutic efficacy.* Cancer Res, 2006. **66**(20): p. 10073-82.

68. Medina, O.P., et al., *Radionuclide imaging of tumor xenografts in mice using a gelatinase-targeting peptide.* Anticancer Res, 2005. **25**(1A): p. 33-42.

69. Schiffelers, R.M., et al., *Anti-tumor efficacy of tumor vasculature-targeted liposomal doxorubicin.* J Control Release, 2003. **91**(1-2): p. 115-22.

70. Lestini, B.J., et al., *Surface modification of liposomes for selective cell targeting in cardiovascular drug delivery.* J Control Release, 2002. **78**(1-3): p. 235-47.

71. Pan, X.Q., H. Wang, and R.J. Lee, *Antitumor activity of folate receptor-targeted liposomal doxorubicin in a KB oral carcinoma murine xenograft model.* Pharm Res, 2003. **20**(3): p. 417-22.

72. Pan, X.Q. and R.J. Lee, *In vivo antitumor activity of folate receptor-targeted liposomal daunorubicin in a murine leukemia model.* Anticancer Res, 2005. **25**(1A): p. 343-6.

73. Wu, J., Q. Liu, and R.J. Lee, *A folate receptor-targeted liposomal formulation for paclitaxel.* Int J Pharm, 2006. **316**(1-2): p. 148-53.

74. Gabizon, A., et al., *Tumor cell targeting of liposome-entrapped drugs with phospholipid-anchored folic acid-PEG conjugates.* Adv Drug Deliv Rev, 2004. **56**(8): p. 1177-92.

75. Gabizon, A., H. Shmeeda, and Y. Barenholz, *Pharmacokinetics of pegylated liposomal Doxorubicin: review of animal and human studies.* Clin Pharmacokinet, 2003. **42**(5): p. 419-36.

76. Gabizon, A., et al., *In vivo fate of folate-targeted polyethylene-glycol liposomes in tumor-bearing mice.* Clin Cancer Res, 2003. **9**(17): p. 6551-9.

77. Gerasimov, M., et al., *Further studies on oxygenated tryptamines with LSD-like activity incorporating a chiral pyrrolidine moiety into the side chain.* Journal of Medicinal Chemistry, 1999. **42**(20): p. 4257-63.

78. Yatvin, M.B., et al., *pH-sensitive liposomes: possible clinical implications.* Science, 1980. **210**(4475): p. 1253-5.

79. Connor, J., M.B. Yatvin, and L. Huang, *pH-sensitive liposomes: acid-induced liposome fusion.* Proc Natl Acad Sci U S A, 1984. **81**(6): p. 1715-8.

80. Ellens, H., J. Bentz, and F.C. Szoka, *pH-induced destabilization of phosphatidylethanolamine-containing liposomes: role of bilayer contact.* Biochemistry, 1984. **23**(7): p. 1532-8.

81. Collins, D., D.C. Litzinger, and L. Huang, *Structural and functional comparisons of pH-sensitive liposomes composed of phosphatidylethanolamine and three different diacylsuccinylglycerols.* Biochim Biophys Acta, 1990. **1025**(2): p. 234-42.

82. Drummond, D.C., M. Zignani, and J. Leroux, *Current status of pH-sensitive liposomes in drug delivery.* Prog Lipid Res, 2000. **39**(5): p. 409-60.

83. Venugopalan, P., et al., *pH-sensitive liposomes: mechanism of triggered release to drug and gene delivery prospects.* Pharmazie, 2002. **57**(10): p. 659-71.

84. Meers, P., *Enzyme-activated targeting of liposomes.* Adv Drug Deliv Rev, 2001. **53**(3): p. 265-72.

85. Davidsen, J., et al., *Secreted phospholipase A(2) as a new enzymatic trigger mechanism for localised liposomal drug release and absorption in diseased tissue.* Biochim Biophys Acta, 2003. **1609**(1): p. 95-101.

86. Yatvin, M.B., et al., *Design of liposomes for enhanced local release of drugs by hyperthermia.* Science, 1978. **202**(4374): p. 1290-3.

87. Weinstein, J.N., et al., *Liposomes and local hyperthermia: selective delivery of methotrexate to heated tumors.* Science, 1979. **204**(4389): p. 188-91.

88. Gaber, M.H., et al., *Thermosensitive sterically stabilized liposomes: formulation and in vitro studies on mechanism of doxorubicin release by bovine serum and human plasma.* Pharm Res, 1995. **12**(10): p. 1407-16.

89. Kono, K., *Thermosensitive polymer-modified liposomes.* Adv Drug Deliv Rev, 2001. **53**(3): p. 307-19.

90. Needham, D. and M.W. Dewhirst, *The development and testing of a new temperature-sensitive drug delivery system for the treatment of solid tumors.* Adv Drug Deliv Rev, 2001. **53**(3): p. 285-305.

91. Bondurant, B., A. Mueller, and D.F. O'Brien, *Photoinitiated destabilization of sterically stabilized liposomes.* Biochim Biophys Acta, 2001. **1511**(1): p. 113-22.

92. Shum, P., J.M. Kim, and D.H. Thompson, *Phototriggering of liposomal drug delivery systems.* Adv Drug Deliv Rev, 2001. **53**(3): p. 273-84.

93. Helmlinger, G., et al., *Acid production in glycolysis-impaired tumors provides new insights into tumor metabolism.* Clin Cancer Res, 2002. **8**(4): p. 1284-91.

94. Huang, S.K., et al., *Pharmacokinetics and therapeutics of sterically stabilized liposomes in mice bearing C-26 colon carcinoma.* Cancer Res, 1992. **52**(24): p. 6774-81.

95. Daleke, D.L., K. Hong, and D. Papahadjopoulos, *Endocytosis of liposomes by macrophages: binding, acidification and leakage of liposomes monitored by a new fluorescence assay.* Biochim Biophys Acta, 1990. **1024**(2): p. 352-66.

96. Tycko, B. and F.R. Maxfield, *Rapid acidification of endocytic vesicles containing alpha 2-macroglobulin.* Cell, 1982. **28**(3): p. 643-51.

97. Cevc, G. and H. Richardsen, *Lipid vesicles and membrane fusion.* Adv Drug Deliv Rev, 1999. **38**(3): p. 207-232.

98. Hafez, I.M. and P.R. Cullis, *Roles of lipid polymorphism in intracellular delivery.* Adv Drug Deliv Rev, 2001. **47**(2-3): p. 139-48.

99. Chernomordik, L., *Non-bilayer lipids and biological fusion intermediates.* Chem Phys Lipids, 1996. **81**(2): p. 203-13.

100. Slepushkin, V.A., et al., *Sterically stabilized pH-sensitive liposomes. Intracellular delivery of aqueous contents and prolonged circulation in vivo.* J Biol Chem, 1997. **272**(4): p. 2382-8.

101. Duzgunes, N., et al., *Proton-induced fusion of oleic acid-phosphatidylethanolamine liposomes.* Biochemistry, 1985. **24**(13): p. 3091-8.

102. Mueller, A., B. Bondurant, and D.F. O'Brien, *Visible-Light-Stimulated Destabilization of PEG-Liposomes.* Macromolecules, 2000. **33**(13): p. 4799-4804.

103. Spratt, T., B. Bondurant, and D.F. O'Brien, *Rapid release of liposomal contents upon photoinitiated destabilization with UV exposure.* Biochim Biophys Acta, 2003. **1611**(1-2): p. 35-43.

104. Thompson, D.H., et al., *Triggerable plasmalogen liposomes: improvement of system efficiency.* Biochim Biophys Acta, 1996. **1279**(1): p. 25-34.

105. Wymer, N.J., O.V. Gerasimov, and D.H. Thompson, *Cascade liposomal triggering: light-induced Ca2+ release from diplasmenylcholine liposomes triggers PLA2-catalyzed hydrolysis and contents leakage from DPPC liposomes.* Bioconjug Chem, 1998. **9**(3): p. 305-8.

106. Zhang, Z.Y., et al., *Formation of fibrinogen-based hydrogels using phototriggerable diplasmalogen liposomes.* Bioconjug Chem, 2002. **13**(3): p. 640-6.

107. Zhang, Z.Y. and B.D. Smith, *High-generation polycationic dendrimers are unusually effective at disrupting anionic vesicles: membrane bending model.* Bioconjug Chem, 2000. **11**(6): p. 805-14.

108. Bisby, R.H., C. Mead, and C.G. Morgan, *Wavelength-programmed solute release from photosensitive liposomes.* Biochem Biophys Res Commun, 2000. **276**(1): p. 169-73.

109. Bisby, R.H., C. Mead, and C.G. Morgan, *Active uptake of drugs into photosensitive liposomes and rapid release on UV photolysis.* Photochem Photobiol, 2000. **72**(1): p. 57-61.

110. Davis, S.C. and F.C. Szoka, Jr., *Cholesterol phosphate derivatives: synthesis and incorporation into a phosphatase and calcium-sensitive triggered release liposome.* Bioconjug Chem, 1998. **9**(6): p. 783-92.

111. Ruiz-Arguello, M.B., F.M. Goni, and A. Alonso, *Vesicle membrane fusion induced by the concerted activities of sphingomyelinase and phospholipase C.* J Biol Chem, 1998. **273**(36): p. 22977-82.

112. Goni, F.M. and A. Alonso, *Membrane fusion induced by phospholipase C and sphingomyelinases.* Biosci Rep, 2000. **20**(6): p. 443-63.

113. Villar, A.V., A. Alonso, and F.M. Goni, *Leaky vesicle fusion induced by phosphatidylinositol-specific phospholipase C: observation of mixing of vesicular inner monolayers.* Biochemistry, 2000. **39**(46): p. 14012-8.

114. Villar, A.V., F.M. Goni, and A. Alonso, *Diacylglycerol effects on phosphatidylinositol-specific phospholipase C activity and vesicle fusion.* FEBS Lett, 2001. **494**(1-2): p. 117-20.

115. Papahadjopoulos, D., et al., *Phase transitions in phospholipid vesicles. Fluorescence polarization and permeability measurements concerning the effect of temperature and cholesterol.* Biochim Biophys Acta, 1973. **311**(3): p. 330-48.

116. Merlin, J.L., *Encapsulation of doxorubicin in thermosensitive small unilamellar vesicle liposomes.* Eur J Cancer, 1991. **27**(8): p. 1026-30.

117. Maruyama, K., et al., *Enhanced delivery of doxorubicin to tumor by long-circulating thermosensitive liposomes and local hyperthermia.* Biochim Biophys Acta, 1993. **1149**(2): p. 209-16.

118. Gaber, M.H., et al., *Thermosensitive liposomes: extravasation and release of contents in tumor microvascular networks.* Int J Radiat Oncol Biol Phys, 1996. **36**(5): p. 1177-87.

119. Song, C.W., *Effect of local hyperthermia on blood flow and microenvironment: a review.* Cancer Res, 1984. **44**(10 Suppl): p. 4721s-4730s.

120. Kong, G. and M.W. Dewhirst, *Hyperthermia and liposomes.* Int J Hyperthermia, 1999. **15**(5): p. 345-70.

121. Dewhirst, M.W., et al., *Hyperthermic treatment of malignant diseases: current status and a view toward the future.* Semin Oncol, 1997. **24**(6): p. 616-25.

122. Schild, H.G., *Poly(N-isopropylacrylamide): experiment, theory and application.* Progress in Polymer Science, 1992. **17**(2): p. 163-249.

123. Feil, H., et al., *Effect of comonomer hydrophilicity and ionization on the lower critical solution temperature of N-isopropylacrylamide copolymers.* Macromolecules, 1993. **26**(10): p. 2496-2500.

124. Kono, K., K. Yoshino, and T. Takagishi, *Effect of poly(ethylene glycol) grafts on temperature-sensitivity of thermosensitive polymer-modified liposomes.* J Control Release, 2002. **80**(1-3): p. 321-32.

125. Kono, K., A. Henmi, and T. Takagishi, *Temperature-controlled interaction of thermosensitive polymer-modified cationic liposomes with negatively charged phospholipid membranes.* Biochim Biophys Acta, 1999. **1421**(1): p. 183-97.

126. Ringsdorf, H., et al., *Interactions of liposomes and hydrophobically-modified poly-(N-isopropylacrylamides): an attempt to model the cytoskeleton.* Biochim Biophys Acta, 1993. **1153**(2): p. 335-44.

127. Needham, D., et al., *A new temperature-sensitive liposome for use with mild hyperthermia: characterization and testing in a human tumor xenograft model.* Cancer Res, 2000. **60**(5): p. 1197-201.

128. Pluen, A., et al., *Role of tumor-host interactions in interstitial diffusion of macromolecules: cranial vs. subcutaneous tumors.* Proc Natl Acad Sci U S A, 2001. **98**(8): p. 4628-33.

129. Maeda, H., et al., *Tumor vascular permeability and the EPR effect in macromolecular therapeutics: a review.* J Control Release, 2000. **65**(1-2): p. 271-284.

130. Hobbs, S.K., et al., *Regulation of transport pathways in tumor vessels: role of tumor type and microenvironment.* Proc Natl Acad Sci U S A, 1998. **95**(8): p. 4607-12.

131. Fukumura, D. and R.K. Jain, *Tumor microenvironment abnormalities: causes, consequences, and strategies to normalize.* J Cell Biochem, 2007. **101**(4): p. 937-49.

132. Yuan, F., et al., *Microvascular permeability and interstitial penetration of sterically stabilized (stealth) liposomes in a human tumor xenograft.* Cancer Res, 1994. **54**(13): p. 3352-6.

133. McNeeley, K.M., A. Annapragada, and R.V. Bellamkonda, *Decreased circulation time offsets increased efficacy of PEGylated nanocarriers targeting folate receptors of glioma.* Nanotechnology, 2007. **18**(38): p. 11.

134. Yan, H., et al., *Distribution of free and liposomal doxorubicin after isolated lung perfusion in a sarcoma model.* Ann Thorac Surg, 2008. **85**(4): p. 1225-32.

135. Harasym, T.O., P.R. Cullis, and M.B. Bally, *Intratumor distribution of doxorubicin following i.v. administration of drug encapsulated in egg phosphatidylcholine/cholesterol liposomes.* Cancer Chemother Pharmacol, 1997. **40**(4): p. 309-17.

136. Kong, G., et al., *Efficacy of liposomes and hyperthermia in a human tumor xenograft model: importance of triggered drug release.* Cancer Res, 2000. **60**(24): p. 6950-7.

137. Hauck, M.L., et al., *Phase I trial of doxorubicin-containing low temperature sensitive liposomes in spontaneous canine tumors.* Clin Cancer Res, 2006. **12**(13): p. 4004-10.

138. Ponce, A.M., et al., *Hyperthermia mediated liposomal drug delivery.* Int J Hyperthermia, 2006. **22**(3): p. 205-13.

139. Lindner, L.H., et al., *Novel temperature-sensitive liposomes with prolonged circulation time.* Clin Cancer Res, 2004. **10**(6): p. 2168-78.

140. Huang, S.L. and R.C. MacDonald, *Acoustically active liposomes for drug encapsulation and ultrasound-triggered release.* Biochim Biophys Acta, 2004. **1665**(1-2): p. 134-41.

141. Ebrahim, S., G.A. Peyman, and P.J. Lee, *Applications of liposomes in ophthalmology.* Surv Ophthalmol, 2005. **50**(2): p. 167-82.

142. Mueller, A., Bondurant, B., O'Brien, D.F., *Visible-light-stimulated destabilization of PEG-liposomes.* Macromolecules, 2000. **33**(13): p. 4799-4804.

143. El-Sayed, I.H., X. Huang, and M.A. El-Sayed, *Surface plasmon resonance scattering and absorption of anti-EGFR antibody conjugated gold nanoparticles*

in cancer diagnostics: applications in oral cancer. Nano Lett, 2005. **5**(5): p. 829-34.

144. El-Sayed, I.H., X. Huang, and M.A. El-Sayed, *Selective laser photo-thermal therapy of epithelial carcinoma using anti-EGFR antibody conjugated gold nanoparticles.* Cancer Lett, 2006. **239**(1): p. 129-35.

145. Huang, X., et al., *Cancer cell imaging and photothermal therapy in the near-infrared region by using gold nanorods.* J Am Chem Soc, 2006. **128**(6): p. 2115-20.

146. Huang, X., et al., *Determination of the minimum temperature required for selective photothermal destruction of cancer cells with the use of immunotargeted gold nanoparticles.* Photochem Photobiol, 2006. **82**(2): p. 412-7.

147. Huang, X., et al., *Gold nanoparticles: interesting optical properties and recent applications in cancer diagnostics and therapy.* Nanomed, 2007. **2**(5): p. 681-93.

148. Huang, X., et al., *Plasmonic photothermal therapy (PPTT) using gold nanoparticles.* Lasers Med Sci, 2008. **23**(3): p. 217-28.

149. Huang, X., et al., *The potential use of the enhanced nonlinear properties of gold nanospheres in photothermal cancer therapy.* Lasers Surg Med, 2007. **39**(9): p. 747-53.

150. Jain, P.K., et al., *Noble metals on the nanoscale: optical and photothermal properties and some applications in imaging, sensing, biology, and medicine.* Acc Chem Res, 2008. **41**(12): p. 1578-86.

CHAPTER 3

RATIONAL IDENTIFICATION OF A NOVEL PEPTIDE FOR TARGETING NANOCARRIERS TO 9L GLIOMA

Parts of the following chapter are published in Journal of Biomedical and Material Research: Part A, Jan 15, 2008

3.1 Abstract

Traditional therapies for high grade gliomas are limited in part by collateral damage to normal tissues. Selective delivery of therapies to tumors is, therefore, needed. Here, we report that liposomal nanocarriers coated with a novel oligopeptide enhance uptake by 9L gliosarcoma. A targeting 9 amino acid peptide sequence (RSI) was identified by differential panning of random peptide phage display libraries on 9L cells and rat blood cells and plasma. Peptides were coupled to the surface of liposomal nanocarriers which were subsequently loaded with doxorubicin. The ability of RSI coated liposomes to facilitate drug uptake and cytotoxicity was compared to conventional liposomal nanocarriers and controls. In addition, plasma clearance profiles of the RSI peptide coupled liposomal nanocarriers were evaluated in adult immuno-competent rats. RSI peptide-coupled liposomal nanocarriers enhanced drug uptake by 9L cells by 500% compared to conventional liposomal nanocarriers, and significantly increased cytotoxicity. The plasma half-lives confirmed that the presence of the RSI peptide on the liposomal nanocarriers did not compromise circulation time in the blood in comparison to Stealth liposomal nanocarriers. These data suggest that phage-identified oligopeptides could lead to the development of new tumor selective nanocarriers.

3.2 Introduction

Brain tumors represent the most common solid tumors in children and adolescents and show rising incidence [1-2]. Prognosis remains poor for these therapeutically challenging neoplasms [3] where long-term survivors are rare among patients with high grade gliomas. The median survival time for patients with high-grade gliomas treated with surgery and chemotherapy is a year or less [3]. These highly infiltrative tumors are not amenable to surgical cure, and current chemo- and radio-therapies suffer from a lack of specificity for the tumor tissue with significant untoward effects on uninvolved tissues [4]. Therefore, there is a dire clinical need for alternative approaches that afford selective tumor targeting.

Currently, a primary limiting step in achieving this goal is lack of molecular targeting ligands and appropriate carriers for specific and efficacious treatment of brain tumors. Liposomal nanocarriers are nanocarrier vehicles that show great promise for delivery of therapeutic agents. PEG-coated liposomal nanocarriers (Stealth) [5-6] have small size and long circulation time, which are major advantages for drug delivery, and when administered systemically, liposomal nanocarriers can passively accumulate in tumor tissue, including in high-grade gliomas [7]. Tumors have compromised vasculature that is leakier than normal vasculature. Due to longer blood residence time and presence of ‘leaky’ tumor vasculature, repeated passage of liposomal nanocarriers through the tumor microvascular bed results in much higher concentration of liposomal nanocarriers within the tumor compared to free drug. This is called the enhanced permeability and retention effect [8-11]. Active targeting follows passive accumulation and is achieved by

incorporating receptor-mediated molecular targets on the nanocarriers to promote their specific localization.

High affinity tumor targeting ligands can be readily coupled covalently to the distal ends of nanocarrier PEG chains through a variety of chemical linkages [12]. In fact, one or more ligands may be coupled to the same nanocarrier, potentially conferring added selectivity [13]. We have developed techniques to tightly control the number of targeting ligands on these nanocarriers, a means to finely tune cell-binding selectivity. The principal shortcoming of existing targeting ligands, such as folate and antibodies, is that they significantly compromise circulation time when presented on nanocarriers. Compromised circulation time results in decreased nanocarrier extravasation into tumors [14]. Long circulation is critical for increasing passive accumulation of liposomal nanocarriers in the tumors [15-16]. The extent of passive accumulation, in turn, determines the maxima in the effects of active targeting. Therefore, identification of ligands that afford selective tumor targeting while not compromising circulation time would be greatly advantageous.

Recently, selective cell targeting ligands have been identified using random peptide phage display libraries by employing *in vitro* [17-19] and *in vivo* [20-22] panning approaches. We and others have identified and characterized high avidity cell and tissue-type selective targeting peptide moieties using random peptide phage display libraries by panning *in vitro* on cells [23-25]. Libraries that contain up to 10^{8-9} unique oligopeptide sequences in a small volume afford rapid screening of immense numbers of peptides to identify distinctive cell surface signatures without the prior information about such sites. In this study, we employed random peptide phage display libraries to rationally identify

glioma selective binding peptides that a) permit significantly enhanced nanocarrier uptake in 9L glioma and b) demonstrate that liposomal nanocarriers coated with targeting oligopeptides manifest prolonged circulation times ensuring uncompromised passive accumulation in tumors.

3.3 Materials and Methods

3.3.1 Materials

1,2-distearoyl-*sn*-glycerophosphoethanolamine poly(ethylene glycol)$_{3400}$ maleimide (DSPE-PEG3400-mal) was obtained from NOF Corporation (Tokyo, Japan). 1,2-distearoyl-*sn*-glycerophospho-choline (DSPC) and 1,2-distearoyl-*sn*-glycerophosphoethanolamine poly(ethylene glycol)$_{2000}$ (DSPE-PEG2000) were purchased from Avanti Polar Lipids (Birmingham, AL). A fluorescent phospholipid β-DPH was obtained from Invitrogen (Carlsbad, CA). Cholesterol, paraformaldehyde, and Triton X-100 were purchased from Sigma (St. Louis, MO). RSIEWSGLWGPPVESC (RSI) and WRWGSELISGPPVESC (scrambled negative control) peptides were synthesized by Global Peptide Services (Ft. Collins, CO) using standard fMOC chemistry followed by HPLC purification and sequence confirmation with mass spectroscopy. Dialysis tubing (10,000 and 100,000 molecular weight cut-off) was purchased from Spectra/Por (Dominguez, CA). DC protein assay was obtained from Bio-Rad, (Hercules, CA). A 9L glioma cell line was received as a generous donation from the Neurosurgery Tissue Bank at UCSF. Minimal essential medium containing Earle's balanced salt solution (MEM/EBSS) was purchased from Hyclone (Logan, UT). Gentamicin (50 mg/ml) and fetal bovine serum (FBS) were obtained from Gibco (Carlsbad, CA). Trypsin-EDTA (0.05% trypsin, 0.53 mM EDTA) in Hanks' balanced salt solution was

purchased from Mediatech (Herndon, VA). FluorMountG was obtained from Southern Biotech (Birmingham, AL). Heparin (1000 USP units/ml), isoflurane, and doxorubicin (DXR) were purchased from Baxter Healthcare (Deerfield, IL). Cell Counting Kit-8 (CCK-8) was obtained from Dojindo (Kumamoto, Japan) and Cytotoxicity Colorimetric Assay Kit, (CytoTox 96) was obtained from Promega (Madison, WI). Fisher 344 male rats were purchased from Harlan (Indianapolis, IN).

3.3.2 Cell Culture

9L glioma cell line was maintained in MEM/EBSS medium supplemented with 10% fetal bovine serum and 0.05 mg/ml gentamicin. Cells were passaged by trypsinization and washed with growth medium.

3.3.3 9L glioma-based panning experiments

The linear nonapeptide (LL9) and constrained hexapeptide (CL6) random peptide phage display libraries were prepared as described [23]. Panning was performed on sub confluent (<95%) 9L adherent cells in 162 cm^2 culture flasks for 6 rounds using a modification of a previously described protocol [23, 25]. Briefly, cell layers were washed twice with 10 ml Hanks' balanced salt solution (HBSS), containing 1 mM $CaCl_2$, 1 mM $MgCl_2$, 10 mM HEPES, and 0.5% BSA, pH 7.4 (HBSS(+)). Phage libraries (30 µL containing 3 x 10^{11} pfu) were added to 6 ml HBSS+, supplemented with 5 mM $CaCl_2$ and 10% rat plasma as adsorbent (Cocalico Biologicals, Reamstown, PA) and incubated with gentle rotation for 4 hours. Supernatants were removed and cell layers washed 10 times with HBSS+. Bound and internalized phage particles were recovered by adding 3 ml lysis buffer [25] for 10 minutes. Phage were collected and amplified in K91 *E. coli* overnight and purified, concentrated, re-suspended in buffer, and quantified to generate sub-

libraries for use in the next round of panning [23]. Before the second and each subsequent round of panning, phage sub-libraries were pre-adsorbed on rat blood cells (Cocalico Biologicals). Sub- libraries (30 µL containing 3 x 10^{11} pfu) were incubated with 2 ml washed, packed blood cells from a buffy-coat preparation suspended in 2 ml HBSS+ for 3 hours. Cells were pelleted to remove adsorbed phage. Cell-free supernatants containing non-adsorbed phage were applied to 9L cells as above. After the fourth and fifth panning rounds, 15 randomly selected phage clones were propagated and concentrated for each library [25]. The amino acid sequences of the displayed peptides were deduced for specific phage clones by sequencing the coding nucleotides in the viral DNA [25].

3.3.4 Phage Binding Assays

Phage binding assays were performed with minor modification [23]. In brief, 9L cells were grown to approximately 95% confluence in 96 well plates and washed. 100 µl individual phage clones were added at 10^{10}/ ml in HBSS+ in quadruplicate for 1 hour at 37 C. After washing, bound phage were fixed to cells with 3.7% paraformaldehyde, washed with HBSS+, and detected with horseradish-peroxidase conjugated anti-phage antibody (Amersham) and peroxidase substrate for quantification using a microtiter plate reader. Synthetic peptide inhibition experiments were performed as described [26]. Cells were incubated with primary phage conjugates or unlabeled phage clones in the presence or absence of 1 mM specific or control synthetic peptide and binding to cells assayed as above.

3.3.5 Flow Cytometry

Flow cytometry (FACS) studies with phage clones and blood cells were performed as described [25-26].

3.3.6 Liposome Preparation

Liposomal nanocarriers were formed as described earlier [13, 27]. Briefly, a ratio of 59:40:0 and 57.5:40:1.5 of DSPC: cholesterol: DSPE-PEG2000 was dissolved in 1mL of ethanol at 60^{o}C. 1.5% of DSPE-PEG2000 was used to evade the RES in the plasma clearance studies. 0.01 (mol %) of fluorescent phospholipid (β-DPH) was used to determine phospholipid content and a 0.1 (mol %) of β-DPH for fluorescent microscopy studies. Liposome size was determined by dynamic light scattering (Particle Size Analyzer, Brookhaven Instruments, Holtsville, NY). Liposomal nanocarriers were dialyzed against a phosphate-buffered saline solution to establish an ammonium sulfate gradient for DXR loading.

3.3.7 Lipid-Peptide Conjugate Synthesis

A lipid-PEG-peptide conjugate was synthesized such that it can later be incorporated into liposomal nanocarriers to facilitate targeting. The N-terminal of the peptide was determined to be the active binding site. Therefore, a cysteine residue was attached to the carboxyl terminal of the peptide for conjugation to the lipid-PEG tether. RSI peptide was coupled to DSPE-PEG3400-mal via the sulfide on the cysteine. DSPE-PEG3400-mal was dissolved in water to form a 1mM micellar solution. 1.5 mmoles of the RSI peptides were slowly dissolved in the micellar solution maintaining the pH between 6.7 and 7.2. The solution was stirred for 3hours at room temperature. Unreacted peptides were removed by dialyzing against deionized water in a 10,000 MWCO

membrane overnight. The solution was lyophilized. The final product was analyzed by MALDI-TOFMS acquired on Applied Biosystems 4700 proteomics analyzer. A conjugate was constructed using a scrambled version of the RSI peptide (control) for use as a control.

The amount of reacted peptide was determined by a modified Lowry method (DC protein assay). Peptide content measured by DC protein assay was verified by Beer-Lamberts law by measuring absorbance at 280 nm in a Synergy microplate reader (Bio-Tek, Winooski, VT).

3.3.8 Lipid-Peptide Conjugate Incorporation into Liposomal Nanocarriers

Peptide presenting liposomal nanocarriers were prepared by post-inserting DSPE-PEG3400-peptide micelles to pre-formed liposomal nanocarriers at 60^{o}C. Micelles were formed by dissolving the DSPE-PEG3400-peptide conjugate in deionized water. Unincorporated micelles were removed by dialysis as described previously [13]. The amount of peptide inserted into liposomal nanocarriers was determined by DC protein assay after lysis of liposomal nanocarriers with 20% SDS.

3.3.9 Active Loading of Doxorubicin

Following ligand incorporation, liposomal nanocarriers were loaded with DXR via the ammonium sulfate gradient as described before [28]. Briefly, liposomal nanocarriers and 2 mg/ml DXR solution in 0.9% saline were mixed at a ratio of 0.1 mg DXR per 1 mg of DSPC in the liposomal nanocarriers for all *in vitro* studies. For plasma clearance studies, a 15 mg/ml DXR solution was mixed with liposomal nanocarriers at a ratio of 0.3 mg DXR per 1 mg of DSPC in the liposomal nanocarriers. The liposome/DXR suspension was heated at 60 °C for 1 h. The liposomal nanocarriers were

then cooled immediately on ice and dialyzed in 100 000 MWCO membrane against PBS to remove un-encapsulated DXR. The formulations were sterilized by passing through a 0.2 μm filter. The final DXR concentration after dialysis was determined by lysis of the liposomal nanocarriers with 5% Triton X-100 and measurement of absorbance at 480 nm.

3.3.10 Cellular Liposomal Drug Uptake Experiments

Cellular uptake experiments were conducted using strategies published earlier [13, 29]. The targeting efficiency as a function of peptide ligand number per liposome was determined by *in vitro* incubation of cells with DXR-loaded peptide-liposome formulations. Cells were seeded at a density of $1.5x10^5$ cells per well in a 12 well plate. After 48 hours in culture, cells were utilized for DXR uptake experiments. After removing the culture medium, cells were washed once with PBS. DXR (200 μM) in either free form (free DXR) or liposomally encapsulated form was mixed with culture medium and immediately added to cells. Cells were then incubated for 6 h with the DXR mixture at 37 °C in a 5% CO_2, high humidity environment. Following incubation, cells were placed on ice, washed three times with PBS containing calcium and magnesium to remove extracellular DXR. Cells were then lysed with 500μl of 5% Triton X-100 and the fluorescence intensity of DXR was measured on a fluorescence spectrometer at an excitation/emission of 485/590 nm.

Competitive binding experiments were performed simultaneously to determine if the RSI peptide specifically mediated the cellular uptake of liposomal-DXR. In these experiments, 200 μM of DXR-peptide-liposomal nanocarriers bearing 500 RSI peptides were co-incubated with an excess of free peptide at 4 mM concentration. An amount of 4

mM free peptide is a 100-fold excess over the number of RSI peptides present due to the 500 peptide motifs per liposome level.

3.3.11 Cytotoxicity of RSI-targeted liposomal nanocarriers

9L glioma cells were seeded at a density of $2x10^4$ cells per well of a 24-well plate and incubated for 48 hours prior to incubation with liposomal nanocarriers. 48 hours later, liposomal formulations were mixed with MEM/EBSS medium to a 100μM doxorubicin concentration and added immediately to cells.

Cells were incubated with free DXR or liposomal DXR for 30 minutes at 37^oC and 5% CO_2 in a humidified environment. Cells were then washed three times with fresh medium and re-incubated for 72 hours. The number of viable cells was determined with a water soluble formazan-based assay (CCK-8). The number of dead cells was quantified by a lactate dehydrogenase based assay (CytoTox 96).

3.3.12 Liposome Cellular Localization Imaging

To visualize the cellular localization of peptide-presenting liposomal nanocarriers, cells were seeded at a density of $3x10^3$ cells per well of an eight-well chamber slide for 24 hours. 2 mM liposomal formulations that incorporated 0.1% of a fluorescent lipid β-DPH were incubated with the cells for 10 minutes at 37^oC and 5% CO_2 in a humidified environment. Cells were then placed on ice, washed three times with PBS to remove unbound liposomal nanocarriers, and fixed with 4% paraformaldehyde for 30 minutes. The chambers were removed and slides were coversliped with Fluoromount G. Cells were imaged on a Nikon Eclipse 80*i* microscope using an Optotronics Microfire camera.

3.3.13 Plasma Clearance

All animal work was done according to an approved animal protocol and in strict compliance with NIH Clinical Center Animal Care and Use Committee guidelines and regulations. 10-11 weeks old male Fisher rats weighing 250g were anesthetized under isoflurane and administered DXR-Stealth liposomal nanocarriers (n=4) or DXR-RSI peptide-presenting liposomal nanocarriers (n=4) via tail vein at a dose of 10 mg/kg DXR. 500 µl of blood was collected from the orbital sinus before IV injection and at 0.5, 2, 8, 24, 48, and 72 hours after injection in heparinized gel tubes. Tubes were centrifuged at 3000 rpm for 20 minutes to separate the plasma. Liposomal nanocarriers were lysed as described elsewhere [30]. Briefly, a mixture of 0.75N acidified isopropanol, 10% Triton X100, water, and plasma was prepared to analyze the DXR content. To quantify total DXR content, fluorescent readings were obtained using a fluorescence spectrometer at excitation/emission of 485/590 nm. Plasma samples obtained prior to injection were used to correct for background fluorescence.

3.3.14 Survival Studies

All animal studies were conducted under a protocol approved by the Institutional Animal Care and Use Committee (IACUC) at Georgia Institute of Technology. A rat glioma model was established by surgically implanting $1x10^6$ 9L glioma cells into the frontal lobe of 10-11 week old male Fisher 344 rats. During surgery, anesthesia was maintained through the administration of 2-3% inhalant isoflurane. The incision site was shaved and the animal mounted in a stereotaxic frame. The scalp was opened to expose the skull, and a burr hole was drilled 2 mm anterior and 2 mm lateral to the bregma. 9L glioma cells in 10 µl of Leibovitz's L-15 medium were slowly injected into the frontal

lobe through a 21-gauge needle at a depth of 3 mm. The burr hole was then sealed with bone wax, and the scalp was sutured.

Four days after tumor inoculation, animals were treated with a saline sham, 0 peptide-targeted 'Stealth', or 500 peptide-targeted liposomal DXR i.v. injections (10 mg/kg doxorubicin) via tail vein. Equivalent volumes of 0.9% sterile saline solution were administered to animals receiving sham injections. To a second set of animals, another liposomal dose of 10 mg/kg of doxorubicin was administered 5 days after the first dose (cumulative 20 mg/kg doxorubicin). Tumor growth was allowed to progress until the animal showed signs of morbidity, at which point, interventional euthanasia was administered. Time of death was determined to be the following day.

3.4 Results

3.4.1 Identification of 9L Glioma Selective Binding Peptides

Panning experiments were performed to identify phage clones bearing peptides that selectively bind to the 9L model rat glioma cell line while displaying minimal binding to normal rat blood cells, a potentially major source for nonspecific uptake of injected nanocarriers. Sequences of the displayed random peptides were determined for 15 phage clones per library each after panning rounds 4 and 5 for 60 total sequences. Of these, specific motifs were identified for a subset. As shown in Table 1, three remarkable motif groups were apparent, labeled groups 1-3. In group 1, 9 amino acid long peptides display the WxGxW consensus (bold) with [**R**/**K**][**T**/**S**]x**EW**x**G**x**W** and [**R**/**K**][**T**/**S**]xx**WDG**x**W** motifs, where "x" is any AA. Group 2 clones all displayed the same the **RGDN** motif in a cyclic 6 AA peptide constrained by N and C terminal Cys residues. A similarly constrained 10 AA peptide consensus was **DVF**xx**WM**x**R**x. A set

of clones devoid of consensus motifs is labeled “None” in Table 3.1. Based on searches of public databases, no significant identities to known peptide/protein sequences were found for the other displayed peptides shown. Finding such clear-cut motifs is consistent with high affinity of the sequences for discrete receptors on the 9L cell surface.

Screening experiments were then performed to assess the relative binding selectivity and avidity of the phage clones with the goal of identifying high 9L glioma binding and low blood cell binding. Results of phage binding assays and FACS analyses using adherent 9L glioma and suspension rat blood cells, respectively, are displayed in Table 1. Consistent with their similar peptide motif, group 1 clones clustered as the top 12 binders to 9L cells. By contrast, they ranked in the lower middle to lower half for binding to rat blood cells. Control clones (CTLs group, Table 3.1) included those previously selected for binding blood cells (e.g. FGPNLTGRW-bearing phage (FGP)) [23] and performed as expected in FACS analysis 4. The best differential binding profile was observed for the displayed peptide of the 2nd clone in group 1, RSIEWSGLW (RSI). Thus, the RSI phage clone was chosen for detailed binding studies.

Table 3.1. Summary of the glioma selective binding peptides.

Motifs Groups	Displayed peptide Sequence	Freq	ELISA 9L Glioma cells	FACS Blood Cells
Group 1	W**S**YS**WDG**F**W**	6	1	11
	RS I**EW**S**GL**W	1	2	16
	KSY**EW**P**G**T**W**	2	3	15
	M**RTEW**T**G**V**W**	2	4	17
	KSAS**WDG**L**W**	1	5	24
	SHLT **WDG**T**W**	6	6	19
	VVIQ **WDG**A**W**	1	7	12
	Y**T**VA**WDG**T**W**	3	8	8
	L**TT EW**S**G**T**W**	2	9	14
	G**R**LQ**WDG**A**W**	2	10	13
	RTV**EW**S**G**N**W**	1	11	7
	A**KT**V**WDG**R**W**	1	12	9
Group 2	C **RGD**NFQ C	9	13	4
Group 3	C **DVF**EV**WM**G**R**V C	4	17	20
	C **DVF**TY**WM**R**R**D C	9	18	18
None	KSLLTTMAS	1	19	21
	GWGMEALGA	1	21	23
	RSPN	1	22	22
	CRGTQNTMRARC	1	24	10
CTLs	DLDVSPWDL		14	3
	FGPNLTGRW		15	2
	CVWHPVTGAAVC		16	6
	Wild type		20	1
	DLPTSKINI		23	5

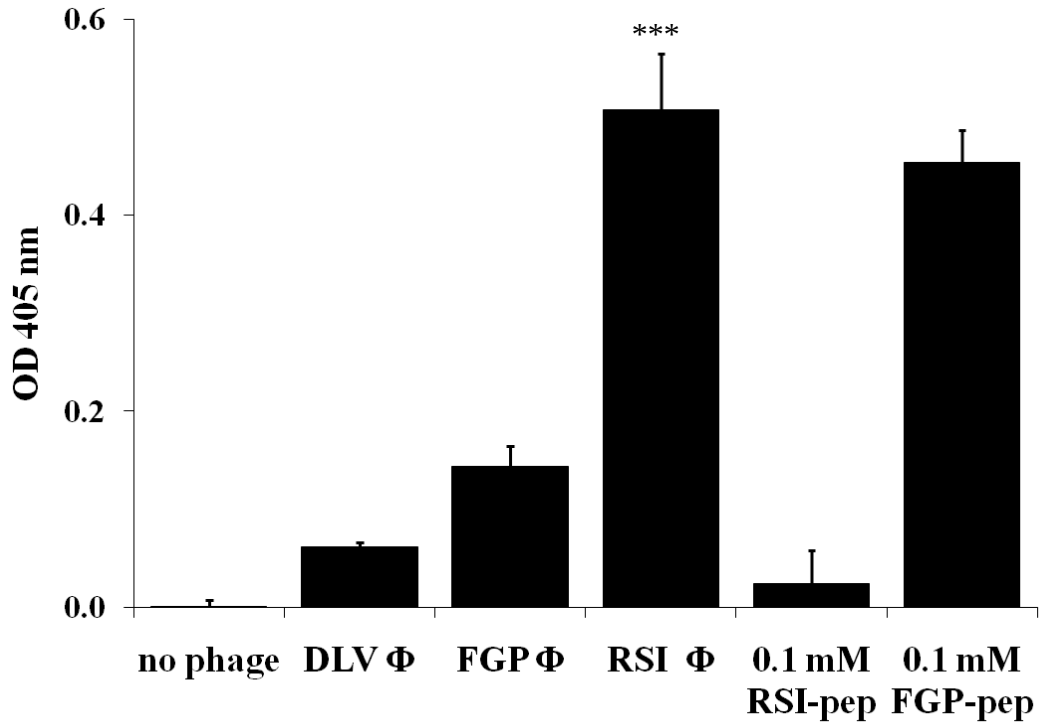

Figure 3.1. RSI phage and peptide selectively bind 9L cells. ELISA was performed with a synthetic version of the RSI peptide to confirm specificity of binding. The RSI Φ displayed significantly higher (* p<0.001) binding to 9L cells compared to control DLV Φ (DLV= DLVTSKINI) and FGP Φ (FGP = FGPNLTGRW). RSI Φ binding was selectively diminished by the 0.1 mM synthetic RSI peptide but not by 0.1 mM control FGPNLTGRW peptide confirming specific binding via the displayed RSI peptide. Data represents the mean ± SD.**

To confirm specificity of binding of RSI at the molecular level, a synthetic peptide version was used in phage binding assay to test whether peptide selectively abrogates binding of RSI phage to adherent 9L glioma cells. As shown in fig. 3.1, the RSI phage (Φ = phage) displayed significantly higher ($p<0.001$) binding to 9L cells compared to control phage bearing peptide DLVTSKINI (DLV) or FGP. DLV and FGP phage displayed peptides that were not related to the RSI primary AA sequence and were therefore chosen as controls. RSI phage binding was selectively abrogated by the 0.1 mM synthetic RSI peptide ($p<0.001$) but not by 0.1 mM control FGP peptide, confirming specific binding via the displayed RSI peptide. Moreover, dose-dependent binding of a biotinylated version of the RSI peptide (0.1 μM to 1 mM) was demonstrable (not shown). In aggregate, these data confirm binding of the RSI peptide to 9L glioma cells.

3.4.2 Targeting Peptide Conjugate and Liposome production

We next produced liposomal nanocarriers bearing the RSI peptide to test *in vitro* binding capability. RSI peptides were conjugated to DSPE-PEG3400 via a maleimide functional group. The final product yield of DSPE-PEG3400-peptide conjugate was 65% as determined by DC protein assay and Beer-Lambert's interpolation method. MALDI-TOFMS and thin layer chromatography (TLC) were used to analyze the product. MALDI-TOFMS confirmed the mass of the conjugate. The mass spectrum had a bell-shaped distribution of 44 Da-spaced lines indicating a singly charged PEG conjugate. The distribution had its mode at 6109 Da, similar to the theoretical molecular mass of 6141 Da (fig. 3.2).

The final product was characterized by TLC showing no unreacted peptide (absence of ninhydrin staining). Cupric sulfate spray indicated complete consumption of

the DSPE-PEG3400-mal (disappearance of the parent spot, Rf=0.36 in $CHCl_3$: MeOH=85:15) into the desired DSPE-PEG3400-peptide conjugate (appearance of a new spot, Rf=0.47 in $CHCl_3$: MeOH=85:15).

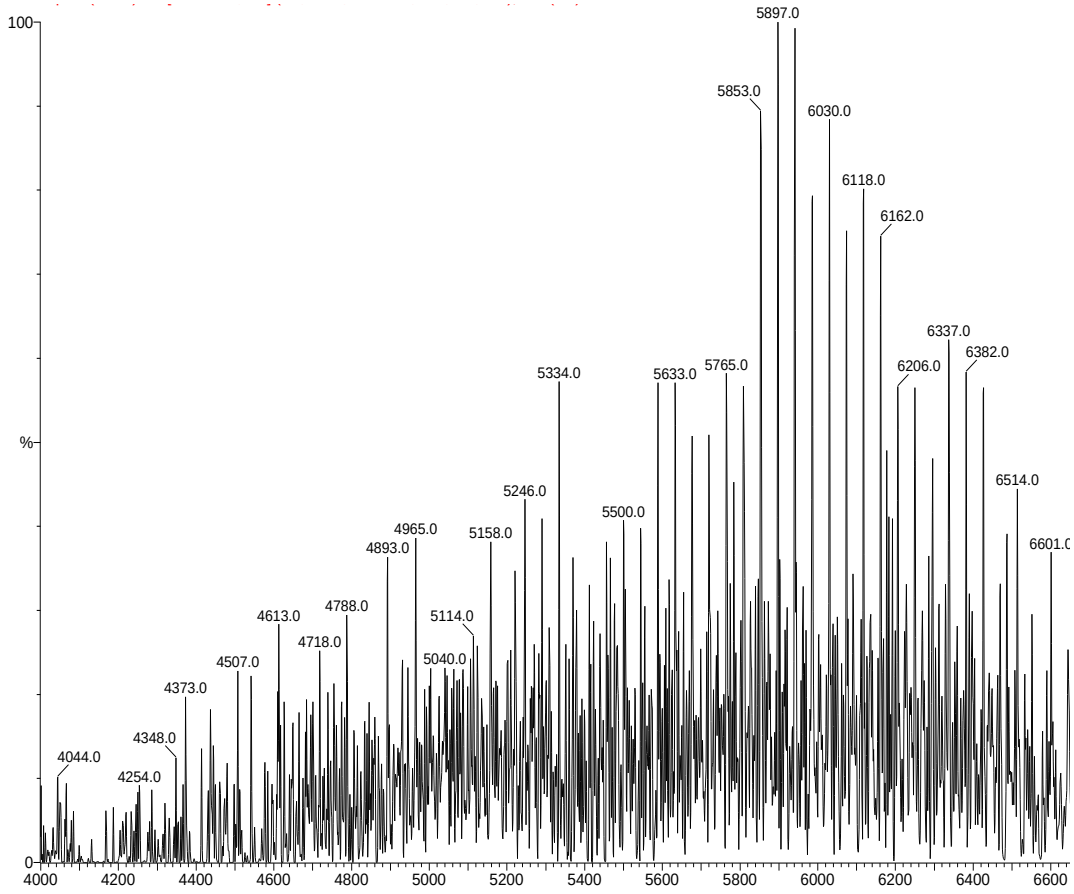

Figure 3.2. MALDI-TOFMS of the DSPE-PEG3400-peptide conjugate.

The liposome size, as determined by DLS, was 98 ± 20 nm. To achieve different number of peptides per liposome, different micellar concentrations were added. The insertion efficiency for the number of conjugated peptides inserted into the liposomal nanocarriers was 80% as determined from the DC protein assay. Therefore, the amount of

micelles added to the liposomal nanocarriers was adjusted to gain the desired number of peptides/liposome.

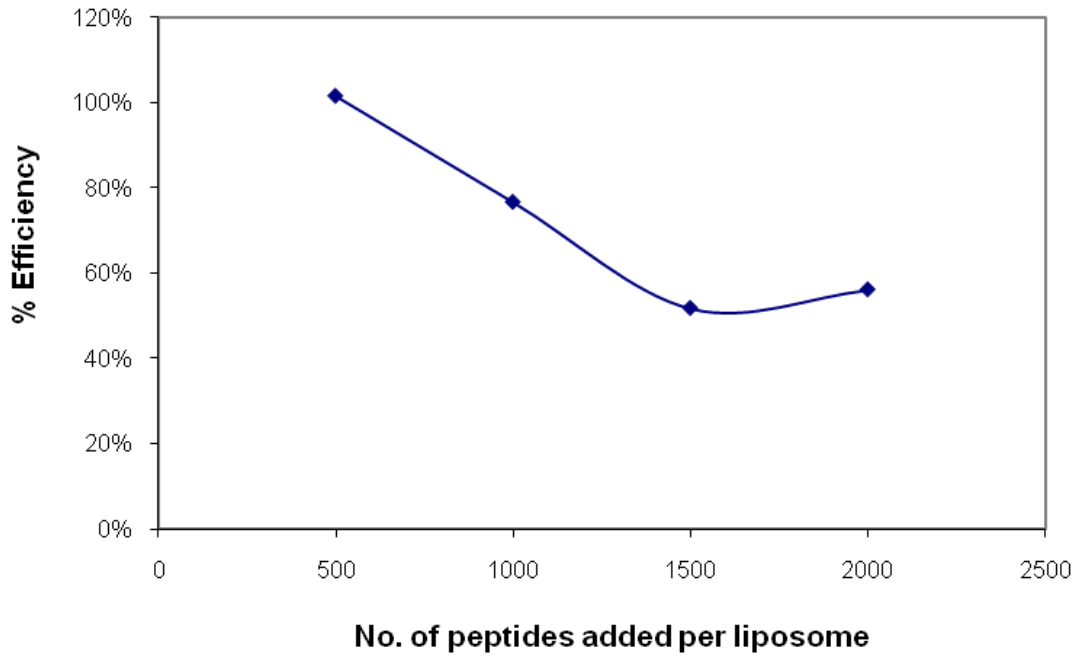

Figure 3.3. Post insertion efficiency of the conjugate DSPE-PEG3400-peptide conjugate onto liposomes with increasing number of peptide conjugate onto the liposomes. Post insertion was 80% efficient up till ~800 peptides per liposomes.

3.4.3 Peptide targeting enhances in vitro delivery of DXR by liposomal nanocarriers

The ability of RSI liposomal nanocarriers to deliver DXR to 9L glioma cells was compared to non-targeting stealth liposomal nanocarriers as a function of number of targeting ligands per liposome. DXR uptake into cells was quantified after 6 h incubation utilizing the fluorescent properties of DXR. As shown in fig. 3.4a, the DXR uptake increased as a function of the number of RSI peptides per liposome. Although data suggest that cell uptake mechanisms were not saturated even at 750 peptides/liposome,

higher peptide content was not assessed because conjugate insertion became inefficient at numbers >1000 (fig 3.3). The uptake of the RSI peptide presenting liposomal nanocarriers was compared with the uptake of the control peptide-presenting liposomal nanocarriers to test the specificity of the RSI peptide to 9L cells. Unlike RSI peptide liposomes the drug payload due to control peptide liposomes did not increase with higher number of peptides on the liposomal surface.

As seen in fig. 3.4b, at 500 peptides of either control or RSI the RSI peptide-presenting liposomal nanocarriers were taken up significantly better than the control peptide-presenting liposomal nanocarriers ($p<0.05$) and conventional non-targeting liposomal nanocarriers (increased by 500%; $p<0.002$). In competition with 100-fold excess of free RSI peptide (4 mM), RSI presenting liposome uptake was reduced approximately 50%. By contrast, RSI peptide had no effect on other liposome preparations.

To establish if the enhanced DXR uptake via the RSI peptide presenting liposomal nanocarriers yields increased cytotoxicity, live and dead 9L cells were counted 72 hours after 30 minute incubation with liposomal nanocarriers. 72 hours is sufficient time for 3-4 cell divisions [31]. 9L cells were seeded at 20,000 cells per well in 24 well plates. DXR at 0 or 100μM in free or liposomal form (conventional non-targeted liposomal nanocarriers, 500 RSI peptide presenting liposomal nanocarriers, and 500 control peptide presenting liposomal nanocarriers) was added for 30 minutes.

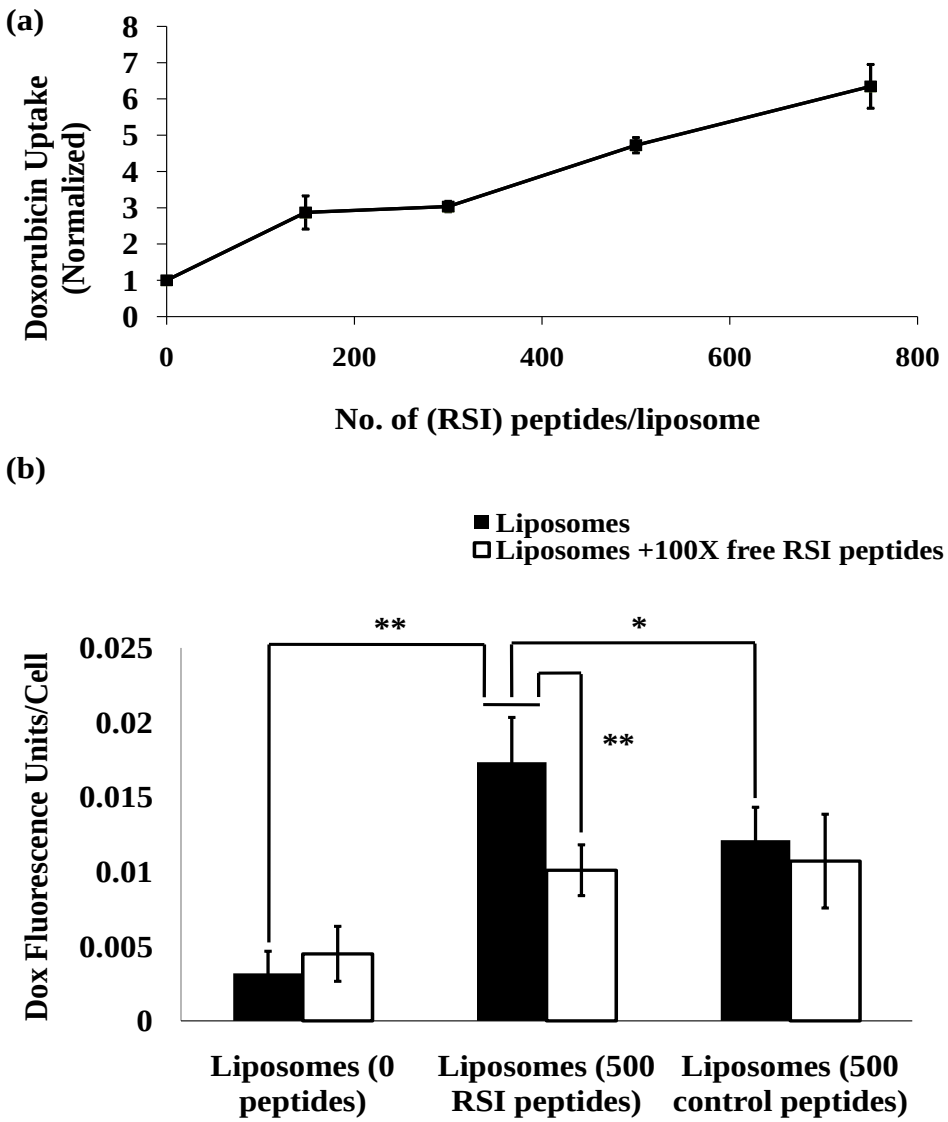

Figure 3.4. Specific and dose dependent uptake of DXR loaded liposomes mediated by targeting RSI peptide. (a) Effect of increasing number of RSI peptides/liposome on the cellular levels of DXR was measured as DXR fluorescence. Fluorescence of the RSI peptide liposomes were normalized to that of the conventional liposomes for comparison purposes. As shown, increasing number of RSI peptides/liposome also increased the drug uptake by 9L cells and the uptake was significantly better than conventional non targeted liposomes (* $p<0.05$). All RSI peptide liposomes were taken up significantly better than the conventional liposomes ($p<0.01$). (b) Comparing uptake of conventional, RSI peptide presenting, and control peptide presenting liposomes. Liposomes with 0 peptides, 500 RSI peptides/liposome, or 500 control peptides/liposome were prepared. 9L cells were incubated with either DXR loaded liposomes or DXR loaded liposomes + 4mM free RSI peptide (~100 fold excess compared to liposomally bound peptide). Cellular DXR fluorescence was measured. Liposomes with 500 RSI peptides/liposome were taken up significantly better than conventional liposomes (**$p<0.002$), 500 control peptide presenting liposomes (* $p<0.05$), and RSI peptide presenting liposomes co incubated with excess of free RSI peptide (** $p<0.01$). Data represents the mean ± SD.**

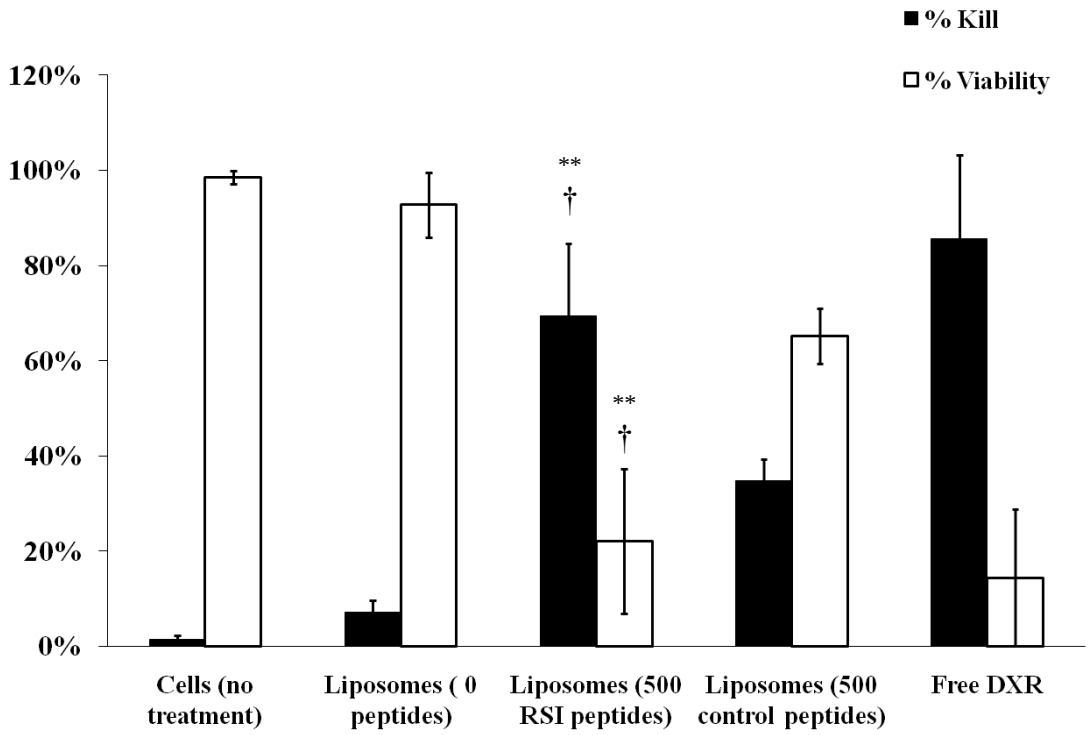

Figure 3.5. Cytotoxic effects of various liposomal formulations on 9L cells. Cells were incubated with various liposomal formulations for 30 minutes. Cells were washed with fresh media and post incubated for another 72 hours. Live cells and dead cells were enumerated. The kill percentage represents the ratio of the number of dead cells to the total number of cells (dead + viable) per well. Similarly, % viability is the ratio of the viable cells to the total number of cells per well. Data represents the mean ± SEM. **p<0.01 compared to untreated cells and cells treated with conventional liposome. † p<0.01 compared to cell treated with control peptide liposomes.

Initial microscope examination of treated and untreated 9L glioma showed no differences in cell density and morphology. After 72 hours, percentages of live cells (a measure of metabolically active cells) and dead cells (measured by the content of lactate dehydrogenase released from dead cells) were determined as a ratio of number of dead cells or live cells to the total number of cells (live + dead) in a given well and are displayed in fig. 3.5. As shown, 76% of cells treated with RSI liposomal nanocarriers were dead in contrast to 35% by control scrambled peptide liposomal nanocarriers and 15% by conventional non-targeted liposomal nanocarriers. Less than 1% of cells were dead in untreated wells. The RSI peptide-presenting liposome treated wells were statistically ($p<0.05$) different from the other treatments. In aggregate, these studies suggest selectively enhanced delivery of liposomal nanocarriers mediated by RSI targeting

To determine the early intracellular localization and selectivity of liposomal uptake, the distribution of fluorescently tagged liposomal nanocarriers with β-DPH was studied by fluorescence microscopy. Fig. 3.6 shows the sub cellular localization of different liposomal formulations after 10 minutes incubation at 37°C followed by cell fixation. In comparison to background cellular fluorescence (fig. 3.6A), non-targeted (fig. 3.6B) and control peptide (fig. 3.6C) liposomal nanocarriers yield minimal to no increase in signal. By contrast, RSI liposomal nanocarriers yield clear and selective increase in signal localized to cytoplasm (fig. 3.6D).

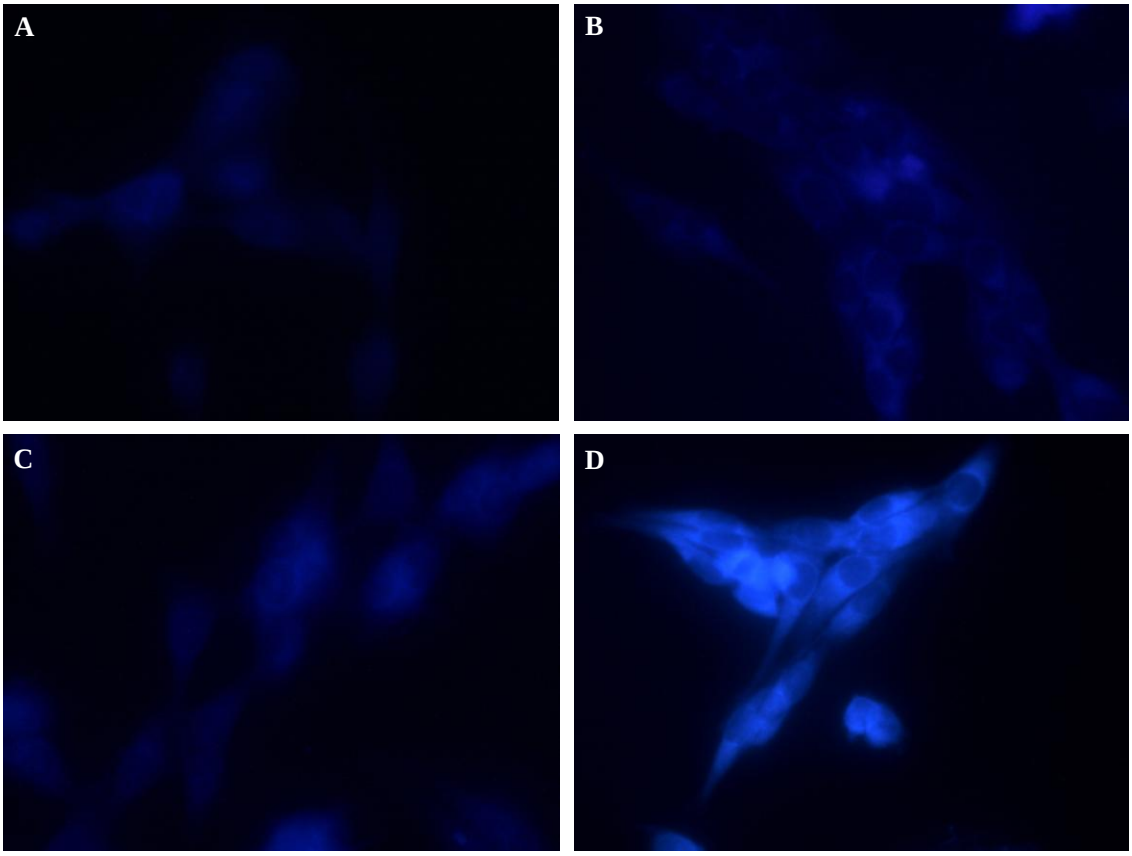

Figure 3.6. Selective uptake of RSI liposomal nanocarriers by 9L cells. Cells were incubated with either conventional, RSI peptide presenting, or control peptide presenting liposomes for 10 minutes and then fixed followed by epifluorescence microscopy using identical gain, exposure time, and target intensities. Cells were treated with (A) no liposomes (B) conventional liposomes (C) control peptide liposomes (D) RSI peptide presenting liposomes (500 peptides/liposome).

3.4.4 Presentation of RSI on liposomal nanocarriers does not diminish plasma half-life

With favorable *in vitro* targeting established for RSI liposomal nanocarriers, we next addressed whether peptide coated liposomal nanocarriers would show extended plasma half-life required for *in vivo* efficacy. Liposomal nanocarriers were formulated

with 1.5% DSPE-PEG2000 to provide Stealth characteristics. RSI peptides were post-inserted onto the liposomal nanocarriers via a longer lipid-PEG tether, as described earlier, in different numbers to examine the effect of increasing peptides/liposome on plasma clearance. The area under the curves (AUCs) were computed and compared for statistical significance. As shown in fig. 3.7, AUC of the liposomal nanocarriers with as many as 500 RSI peptides was statistically the same as the AUC of Stealth liposomal nanocarriers with no peptides. Increasing the number of RSI peptides/liposome greater than 800 accelerated plasma clearance and the AUC decreased by 40% in comparison to Stealth nanocarriers with no peptides.

In addition, the 500 RSI peptides/liposome formulation was compared to 3% Stealth liposomal nanocarriers with no peptides. The plasma clearance half life of 3% Stealth liposomal nanocarriers was statistically the same as that of 500 RSI peptides/liposome formulation (data not shown). These data rule out the effect of increasing PEG concentration on plasma clearance half life. PEG at 1.5% was chosen over 3% PEG to facilitate the post insertion process of lipid-PEG-peptide conjugate. The lipid dose administered (30mg/kg) for the pharmacokinetic study was kept significantly below the RES saturation dose of 280 mg/kg [32].

	0 RSI Liposomes	500RSI Liposomes	850RSI Liposomes
AUC	3142	2839	1916
$T_{1/2}$	25.43	23.32	10.2
$T_{1/2(fast)}$	0.940833	0.877	0.458152
$T_{1/2(slow)}$	75.83667	45.180	21.28333

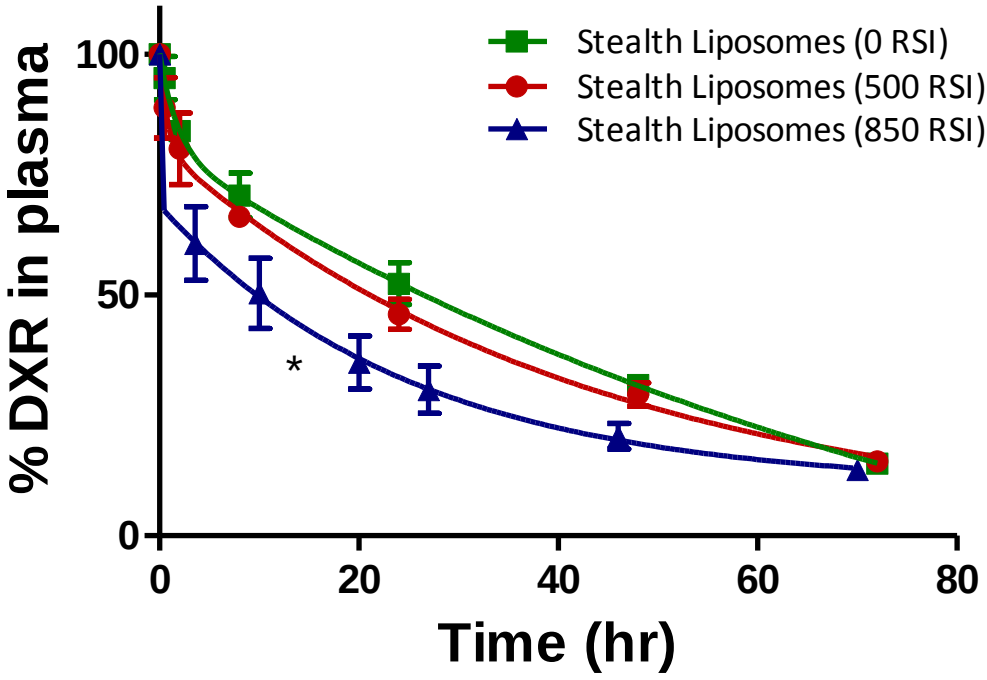

Figure 3.7. Plasma clearance profiles. Stealth liposomes (1.5% PEG2000) were compared to Stealth RSI peptide presenting liposomes. 4 animals each were injected via the tail vein with 10 mg/kg of DXR. Blood was collected through the orbital's sinus at 0.5, 2, 8, 24, 48, and 72 hours. Blood was collected at 3, 10, 20, 27, 46, and 70 hours for the case of 850 RSI peptide/liposome formulation. DXR concentrations in the blood were compared, plasma half lives, and the areas under the curves (AUCs) were evaluated. The AUCs of Stealth non-targeted versus Stealth 500 RSI peptide liposome formulations were not statistically different from each other. However, the clearance profile of the Stealth 850 RSI peptide liposomes were statistically different from the other two formulations ($p<0.05$). Data represents the mean ± SEM.

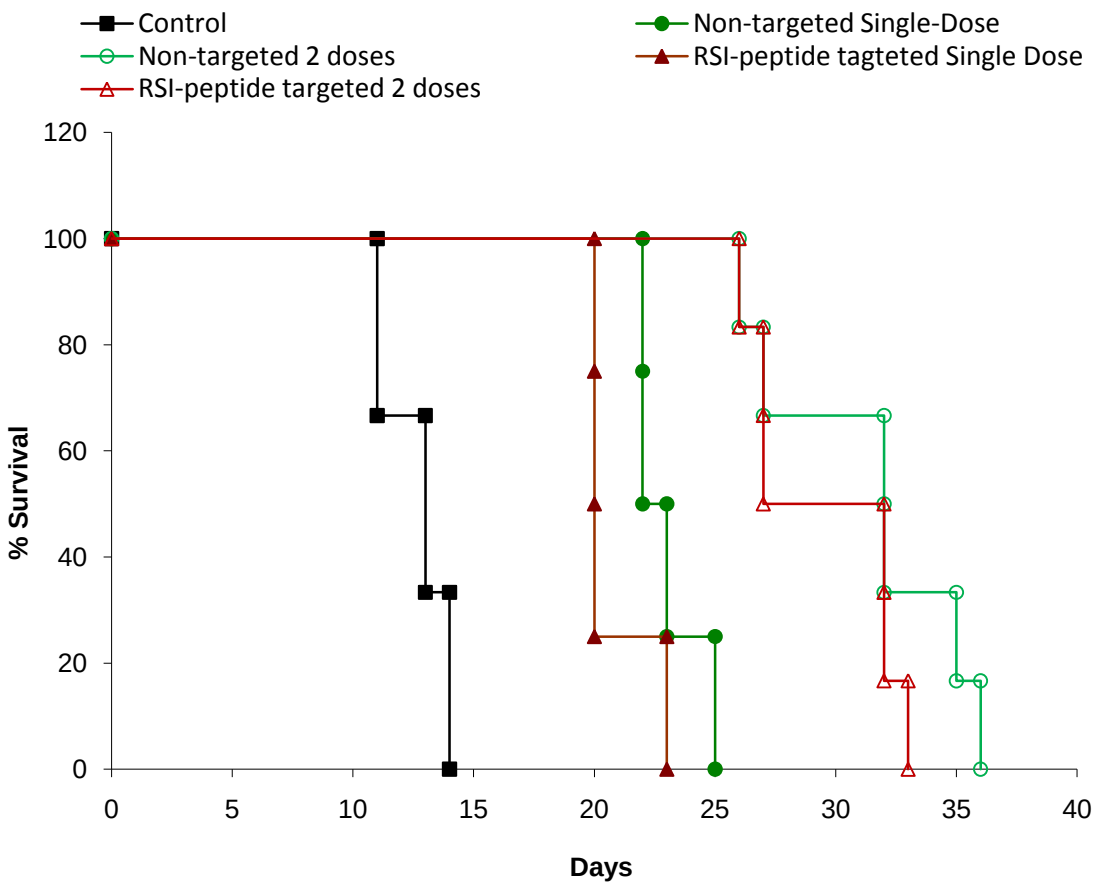

Figure 3.8. Use of RSI peptide to target liposomal DXR does not prolong survival of tumor-bearing rats. Animals received saline sham, non-targeted, or 500 RSI peptide-targeted liposomal DXR i.v. 4 days after tumor inoculation. A different set of animals received 2 doses at 4 days and 9 days after tumor inoculation. Both liposomal treatments were able to prolong survival of tumor-bearing rats compared to saline-treated controls. 2 doses were better at increasing survival than a single dose. However, there was no effect of RSI peptide on liposomes in prolonging survival when compared to non-targeted liposomes.

3.4.5 RSI peptide targeted liposomes did not improve survival

All animals received first treatment 4 days after tumor inoculation. As seen in fig 3.8 survival times of liposomal DXR treated animals were improved compared to saline-treated controls, however, there was no significant difference in survival between the groups receiving either non-targeted or 500 RSI peptide-targeted liposomal doxorubicin ($p<0.05$). To investigate the impact of multiple treatment administration on therapeutic efficacy, additional survival studies were conducted on tumor bearing rats receiving either non-targeted or 500 RSI peptide-targeted liposomal DXR. Animals received treatments 4 days after tumor inoculation, and a subsequent treatment 9 days after tumor inoculation. Survival was monitored, and the results of this study are exhibited in fig. 3.8. No improvement in survival resulted upon increasing the number of doses between animals receiving non-targeted liposomal DXR compared to those receiving 500 RSI peptide-targeted liposomal DXR. However, there was a significant increase in survival times of animals when comparing single treatment to animals receiving 2 treatments.

3.5 Discussion

The major shortcomings of the current generation of actively targeted nanocarriers are either lack of specificity or reduced efficacy due to ineffective tumor dosing stemming from decreased circulation time.

Recent studies have indicated successful targeting of liposomal nanocarriers to solid tumors by use of monoclonal antibodies and antibody fragments [33-34]. In these studies, the removal of the Fc portion of the IgG helped reduce antigenicity and increase efficacy [35]. However, the mass scale production and use of monoclonal antibodies and fragments is time and cost inefficient. Antibody therapy has been more beneficial in the

case of lymphoma or leukemia than solid tumors because of their enhanced accessibility to monoclonal antibodies [36]. In fact, one antibody or antibody fragment for targeted nanocarriers is insufficient in treating solid cancer which may be due to the incidence of multiple parallel or compensatory oncogenic pathways that allow tumor cells to escape and survive [37]. Therefore, use of combination of targeting ligands may help increase specificity to tumors and in turn, increase efficacy [27].

Phage panning of random peptide libraries features rapid screening of immense numbers of peptides to identify distinctive cell surface signatures without the benefit of prior information about such sites or knowledge about target cell biology. Unlike antibody technology, phage display offers the advantages of facilitating the identification of immunogenic as well as non-immunogenic structures, without bias as to which may be of therapeutic importance. Isolated phage clones bearing cell targeting peptides can be rapidly prepared for detailed analyses, including DNA sequencing to determine displayed peptide amino acid sequences. Peptides that target breast, prostate, and nasopharyngeal cancer have been identified as well by others [38-40]. Interestingly, a phage-derived small peptide was identified and used to guide an MRI contrast agent to image atherosclerotic plaques [41]. Thus, random-peptide phage display libraries represent a powerful combinatorial technology to help identify selective molecular targeting moieties.

One major problem associated with the use of targeting moieties on liposome surface is the loss of circulation time in the plasma. Folate targeted liposomal nanocarriers are a good example of ineffective targeting due to loss of plasma half-life [15-16]. In other studies, we have shown that folate targeted liposomes are cleared 3

times faster than Stealth liposomes from the blood circulation. Enhanced plasma clearance of folate targeted liposomes, in turn, decreases the passive accumulation at the tumor site. Passive accumulation, resulting from 'leaky' tumor vasculature, is directly proportional to the AUC for plasma drug clearance when operating below lipid RES saturation limits. The benefits of active targeting of liposomal nanocarriers can only be reaped by not compromising the passive accumulation component due to "leaky" vasculature [42-43] at the tumor sites. We have made the important observation here that the use of a small peptide as targeting moiety on liposomal nanocarriers at sizeable number per carrier does not compromise passive accumulation necessary to achieve increased drug efficacy by active targeting.

This study suggests that the use of peptides, identified through phage display, on the surface of liposomal nanocarriers can result in enhanced specificity and uptake of chemotherapeutics by tumors. The peptide (RSI) used here was rationally selected for maximal binding to 9L glioma cells and minimal binding to blood cells. Initial FACS analysis demonstrated relatively reduced binding of the RSI peptide to blood cells with more rigorous *in vivo* confirmation through plasma clearance studies that confirmed no compromised in plasma half life for RSI liposomal nanocarriers. In fact, the strength of our peptide selection techniques lies in our ability to screen peptides that minimally bind to blood cells, which can thus evade the RES *in vivo* and have high selectivity towards the desired cell type.

Liposomal nanocarriers are good candidates for their use as therapeutics nanocarriers *in vivo* for several reasons. They are easy to formulate and acquiescent to surface modification with targeting moieties. They can stably carry a variety of

therapeutics. Importantly, the presence of PEG chains provide for long circulation times in the blood. In the present study, PEG was used to sterically stabilize liposomal nanocarriers for *in vivo* application. However, as PEG promotes steric hindrance [44-45] for interaction of targeting moieties with the cell surface, the RSI peptide was conjugated to the end of a long spacer lipid-PEG molecule (DSPE-PEG3400-mal) that could be easily inserted into the liposome. DXR was the chosen as the preferred drug due to its fluorescent properties that enable both its detection intracellularly, and its ability to remotely load in the liposome [28, 46] with high efficiency >95% [47]. DXR is also non leaky due to the formation of stable precipitates inside the liposomal vesicle, and it is FDA approved for use in liposomal nanocarriers (DOXIL).

The RSI peptide liposomal nanocarriers were successful in delivering high payload (up to a six fold increase compared to the conventional non-targeted liposomes) of the drug DXR to the 9L cells, in a fashion that increased with higher number of peptides on the surface of the liposomal nanocarriers (fig. 3.4a). The number of peptides that could be tethered on the liposomal nanocarriers was limited as the method of post-insertion of lipid-peptide conjugates in numbers >1200 per liposome became highly inefficient. In addition, plasma half life was reduced when more than 500 peptides were used per nanocarrier. Nevertheless, as seen from the DXR uptake study, when 500 RSI peptides were presented on the liposomal nanocarriers, significantly increased cellular DXR levels were observed as compared to liposomal nanocarriers with no peptides. The requirement for the specific RSI peptide sequence is evident suggested by the significant reduction in DXR delivery when a scrambled version of the RSI peptide was used. Although, it can be argued that the effect of the scrambled peptide is larger than the non-

targeted liposomes. This effect can be attributed to the preservation of the phage sequence (GPPVESC) on the scrambled peptide. Therefore, one may conclude that the phage part of the peptide may have had a significant role in binding to the cells. In a competitive environment where RSI liposomes were presented to the cells in the presence of excess of free RSI peptides, RSI liposome-mediated DXR delivery was significantly reduced indicating increased uptake specifically due to the RSI peptide.

From the cytotoxicity experiments, it was observed 72 hours after treatment with DXR-RSI-liposomal nanocarriers that a large number of cells died. These data confirm that DXR payload was cellular uptake and not merely surface binding. DXR primarily kills cells by binding to topoisomerase II and disrupting the DNA base pairs during the cell cycle; therefore, it is important that DXR reaches the cell's interior. However, the mechanism by which RSI peptide facilitates cellular uptake is not known. The fluorescence micrograph images of 9L cells treated with DXR free liposomal nanocarriers presenting RSI peptide also confirm that the liposomal nanocarriers, indeed, reach the cytoplasm. 9L cells were also treated with free RSI peptide to rule out any cytotoxic effects of the peptide (data not shown). There were no differences found in the viability of the untreated cells and the cells treated with free RSI peptide. This result argues that cytotoxicity was medicated by DXR and RSI peptides.

In the survival studies, we failed to observe an improvement in survival of tumor bearing animals compared to non targeted formulations. We followed these animals with a second dose. There was overall improvement in survival due to multiple doses. However, the presence of the 9L tumor binding peptide (RSI) did not have any effect on

the survival of tumor bearing mice receiving liposomal doxorubicin. Such outcome could be attributed to a number of factors.

It is likely that the 9L tumor cells may have changed *in vivo* compared to their phenotype *in vitro*. Therefore, the binding of the RSI peptide to the tumors would be affected and the peptide presenting liposomes would be then similar to non-targeted liposomes in their outcome. *In vivo* environment is significantly different than what can be replicated *in vitro*. The RSI peptide could have been competed out by other peptides and proteins in the microenvironment of the tumor cells, in turn, leading to less liposomal uptake of the RSI targeted liposomes. In comparison to folate targeting liposomes that binds 9L cells about 18 times more than non-targeted liposomes, RSI-peptide presenting liposomes were about 3.5 times better than non-targeted liposomes *in vitro*. The gain seen *in vitro* may have been in significant *in vivo*, and several doses needed to be administered before a therapeutic difference could be registered. Alternatively, it is likely that once extravasated, the liposomes do not penetrate far into the tumor tissue. Liposomes are big particles and interstitial diffusion is limited. Presence of targeting moieties, therefore, may not be useful in solid tumors due to limited diffusion of liposomal particle.

3.6 Conclusions

One potential advantage of the approach employed here is in rapid identification of a specific peptide for a patient's tumor. The phage identified RSI peptide for 9L gliomas in this study is an example of a technique that can be extended to tumor lines of any kind. The rationale for using a rat glioma line was to enable us to test nanocarrier targeting in an immune-competent animal where the RES is capable of detecting and eliminating drugs from the body. The non-improvement in survival of tumor bearing

animals should not necessarily discredit the strength of the technique, reported here, in being able to personalize treatment for solid tumors.

Using the phage display technique, a variety of peptides could be identified at the same time for use as targeting moieties. This could lead to the development of a nanocarrier system with high avidity and selectivity for tumors without compromising tumor dosing due to decreased passive accumulation.

Acknowledgements

This work was supported through a translational research award from the Wallace H Coulter Foundation (RVB and DLJ), the National Science Foundation (RVB), the Georgia Cancer Coalition Distinguished Cancer Scholar award (RVB), the NIH (DK60647 and DK064399, DLJ), the Georgia Tech – Emory Fund for Innovative Cancer Technologies (DLJ and RVB), the Nora Redman Foundation (RVB), and the Graduate Assistance in Areas of National Need: Fellowship in Drug and Gene Therapy Development at Georgia Tech (P200A030077, AA). Prof. Ananth Annapragada (UT Houston), Efstathios Karathanasis, Kathleen McNeeley, and Chen-Yu Kao are acknowledged for valuable discussions. Ben Roller and Lynn Replogle are acknowledged for their help with the *in vitro* studies.

3.7 References

1. Finlay, J.L. and S. Zacharoulis, *The treatment of high grade gliomas and diffuse intrinsic pontine tumors of childhood and adolescence: a historical - and futuristic - perspective.* J Neurooncol, 2005. **75**(3): p. 253-66.

2. Siegel, M.J., J.L. Finlay, and S. Zacharoulis, *State of the art chemotherapeutic management of pediatric brain tumors.* Expert Rev Neurother, 2006. **6**(5): p. 765-79.

3. Chang, S.M., et al., *Standard treatment and experimental targeted drug therapy for recurrent glioblastoma multiforme.* Neurosurg Focus, 2006. **20**(4): p. E4.

4. Perry, A. and R.E. Schmidt, *Cancer therapy-associated CNS neuropathology: an update and review of the literature.* Acta Neuropathol (Berl), 2006. **111**(3): p. 197-212.

5. Papahadjopoulos, D., et al., *Sterically stabilized liposomes: improvements in pharmacokinetics and antitumor therapeutic efficacy.* Proc Natl Acad Sci U S A, 1991. **88**(24): p. 11460-4.

6. Zalipsky, S., et al., *Long circulating, cationic liposomes containing amino-PEG-phosphatidylethanolamine.* FEBS Lett, 1994. **353**(1): p. 71-4.

7. Sharma, U.S., et al., *Liposome-mediated therapy of intracranial brain tumors in a rat model.* Pharm Res, 1997. **14**(8): p. 992-8.

8. Duncan, R., *Polymer conjugates for tumour targeting and intracytoplasmic delivery. The EPR effect as a common gateway?* Pharm Sci Technolo Today, 1999. **11**(2): p. 441-449.

9. Maeda, H., et al., *Tumor vascular permeability and the EPR effect in macromolecular therapeutics: a review.* J Control Release, 2000. **65**(1-2): p. 271-284.

10. Maeda, H., *The enhanced permeability and retention (EPR) effect in tumor vasculature: the key role of tumor-selective macromolecular drug targeting.* Adv Enzyme Regul, 2001. **41**: p. 189-207.

11. Takeuchi, H., et al., *Passive targeting of doxorubicin with polymer coated liposomes in tumor bearing rats.* Biol Pharm Bull, 2001. **24**(7): p. 795-799.

12. Harasym, T.O., et al., *Poly(ethylene glycol)-modified phospholipids prevent aggregation during covalent conjugation of proteins to liposomes.* Bioconjug Chem, 1995. **6**(2): p. 187-94.

13. Saul, J.M., et al., *Controlled targeting of liposomal doxorubicin via the folate receptor in vitro.* J Control Release, 2003. **92**(1-2): p. 49-67.

14. Gabizon, A., et al., *In vivo fate of folate-targeted polyethylene-glycol liposomes in tumor-bearing mice.* Clin Cancer Res, 2003. **9**(17): p. 6551-9.

15. Gabizon, A.A., H. Shmeeda, and S. Zalipsky, *Pros and cons of the liposome platform in cancer drug targeting.* J Liposome Res, 2006. **16**(3): p. 175-83.

16. McNeeley, K.M., A. Annapragada, and R.V. Bellamkonda, *Decreased circulation time offsets increased efficacy of PEGylated nanocarriers targeting folate receptors of glioma.* Nanotechnology, 2007. ***In Press***.

17. Spear, M.A., et al., *Isolation, characterization, and recovery of small peptide phage display epitopes selected against viable malignant glioma cells.* Cancer Gene Ther, 2001. **8**(7): p. 506-11.

18. Samoylova, T.I., et al., *Phage probes for malignant glial cells.* Mol Cancer Ther, 2003. **2**(11): p. 1129-37.

19. Ho, I.A., P.Y. Lam, and K.M. Hui, *Identification and characterization of novel human glioma-specific peptides to potentiate tumor-specific gene delivery.* Hum Gene Ther, 2004. **15**(8): p. 719-32.

20. Schluesener, H.J. and T. Xianglin, *Selection of recombinant phages binding to pathological endothelial and tumor cells of rat glioblastoma by in-vivo display.* J Neurol Sci, 2004. **224**(1-2): p. 77-82.

21. Kolonin, M.G., et al., *Synchronous selection of homing peptides for multiple tissues by in vivo phage display.* Faseb J, 2006. **20**(7): p. 979-81.

22. Li, X.B., H.J. Schluesener, and S.Q. Xu, *Molecular addresses of tumors: selection by in vivo phage display.* Arch Immunol Ther Exp (Warsz), 2006. **54**(3): p. 177-81.

23. Mazzucchelli, L., et al., *Cell-specific peptide binding by human neutrophils.* Blood, 1999. **93**(5): p. 1738-48.

24. Jaye, D.L., et al., *Novel G protein-coupled responses in leukocytes elicited by a chemotactic bacteriophage displaying a cell type-selective binding peptide.* J Immunol, 2001. **166**(12): p. 7250-9.

25. Jaye, D.L., et al., *Use of real-time polymerase chain reaction to identify cell- and tissue-type-selective peptides by phage display.* Am J Pathol, 2003. **162**(5): p. 1419-29.

26. Jaye, D.L., et al., *Direct fluorochrome labeling of phage display library clones for studying binding specificities: applications in flow cytometry and fluorescence microscopy.* J Immunol Methods, 2004. **295**(1-2): p. 119-27.

27. Saul, J.M., A.V. Annapragada, and R.V. Bellamkonda, *A dual-ligand approach for enhancing targeting selectivity of therapeutic nanocarriers.* J Control Release, 2006. **114**(3): p. 277-87.

28. Bolotin, E.M., et al., *Ammonium sulfate gradients for efficient and stable remote loading of amphipathic weak bases into liposomes and ligandoliposomes.* J Liposome Res, 1994. **4**(1): p. 455-479.

29. Eavarone, D.A., X. Yu, and R.V. Bellamkonda, *Targeted drug delivery to C6 glioma by transferrin-coupled liposomes.* J Biomed Mater Res, 2000. **51**(1): p. 10-4.

30. Charrois, G.J. and T.M. Allen, *Drug release rate influences the pharmacokinetics, biodistribution, therapeutic activity, and toxicity of pegylated liposomal doxorubicin formulations in murine breast cancer.* Biochim Biophys Acta, 2004. **1663**(1-2): p. 167-77.

31. Nomura, K., et al., *Perturbed cell kinetics of 9L rat brain tumor cells following dianhydrogalactitol.* Cancer Treat Rep, 1978. **62**(12): p. 2055-61.

32. Allen, T.M. and C. Hansen, *Pharmacokinetics of stealth versus conventional liposomes: effect of dose.* Biochim Biophys Acta, 1991. **1068**(2): p. 133-41.

33. Park, J.W., et al., *Anti-HER2 immunoliposomes for targeted therapy of human tumors.* Cancer Lett, 1997. **118**(2): p. 153-60.

34. Gupta, B. and V.P. Torchilin, *Monoclonal antibody 2C5-modified doxorubicin-loaded liposomes with significantly enhanced therapeutic activity against intracranial human brain U-87 MG tumor xenografts in nude mice.* Cancer Immunol Immunother, 2007.

35. Siwak, D.R., A.M. Tari, and G. Lopez-Berestein, *The potential of drug-carrying immunoliposomes as anticancer agents. Commentary re: J. W. Park et al., Anti-HER2 immunoliposomes: enhanced efficacy due to targeted delivery. Clin. Cancer Res., 8: 1172-1181, 2002.* Clin Cancer Res, 2002. **8**(4): p. 955-6.

36. Holliger, P. and P.J. Hudson, *Engineered antibody fragments and the rise of single domains.* Nat Biotechnol, 2005. **23**(9): p. 1126-36.

37. Sathornsumetee, S. and J.N. Rich, *New approaches to primary brain tumor treatment.* Anticancer Drugs, 2006. **17**(9): p. 1003-16.

38. Arap, W., R. Pasqualini, and E. Ruoslahti, *Cancer treatment by targeted drug delivery to tumor vasculature in a mouse model.* Science, 1998. **279**(5349): p. 377-80.

39. Landon, L.A. and S.L. Deutscher, *Combinatorial discovery of tumor targeting peptides using phage display.* J Cell Biochem, 2003. **90**(3): p. 509-17.

40. Lee, T.Y., et al., *A novel peptide specifically binding to nasopharyngeal carcinoma for targeted drug delivery.* Cancer Res, 2004. **64**(21): p. 8002-8.

41. Nahrendorf, M., et al., *Noninvasive vascular cell adhesion molecule-1 imaging identifies inflammatory activation of cells in atherosclerosis.* Circulation, 2006. **114**(14): p. 1504-11.

42. Jain, R.K., *Tumor angiogenesis and accessibility: role of vascular endothelial growth factor.* Semin Oncol, 2002. **29**(6 Suppl 16): p. 3-9.

43. Gabizon, A. and F. Martin, *Polyethylene glycol-coated (pegylated) liposomal doxorubicin. Rationale for use in solid tumours.* Drugs, 1997. **54 Suppl 4**: p. 15-21.

44. Harris, J.M., N.E. Martin, and M. Modi, *Pegylation: a novel process for modifying pharmacokinetics.* Clin Pharmacokinet, 2001. **40**(7): p. 539-51.

45. Eto, Y., et al., *PEGylated adenovirus vectors containing RGD peptides on the tip of PEG show high transduction efficiency and antibody evasion ability.* J Gene Med, 2005. **7**(5): p. 604-12.

46. Haran, G., et al., *Transmembrane ammonium sulfate gradients in liposomes produce efficient and stable entrapment of amphipathic weak bases.* Biochim Biophys Acta, 1993. **1151**(2): p. 201-15.

47. Fritze, A., et al., *Remote loading of doxorubicin into liposomes driven by a transmembrane phosphate gradient.* Biochim Biophys Acta, 2006. **1758**(10): p. 1633-40.

CHAPTER 4

SYNERGISTIC APPLICATION OF GOLD NANORODS AND THERMALLY SENSITIVE LIPOSOMES FOR SOLID TUMORS

4.1 Introduction

Nanocarriers have become popular in delivering therapeutics primarily due to their ability to shield the drug and prevent unwanted tissue exposure. Nanochemotherapy benefits from effectively evading the reticulo-endothelial system (RES) and delivering high payloads of the drug at the tumor site compared to healthy tissue [1-2]. Liposomes are long circulating [3] and are the only nanochemotherapeutics approved for clinical use by FDA. Their long circulation enables increased passive accumulation in the tumor due to enhanced permeation and retention effect. However, once extravasated, nanocarriers accumulate close to the blood vessels and further tissue diffusion is limited [4]. In addition, the release of the drug from these nanocarriers, once extravasated, is very slow [5]. Since their discovery, much research has been conducted to improve liposomal nanocarrier delivery for higher drug payloads by incorporating targeting ligands or triggering content release at the specific site. Targeted systems require tumor specific ligand identification. In addition, such liposomes, after extravasation, are trapped by the cells close to the endothelium and suffer deeper tissue penetration [6]. Several triggered release systems have been fabricated including triggers like pH, light, enzymes, and heat. However, the stability of such systems in the blood circulation remains a challenge [7]. In

turn, the intrinsic characteristics of liposomal nanocarriers for protecting the drug and reducing systemic toxicity are lost.

Much effort has been made to optimize the composition of triggerable nanoparticle systems without much success. Thermosensitive liposomes have been investigated for controlled drug delivery [8]. However, the traditional methods used to trigger the release of the drug from the liposomes lead to exposure of healthy tissue to chemotherapeutics. In addition, these methods also expose healthy tissue to hyperthermic temperatures and can only be used effectively for peripherally located tumors. Development of a remote triggering mechanism can help control the release of the drug from the liposomes. Recently, there has been advancement in the field of photothermal hyperthermia mediated by laser light, particularly near infrared (NIR). To this effect, noble metal nanoparticles are very useful for photothermal therapy due to their enhanced absorption and non-bleaching characteristic. Plasmonic nanoparticles exhibit strong absorption in visible as well as NIR due to surface plasmon resonance oscillations [9-12]. Gold nanorods (GNRs) are particularly attractive as they can be tuned to absorb in the NIR region that enables their use in biological tissue. NIR light has been reported to have a penetration depth of up to 10 cm [13]. As described earlier, GNRs can accumulate specifically in tumor tissue due to EPR effect [14]. Use of GNRs, therefore, enables noninvasive and spatially controlled heating of desired tissue. By optimizing the shape and amount of the GNRs administered and the power of the laser, one can achieve precise and controlled temperature increase.

In this study, we explored the possibility of formulating a relatively plasma stable thermosensitive liposomal formulation to reduce systemic toxicity. We employed GNRs

to noninvasively and spatially trigger the release of the chemotherapeutic drug from the thermosensitive liposomes after their passive accumulation in the tumor. In doing so, we were able to achieve control over drug release at the desired site. The synergistic application of GNRs with thermosensitive liposomes led to increased therapeutic efficacy.

4.2 Materials and Methods

4.2.1 Materials

1,2-distearoyl-*sn*-glycerophospho-choline (DSPC), 1,2-dimyristoyl-sn-glycero-3-phosphocholine (DMPC) and 1,2-distearoyl-*sn*-glycerophosphoethanolamine poly(ethylene glycol)$_{2000}$ (DSPE-PEG2000) were purchased from Genzyme Pharmaceuticals (Cambridge, MA). Cholesterol, paraformaldehyde, and Triton X-100 were purchased from Sigma (St. Louis, MO). Dialysis tubing (10,000 and 100,000 molecular weight cut-off) was purchased from Spectra/Por (Dominguez, CA). U87-MG human glioma cell line was purchased from American Type Culture Collection (Manassas, VA). DMEM and trypsin-EDTA (0.05% trypsin, 0.53 mM EDTA) in Hanks' balanced salt solution was purchased from Mediatech (Manassas, VA). Doxorubicin (DXR) was purchased from Bedford Labratories (Bedford, OH). Cell Counting Kit-8 (CCK-8) was obtained from Dojindo (Kumamoto, Japan). Nu/nu mice were purchased from Charles River Laboratories International, Inc. (Wilmington, MA).

4.2.2 Cell Culture

U-87 MG were acquired from ATCC and maintained as per ATCC recommendation.

4.2.3 Liposome Preparation

Liposomal nanocarriers were formed as described earlier [15-16]. Briefly, x: 97-x:3 DPPC/DSPC/PEG or a ratio of 57-x:40-x:3 of DPPC:Cholesterol:DSPE-PEG2000 or 57:3:30:3 DPPC:DMPC:Cholesterol:DSPE-PEG2000 was used to identify a thermosensitive formulation. A non-thermosensitive stealth liposomal formulation of DPPC:Cholesterol:DSPE-PEG2000 in the ratio 57:40:3 respectively (NTSL) was used as control in all in vivo studies. The lipid mixture was dissolved in 1ml of ethanol at 60^{o}C. Liposome size was determined by dynamic light scattering (Particle Size Analyzer, Brookhaven Instruments, Holtsville, NY). Liposomal nanocarriers were dialyzed against a phosphate-buffered saline solution to establish an ammonium sulfate gradient for DXR loading.

4.2.4 Active Loading of Doxorubicin

Following ligand incorporation, liposomal nanocarriers were loaded with DXR via the ammonium sulfate gradient as described before [17]. Briefly, liposomal nanocarriers and 5 mg/ml DXR solution in 0.9% saline were mixed at a ratio of 0.1 mg DXR per 1 mg of phospholipid in the liposomal nanocarriers. The liposome/DXR suspension was heated at 45 °C for 30 minutes. The liposomal nanocarriers were then cooled immediately on ice and dialyzed in 100 000 MWCO membrane against PBS to remove un-encapsulated DXR. The formulations were sterilized by passing through a 0.2 μm filter. The final DXR concentration after dialysis was determined by lyses of the liposomal nanocarriers with 5% Triton X-100 and measurement of absorbance at 480 nm.

4.2.5 Liposomal Leak Studies

Liposomal DXR was diluted to a final concentration of 1 µg/ml in 50% FBS solution and heated in circulating water bath at 37°C for 24 hours. The samples were placed in water bath at 43°C for 10 minutes in order to quantify drug release and then transferred back to the water bath at 37°C. 24 hours later all samples were analyzed for the amount of drug released. 100% release was the intensity after the addition of detergent Triton X-100, while 0% (no release) was the intensity measured for 50% FBS solution [18]. DXR intensity was measured at 485/590 excitation and emission wavelength in a spectrophotometer.

$$\%\text{release} = \frac{(\text{Sample Intensity})_{\text{T}} - (\text{Sample Intensity})_{25^{\circ}\text{C}}}{(\text{Max Intensity})_{\text{lysed}} - (\text{Sample Intensity})_{25^{\circ}\text{C}}}$$

where T = time

4.2.6 In vitro Cell Cytotoxicity Studies

U87-MG glioma cells were seeded at a density of $2x10^4$ cells per well of a 24-well plate and incubated for 48 hours prior to incubation with liposomal nanocarriers. 48 hours later, liposomal formulations were mixed with cell media to a different doxorubicin concentration and added immediately to cells.

Cells were incubated with free DXR or liposomal DXR for 20 minutes at 37^{o}C or 43^{o}C and 5% CO_2 in a humidified environment. All wells were then incubated at 37^{o}C for additional 4 hours. Cells were then washed three times with fresh medium and re-incubated for 72 hours. The numbers of viable cells were determined with a water soluble formazan-based assay (CCK-8).

4.2.7 In vivo Therapeutic Studies

All animal studies were conducted under a protocol approved by the Institutional Animal Care and Use Committee (IACUC) at Georgia Institute of Technology. For the tumor model, the U87-MG human glioma cell line was used. A 100 µL aliquot containing $2x10^6$ cells was subcutaneously injected using a 26-gauge needle into the right shoulder of 6-8 weeks old female nude mice. Caliper measurements were used to estimate tumor size and the tumor volume was calculated as:

$$V_{tumor} = \frac{a \times b^2}{2}$$

where a and b are the maximum and minimum diameters respectively [19-20]

When tumors were about ~45-75 mm^3, animals were treated with a saline sham, TSL, NTSL liposomal DXR i.v. injections (10, 5, and 2.5 mg/kg doxorubicin) via tail vein with or without GNRs. Equivalent volumes of 0.9% sterile saline solution were administered to animals receiving sham injections. Tumor growth was allowed to progress until the tumors were 1.5 cm or showed signs of ulceration, at which point, interventional euthanasia was administered. Time of death was determined to be the day of euthanasia.

4.2.8 In vivo Apoptotic Imaging

All animals used for in vivo fluorescence imaging were fed Teklad 2916 chlorophyll free diet for 10 days prior to imaging to reduce autofluorescence [21]. Tumor bearing mice, received 100 µl of Annexin-Vivo 72 hours after treatment administration. All animals were imaged using IVIS Lumina (Caliper Life Sciences, Hopkinton, MA). Images were acquired using the appropriate filter set at 2, 4, and 48 hours after administering the imaging agent.

For analysis, images were loaded together to normalize all images to one color scale. A region of interest (ROI) around the tumor was drawn and the fluorescence intensity was quantified for each time point. For comparison between groups, each animal's tumor volume was used to normalize the fluorescence intensity per cubic millimeter of the tissue. Values obtained were then averaged for the respective group for statistical analysis.

4.2.9 Statistical Analysis

Means were determined for each variable in this study and the resulting values from each experiment were subjected to an analysis of variance (ANOVA) with Tukey post-hoc pairwise comparisons. Significance was determined using a 95% confidence level.

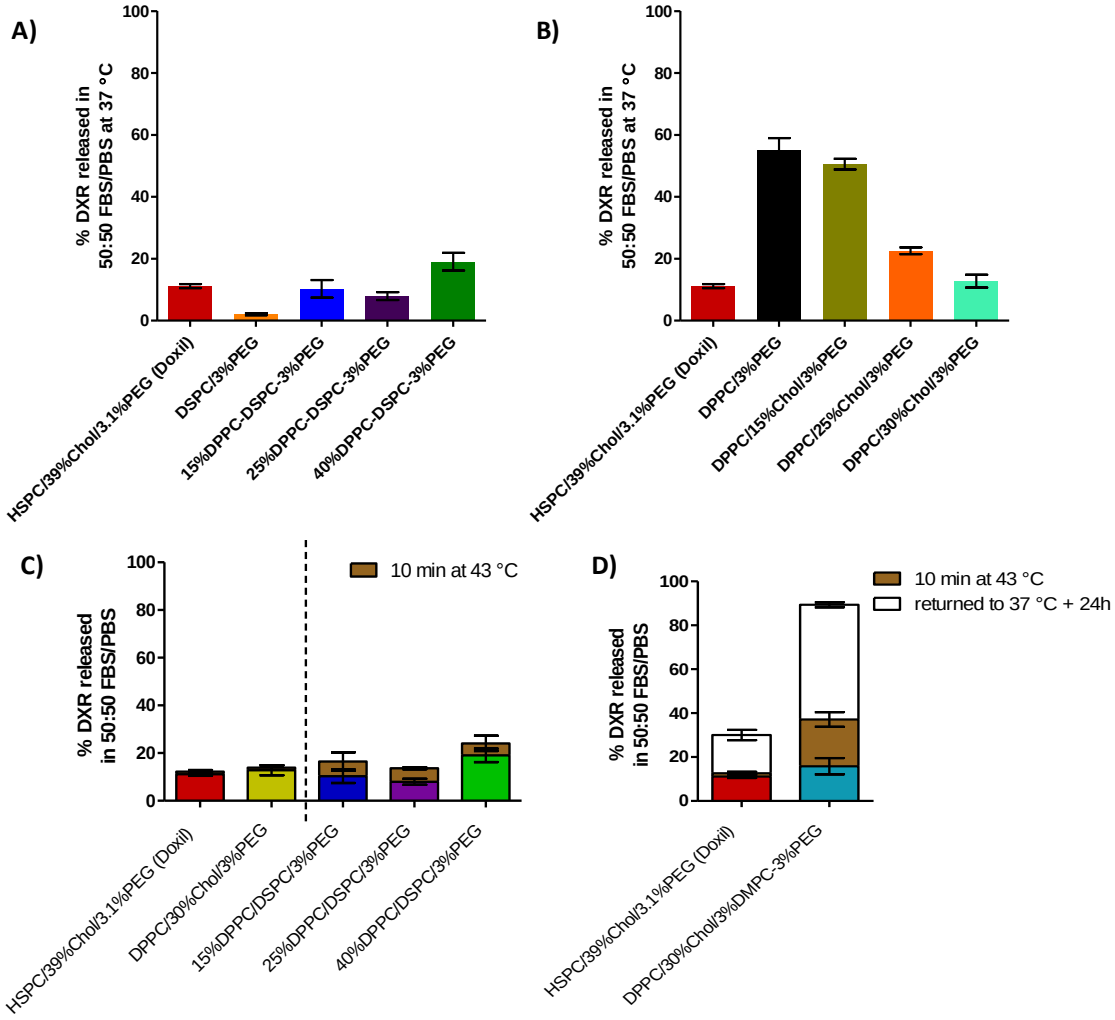

Figure 4.1. Release of DXR from liposomes. A) Liposomes with varying combinations of DSPC/DPPC and without cholesterol were formulated and and amount of DXR released after 24 hours at 37 °C was quantified. B) Liposomes with varying cholesterol content were formulated and amount of DXR released after 24 hours at 37 °C was quantified. C) Liposomes comparable in stability to Doxil were selected from B) and C). After 24 hours at 37 °C, liposomes were transferred to higher temperature of 43 °C and DXR release was quantified indicated by brown bars (■) and almost all formulations failed to show a burst release. D) Small amount of DMPC was added to DPPC liposomes in order to achieve thermosensitivity. DPPC/30%Chol/3%DMPC/3%PEG showed comparable stability after a 24 hour period at 37 °C to Doxil and was able to show significant amount of DXR release upon heating. After heating at 43 °C, liposomal formulations were transferred back to 37 °C water bath and their release was quantified after another 24 hours indicated by white bars (□). Doxil still carried DXR very stably. In contrast, DPPC/30%Chol/3%DMPC/3%PEG (TSL) formulation lost most of the drug.

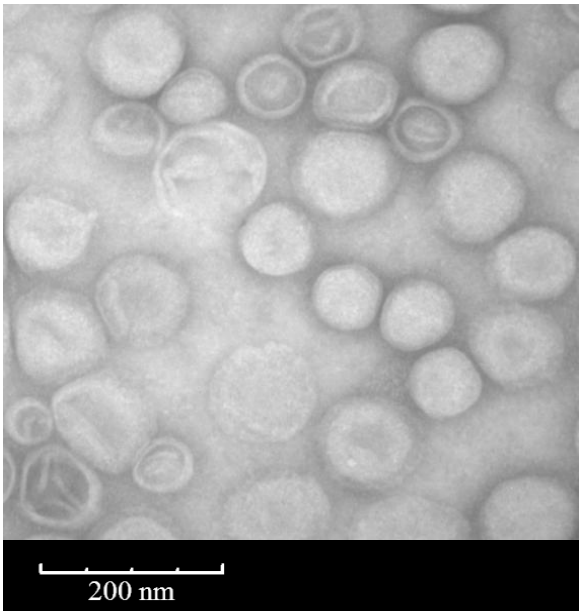

Figure 4.2. TEM image of negatively stained TSLs. Scale bars are 200 nm.

4.3 Results and Discussion

4.3.1 Controlled Release of Chemotherapeutic Drug from Liposomes

Thermosensitive liposomes reported in the literature suffer from excessive drug loss from the nanocarriers at physiological temperature in contrast to FDA approved Doxil composed of HSPC/39%Chol/3.1%PEG. Loss of drug at physiological temperature compromises passive drug accumulation in the tumor and increases systemic cytotoxicity. Several liposomal formulations were fabricated and tested for drug encapsulation stability at physiological temperature and release at 4-5 ˚C elevated temperature. Liposomes were diluted at 1 µg/ml in 50:50 mixtures of FBS/PBS [18]. Liposome aliquots were heated at various temperatures and times and the fluorescence of doxorubicin released from the liposomes was quantified to assess % drug released. It was found that DPPC liposomes, devoid of any cholesterol, rendered the liposomes highly

unstable and liposomes did not carry the drug stably over extended periods of time at physiological temperatures (Fig 4.1B). In 24 hours, DPPC liposomes lost more than 50% of the encapsulated DXR. DSPC liposomes, on the other hand, do not release any DXR at 37 ˚C, which could be attributed to the fact that they have very high transition temperature of 55 ˚C preventing leakiness. Addition of varying amounts of DPPC to DSPC liposome did not affect their stability, but DXR was also not released from these formulations upon heating at 43 ˚C (fig. 4.1C). These results are in contrast to earlier reports where calcein was reported to be released from such liposomes at a temperature of 37-45 ˚C [22]. The differences can be attributed to the fact that calcein that is passively loaded is easier to release upon heating. However, a remotely loaded drug like DXR is more difficult to release. DXR, upon remote loading is trapped inside the liposomes as precipitates of the sulfate. The slight increase in release of DXR upon heating to 43 ˚C, in the case of DPPC/DSPC liposomes, could be due to increase in DXR solubility in comparison to its solubility at 37 ˚C. Increase in DXR solubility may enable its outward movement recorded as released DXR. Therefore, it can be concluded that every thermosensitive formulation needs to be optimized for the chemotherapeutic drug of choice. DPPC liposomes were also fabricated by inclusion of varying amounts of cholesterol (fig 4.1B). It was found that 30% cholesterol in DPPC liposomes results in very small loss of DXR over a 24 hour period at 37 ˚C. However, these liposomes, also, do not exhibit any thermosensitivity at 43 ˚C, which is higher than DPPC phase transition. Cholesterol, therefore, has a stabilizing effect on DPPC membrane as shown here and in earlier reports [23]. As shown in fig 4.1C, it was found that inclusion of 30% cholesterol and small amounts (3%) of very low transition temperature (23 °C) lipid

DMPC resulted in a liposome (DPPC/30%Chol/3%DMPC/3%PEG, TSL) that would carry its content stably at physiological temperature and released DXR at 43 ˚C when heated for 10 minutes. Reduction of cholesterol to 25% in these liposomes reduced their stability at 37 ˚C. It was also seen that after heating for 10 minutes and placing TSLs back in 37 ˚C for another 24 hours resulted in complete loss of DXR from these liposomes (fig 4.1D). Such a characteristic could be very useful in causing the liposomes to lose their contents quickly after reaching the tumor instead over a period of time. TSLs were also heated for 10 minutes at various temperatures from 37 °C to 45 °C to determine the maximum release temperature. For all further release studies, TSLs were heated at 43 °C. Fast release of the chemotherapeutic can result in better bioavailability of the drug and higher apoptosis rate as is explained later in this report. For further therapeutic studies, DPPC/30%Chol/3%DMPC/3%PEG was chosen as the thermosensitive liposomal formulation for its better stability over other formulations and ability to release drug at elevated temperatures.

4.3.2 In vitro Cytotoxicity Studies

Cytotoxicity of TSL formulation was determined by evaluating cell viability to ensure that the extent of DXR release at 43 ˚C was cytotoxic in comparison to NTSL (fig. 4.3). Untreated cells remained unaffected by temperature change with the viability of cells being at 100%. Cells exposed to empty liposomes (NTSLs or TSLs) also did not show change in viability at either temperature. Cell viability, also, remained unaffected upon treatments with NTSLs, did not depict any significant change due to change in temperature and exhibited approximately 70-90% viability under all conditions (fig. 4.3). TSLs, however, demonstrated a significant increase in cytotoxicity over NTSLs at 43 ˚C

($p < 0.001$) at all DXR concentrations confirming the release of DXR from TSLs, and thereby, the cytotoxic effect at higher temperature. Free DXR depicted an LC_{50} at 10 µg/ml DXR concentration. TSLs did not show an increase in cytotoxicity at 37 ˚C and the results were comparable to cells treated with NTSLs. However, at 43 ˚C TSLs depicted an LC_{50} between 30 and 60 µg/ml.

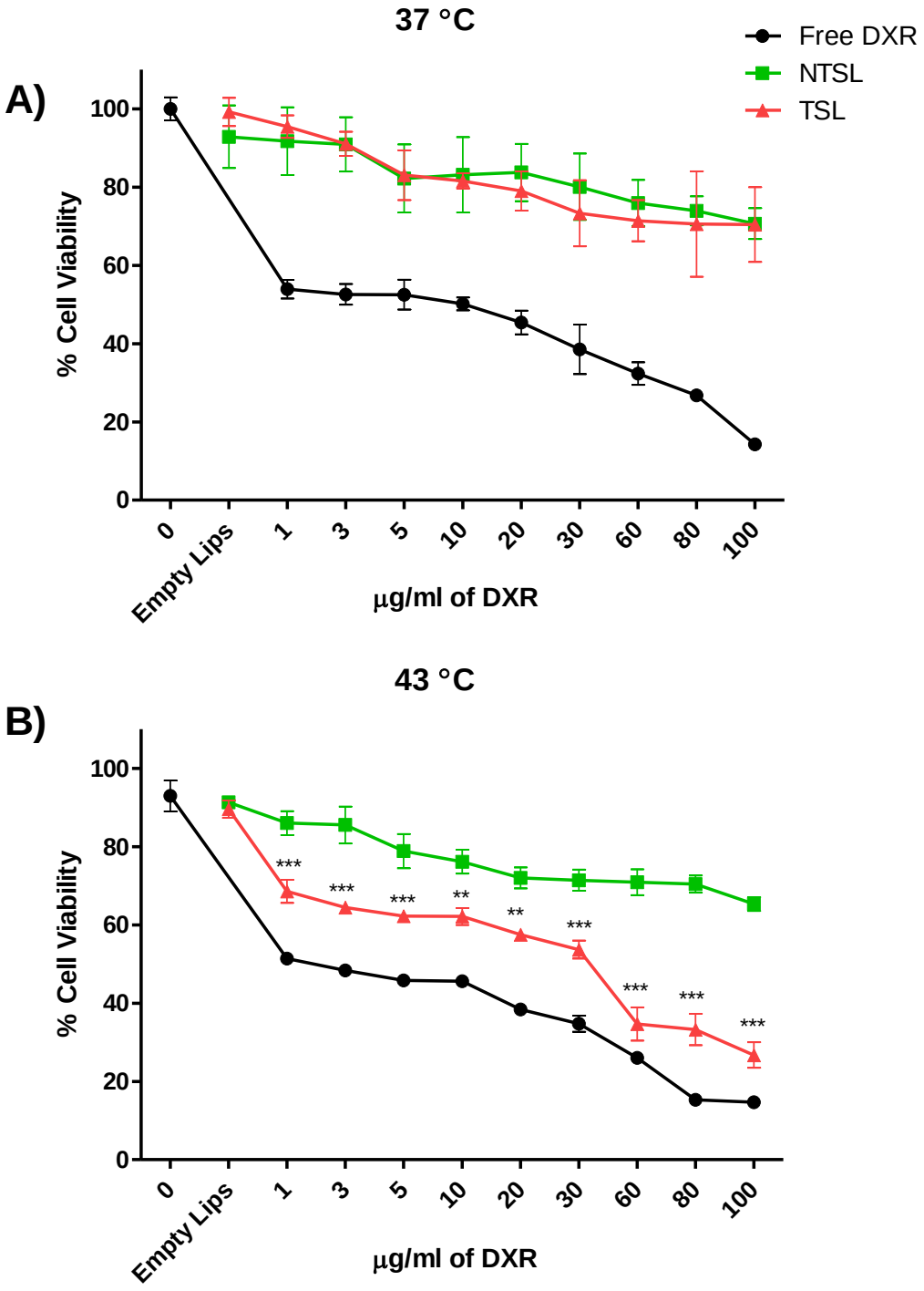

Figure 4.3. In vitro heat mediated cell cytotoxicity of liposomal formulation. Cells were treated with free DXR, non thermosensitive liposomes (NTSL), or thermosensitive liposomes (TSL) with varying DXR concentrations at A) 37 ˚C or B) 43 ˚C. Cell cytotoxicity was measured by modified MTT assay (CCK8). Cells treated with TSL showed significant increase in cytotoxicity at 43 ˚C in comparison to NTSL (p < 0.01, or ***p < 0.001) at all DXR concentrations. TSL were significantly cytotoxic at 43 ˚C in comparison to at 37 ˚C (p < 0.001). Data represented is mean ± S.D.**

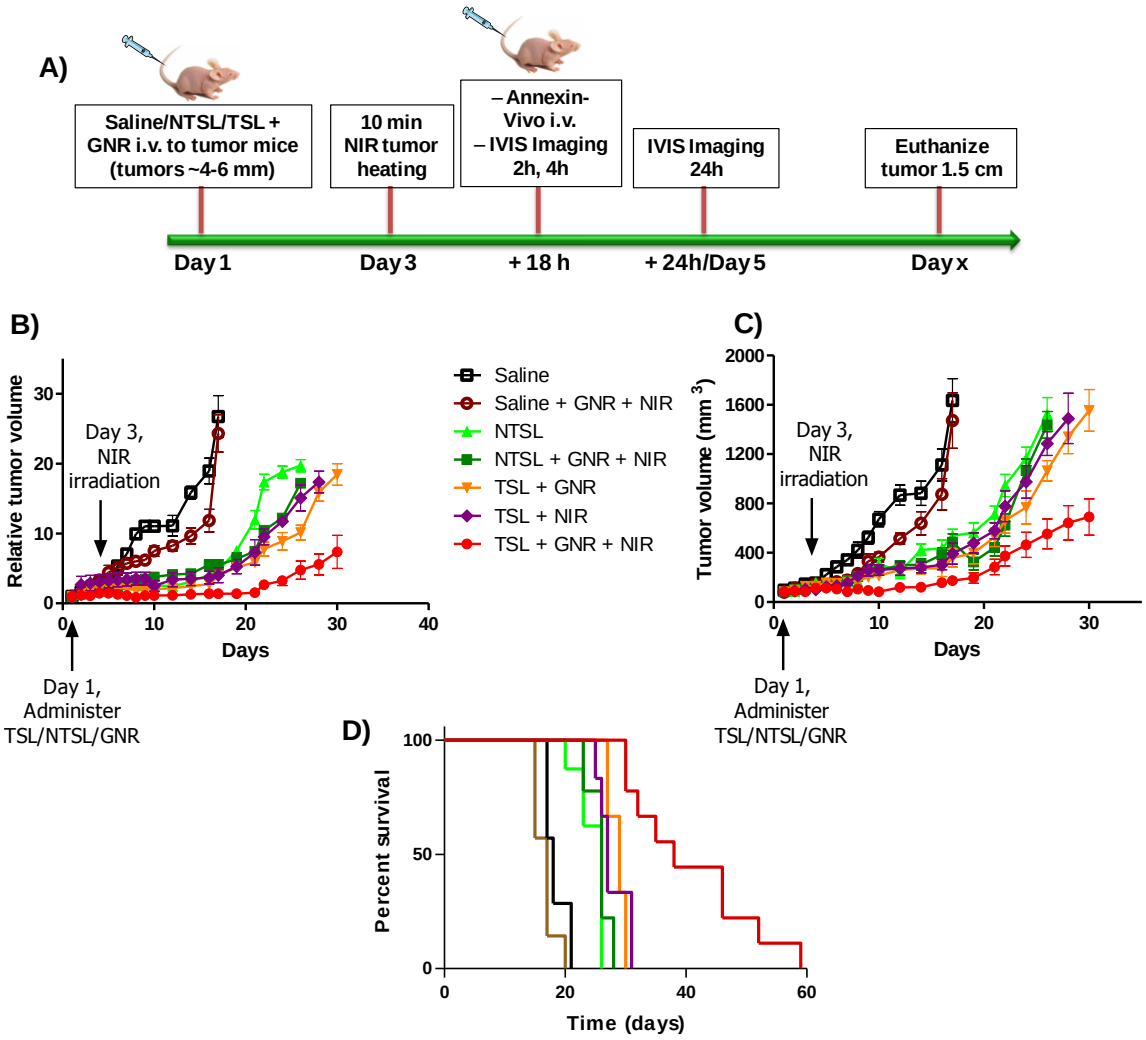

Figure 4.4. Therapeutic efficacy. Nude mice were injected with $2x10^6$ U87-MG. A) Schematic of treatment administration and in vivo imaging. B) Relative tumor volume after treatment administration in different groups (n = ~6-9) was measured everyday for the first 10 days and every other day after day 10. Mice received either liposomal DXR (2.5 mg/kg) or saline in combination with GNRs at 5 pmol/kg of rods. 48 hours later, mice received NIR irradiation with a laser (808 nm, 0.5 W/cm^2) for 10 minutes. TSL + GNR + NIR were significantly different from the saline groups (day 6-17, p <0.001). Animals that were treated with TSL + GNR + NIR were significantly different from all other liposomal treatment groups (day 19-26, p < 0.001). Data represented is mean ± S.E.M. C) Absolute tumor volumes for various treatments. Data represented is mean ± S.E.M. D) Percent survival for different treatments groups (n = ~6-9). Mantel-Cox analysis indicated that TSL + GNR + TSL was significantly different from all other groups (p <0.0001).

4.3.3 In vivo Drug Studies

Further, to assess the cytotoxic effect and therapeutic efficacy of the TSL triggered via GNRs in NIR, we used a xenograft mouse model of human glioma U87-MG. In this study, we co-injected the liposomal drug and GNRs and waited for 48 hours to heat the tumors. In doing so, we wanted to assess the capability of the GNRs in disrupting the liposomes in vivo, as well as, compare the effect of burst release of the drug from the nanaocarriers to drug being released from non-disruptable nanocarriers for long periods of time after passive accumulation. Animals received liposomal DXR or saline +/- GNR (fig. 4.3A) when the tumor size was ~4-6 mm. The average temperature recorded using a thermo-probe in all animal tumors heated via GNRs was 43 ± 1˚C. All animal tumors that did not receive GNRs but were irradiated with NIR recorded an average of 39 ± 1˚C. The basal temperature of tumors before NIR irradiation was 34-35˚C primarily due to loss of heat as animals were anesthetized for NIR irradiation.

We found that GNR mediated heating of TSL was highly effective in suppressing tumor progression. As seen in fig. 4.3B, animals that received TSL + GNR + NIR did not show increase in the size of tumors up till day 21. All saline treated animals, in contrast, showed exponential increase in tumor size. All other liposomal treatments with or without GNR/NIR were also able to suppress tumors on an average till day 17. There was a significant difference in the ability to suppress tumors overall between TSL + GNR + NIR treatment and all other treatments ($p < 0.001$). In addition, TSL + GNR + NIR treatment was successful in extending overall survival (median survival = 38 days, fig 4.3C). In contrast, saline treated animals +/- GNR mediated heating did not show such pronounced effects with median survival of 17 days. Animals that received either NTSL

+/- GNR mediated heating or TSL +/- NIR, were also, less successful in prolonging survival in comparison to TSL + GNR + NIR treatment. All animals receiving liposomal DXR at 2.5 mg/kg showed significant tumor suppression in comparison to saline treated animals with or without GNRs mediated heating. In our studies, we tested 10 mg/kg and 5 mg/kg DXR doses as well; however, animals did not tolerate these doses very well and were not further investigated.

Increased animal survival indicates that GNR mediated heating results in increased bioavailability of DXR trapped in TSLs. The incapability of NTSL heated via GNRs in reducing tumor progression shows that the drug is not able to escape the nanocarrier. Therefore, the cytotoxic effects of the drug are also suppressed. It can be concluded that GNRs can be effectively used to remotely and locally trigger the release of the drug from nanocarriers, thereby, promoting drug distribution and bioavailability.

To demonstrate the immediate effect of drug release from the nanocarriers on cell viability in vivo, we used Annexin-Vivo 750. Annexin injected 18 hours after NIR irradiation was able to bind to apoptotic cells and reveal information about immediate cell death induced by drug release.

4.3.4 Apoptosis Imaging

In vivo fluorescence imaging provides inexpensive and rapid assessment of real-time biological processes [24-25] in contrast to MRI or histological techniques. To assess the short term effect of various drug treatments, we measured and quantified the extent of apoptosis at the tumor site using an in vivo fluorescence modality. Apoptotic agent Annexin-Vivo (excited at: 740, and emission collected at: 780 nm) was administered 18 hours after the tumors were heated via NIR (see fig 4.3A). Imaging conducted at 2, 4 and

24 hours post annexin administration, fluorescent signal was quantified for each animal, and normalized by their respective tumor volume determined via calipers to obtain a per cell apoptosis intensity. A signal enhancement was found at all time points for animal tumors that received TSLs and were heated via GNRs using NIR. Tables 4.1 and 4.2 show the average increase in signal quantified per millimeter cube and the related statistics respectively. Enhancement in signal intensity can be attributed to increase in annexin binding at the tumor site. At 24 hours, when all treatment groups showed reduction in annexin intensity, in comparison, TSL + GNR + NIR group showed the maximum fluorescent signal per cubic millimeter indicating retention of annexin at the tumor after clearance of annexin from the blood pool (fig 4.6A and fig 4.5). Annexin clearance could be easily detected through the kidneys as the fluorescence recorded in this area was much higher than the tumor. As a result, the CCD was flooded with photons from the kidney area and could not detect differences in the tumor apoptosis in uncovered animals. Therefore, animals had to be covered with a black paper to cover the kidneys and reveal the differences in the annexin accumulation in the tumors.

Apoptosis imaging can be used as a powerful tool to assess the success of a treatment in suppressing the tumor. When comparing the survival of the animals to the fluorescent intensity obtained at 24 h, we find that the fluorescence intensity is somewhat indicative of the length of survival (fig 4.6B). The graph is segmented into two distinct areas with animals surviving less than 30 days showing lower signal intensity and animals above 30 day showing much higher signal intensity. The correlation is somewhat independent of the type of treatment. All saline animals, although, showed much lower

signal intensity. The correlation co-efficient was 0.4998, and hence, apoptosis imaging in this study cannot be reliably used as a predictor of survival.

Table 4.1. Fluorescence intensity per cubic millimeter obtained for 2, 4, and 24h time *in* vivo apoptosis imaging for different treatment groups.

	2h		4h		24h	
FI p/s/mm^3	**Mean**	**S.D.**	**Mean**	**S.D.**	**Mean**	**S.D.**
Saline	3.59E+06	5.11E+05	2.66E+06	6.40E+05	1.27E+06	9.01E+05
Saline + GNR + NIR	3.07E+06	8.73E+05	3.09E+06	1.58E+06	1.72E+06	7.85E+05
NTSL	2.01E+06	5.15E+05	4.60E+06	2.79E+06	1.79E+06	1.16E+06
NTSL + GNR + NIR	2.76E+06	5.35E+05	5.44E+06	3.30E+06	1.50E+06	1.17E+06
TSL + GNR	2.61E+06	5.20E+05	4.49E+06	3.05E+06	2.09E+06	1.55E+06
TSL + NIR	2.17E+06	4.73E+05	4.00E+06	3.00E+06	1.96E+06	1.56E+06
TSL + GNR + NIR	8.35E+06	3.59E+06	9.13E+06	4.08E+06	5.49E+06	2.12E+06

Table 4.2. Bonferroni statistical comparison between TSL + GNR + NIR and different treatment groups for 2, 4, and 24h time *in* vivo apoptosis imaging.

	Saline	**Saline + GNR + NIR**	**NTSL**	**NTSL + GNR + NIR**	**TSL + GNR**	**TSL + NIR**
2h	$p < 0.05$	$p < 0.01$	$p < 0.001$	$p < 0.01$	$p < 0.001$	$p < 0.001$
4h	$p < 0.001$	$p < 0.001$	$p < 0.001$	$p < 0.01$	$p < 0.001$	$p < 0.001$
24h	$p < 0.01$	$p < 0.01$	$p < 0.01$	$p < 0.01$	$p < 0.01$	$p < 0.01$

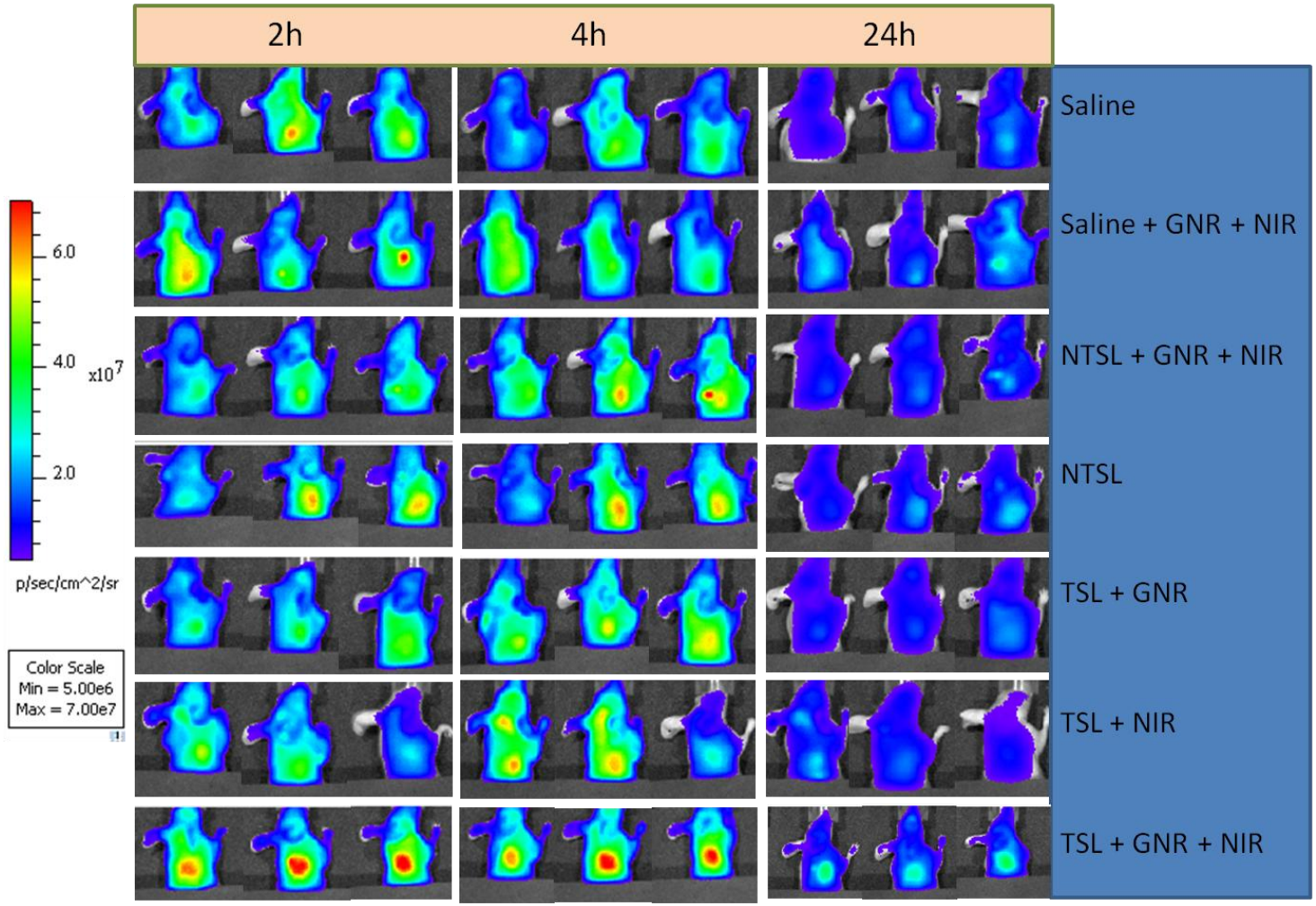

Figure 4.5. In vivo imaging representative images from 2, 4, and 24 hours for different treatment groups.

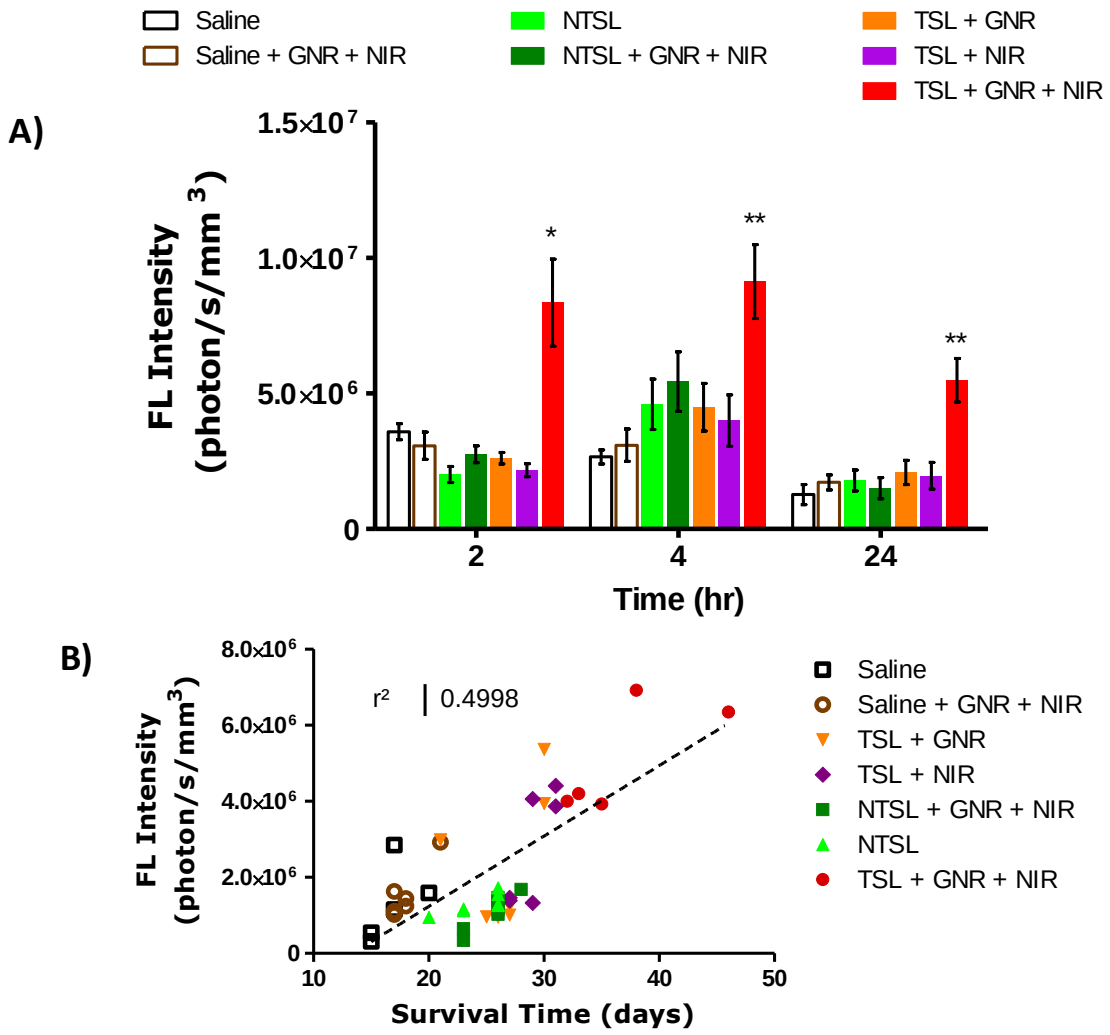

Figure 4.6. In vivo apoptosis imaging shows higher accumulation and retention of apoptosis marker Annexin-Vivo 750. A) Different groups of tumor bearing animals, 18 h post NIR irradiation, were administered Annexin-vivo 750 i.v. and were imaged at 2, 4, and 24 hours. Fluorescence intensity (FL) acquired in photons/s was quantified by drawing a region of interest around the tumor. The resulting flux was then normalized by each animal's tumor volume measured using calipers. Animals treated with TSL+GNR+NIR were significantly different from all other groups at all time points (2h *p <0.05, 4h & 24h **p <0.01, at the least for all groups). B) Correlation of apoptosis quantification obtained from imaging to animal survival at 24h (n = ~4-6). The survival time is somewhat correlated to the apoptosis seen from in vivo imaging.

In this report we identified a thermosensitive liposomal formulation that can stably carry DXR in the plasma over a period of 24 hours and release its contents when heated at 43 °C. We used GNRs to heat this TSL formulation remotely in an in vivo xenograft model. The GNRs were highly effective in releasing the DXR from TSLs as was seen from increased survival of animals receiving TSLs heated via GNRs. The synergistic effect of GNRs and TSL in this study proves the principle that liposomes can be disrupted remotely and can be, especially, useful in treating tumors without the toxic exposure of the chemotherapeutic to surrounding normal tissue. The combination can provide a strong tool in increasing the effects of a chemotherapeutic. As demonstrated earlier, such a combination can also be used to increase the accumulation of the chemotherapeutic in the tumor region [14, 26]. In this study, we demonstrated that when same amount of liposomal drug accumulates passively in a tumor, the effect of release of the chemotherapeutic from a nanocarrier is much more beneficial than the drug being slowly released from the nanocarrier over time. Using GNRs to cause higher drug accumulation at the tumor site and then using a second NIR pulse to disrupt the liposomes may significantly enhance the effects of chemotherapy and reduce the overall drug administered systemically.

The major drawback of thermally induced triggered release therapy is that it requires the localization of the tumor. In case of metastatic tumors, this can be a disadvantage to using thermally triggered liposomes for chemotherapy. Using GNRs may allow for non invasive tracking of tumor using optical coherence tomography and photoacoustic tomography [27]. Using the approach, described here, for remote

disruption of liposomes with GNRs can allow for tracking of tumor in vivo and following up with thermally destabilizable liposomal chemotherapy. The study presented here is a proof of principle that remote triggering of thermosensitive liposomes is achievable and allows for point specific treatment.

4.4 References

1. Maeda, H., et al., *Tumor vascular permeability and the EPR effect in macromolecular therapeutics: a review.* J Control Release, 2000. **65**(1-2): p. 271-284.
2. Maeda, H., *The enhanced permeability and retention (EPR) effect in tumor vasculature: the key role of tumor-selective macromolecular drug targeting.* Adv Enzyme Regul, 2001. **41**: p. 189-207.
3. Woodle, M.C. and D.D. Lasic, *Sterically stabilized liposomes.* Biochim Biophys Acta, 1992. **1113**(2): p. 171-99.
4. Yuan, F., et al., *Microvascular permeability and interstitial penetration of sterically stabilized (stealth) liposomes in a human tumor xenograft.* Cancer Res, 1994. **54**(13): p. 3352-6.
5. Andresen, T.L., S.S. Jensen, and K. Jorgensen, *Advanced strategies in liposomal cancer therapy: problems and prospects of active and tumor specific drug release.* Prog Lipid Res, 2005. **44**(1): p. 68-97.
6. Peer, D., et al., *Nanocarriers as an emerging platform for cancer therapy.* Nat Nanotechnol, 2007. **2**(12): p. 751-60.
7. Drummond, D.C., et al., *Pharmacokinetics and in vivo drug release rates in liposomal nanocarrier development.* J Pharm Sci, 2008. **97**(11): p. 4696-740.

8. Needham, D. and M.W. Dewhirst, *The development and testing of a new temperature-sensitive drug delivery system for the treatment of solid tumors.* Adv Drug Deliv Rev, 2001. **53**(3): p. 285-305.

9. Jain, P.K., et al., *Noble metals on the nanoscale: optical and photothermal properties and some applications in imaging, sensing, biology, and medicine.* Acc Chem Res, 2008. **41**(12): p. 1578-86.

10. Huang, X., et al., *Gold nanoparticles: interesting optical properties and recent applications in cancer diagnostics and therapy.* Nanomedicine (Lond), 2007. **2**(5): p. 681-93.

11. El-Sayed, I., et al., *Effect of plasmonic gold nanoparticles on benign and malignant cellular autofluorescence: a novel probe for fluorescence based detection of cancer.* Technol Cancer Res Treat, 2007. **6**(5): p. 403-12.

12. Huang, X., et al., *Plasmonic photothermal therapy (PPTT) using gold nanoparticles.* Lasers Med Sci, 2008. **23**(3): p. 217-28.

13. Weissleder, R., *A clearer vision for in vivo imaging.* Nat Biotechnol, 2001. **19**(4): p. 316-7.

14. Park, J.H., et al., *Cooperative nanomaterial system to sensitize, target, and treat tumors.* Proc Natl Acad Sci U S A, 2010. **107**(3): p. 981-6.

15. Saul, J.M., et al., *Controlled targeting of liposomal doxorubicin via the folate receptor in vitro.* J Control Release, 2003. **92**(1-2): p. 49-67.

16. Saul, J.M., A.V. Annapragada, and R.V. Bellamkonda, *A dual-ligand approach for enhancing targeting selectivity of therapeutic nanocarriers.* J Control Release, 2006. **114**(3): p. 277-87.

17. Bolotin, E.M., et al., *Ammonium sulfate gradients for efficient and stable remote loading of amphipathic weak bases into liposomes and ligandoliposomes.* J Liposome Res, 1994. **4**(1): p. 455-479.

18. Gaber, M.H., et al., *Thermosensitive sterically stabilized liposomes: formulation and in vitro studies on mechanism of doxorubicin release by bovine serum and human plasma.* Pharm Res, 1995. **12**(10): p. 1407-16.

19. Tomayko, M.M. and C.P. Reynolds, *Determination of subcutaneous tumor size in athymic (nude) mice.* Cancer Chemother Pharmacol, 1989. **24**(3): p. 148-54.

20. Euhus, D.M., et al., *Tumor measurement in the nude mouse.* J Surg Oncol, 1986. **31**(4): p. 229-34.

21. Troy, T., et al., *Quantitative comparison of the sensitivity of detection of fluorescent and bioluminescent reporters in animal models.* Mol Imaging, 2004. **3**(1): p. 9-23.

22. Paasonen, L., et al., *Gold nanoparticles enable selective light-induced contents release from liposomes.* J Control Release, 2007. **122**(1): p. 86-93.

23. Hunt, C.A., *Liposomes disposition in vivo. V. Liposome stability in plasma and implications for drug carrier function.* Biochim Biophys Acta, 1982. **719**(3): p. 450-63.

24. Ghoroghchian, P.P., M.J. Therien, and D.A. Hammer, *In vivo fluorescence imaging: a personal perspective.* Wiley Interdiscip Rev Nanomed Nanobiotechnol, 2009. **1**(2): p. 156-67.

25. Graves, E.E., R. Weissleder, and V. Ntziachristos, *Fluorescence molecular imaging of small animal tumor models.* Curr Mol Med, 2004. **4**(4): p. 419-30.

26. Park, J.H., et al., *Cooperative nanoparticles for tumor detection and photothermally triggered drug delivery.* Adv Mater, 2010. **22**(8): p. 880-5.

27. Wei, A., A.P. Leonov, and Q. Wei, *Gold nanorods: multifunctional agents for cancer imaging and therapy.* Methods Mol Biol, 2010. **624**: p. 119-30.

CHAPTER 5

REMOTE TRIGGERED RELEASE OF LIPOSOMES IN A RODENT BRAIN TUMOR MODEL

5.1 Introduction

Passively accumulated long circulating liposomes, after extravasation, exhibit very slow release, hence, not enough therapeutic efficacies [1]. In addition, delivery of liposomes to solid tumors is limited by elevated interstitial pressures and inability to diffuse beyond the perivascular space [2]. The ideal chemotherapeutic liposome should be able to retain the drug, evade the RES, target the tumor, and release the drug within the tumor [3]. Many efforts have been directed towards triggered release in response to a specific stimulus at target site. To obtain controlled release, the carrier/drug relationship must change from the stable state for carrying drugs in the circulation, to rapid instability to release the drug at the tumor site. In the late 1970s, Yatvin et al. proposed the use of pH sensitive and thermosensitive liposomes to trigger this change. However, when fabricating triggerable liposomes, the ability of such liposomes to carry their payload stably in the circulation is compromised.

In chapter 4, we fabricated stable thermosensitive liposomes that would enable rapid drug release at the tumor site. In addition, we administered gold nanorods to a xenograft model of human U87-MG gliomas to achieve point specific heating. In this chapter, we substitute the chemotherapeutic with a water soluble dye ADS645WS in the thermosensitive liposomes and co-administer it with the gold nanorods in an orthotopic

brain tumor model. We show that the gold nanorod mediated disruption of the liposomes enables enhanced distribution of the dye in the tumor. Therefore, disruption of liposomes with GNRs is achievable and beneficial for rapid drug distribution.

5.2 Materials and Methods

5.2.1 Materials

1,2-distearoyl-*sn*-glycerophospho-choline (DSPC), 1,2-dimyristoyl-sn-glycero-3-phosphocholine (DMPC) and 1,2-distearoyl-*sn*-glycerophosphoethanolamine poly(ethylene glycol)$_{2000}$ (DSPE-PEG2000) were purchased from Genzyme Pharmaceuticals (Cambridge, MA). Cholesterol, paraformaldehyde, and Triton X-100 were purchased from Sigma (St. Louis, MO). Dialysis tubing (10,000 and 100,000 molecular weight cut-off) was purchased from Spectra/Por (Dominguez, CA). A 9L glioma cell line was received as a generous donation from the Neurosurgery Tissue Bank at UCSF. U87-MG human glioma cell line was purchased from American Type Culture Collection (Manassas, VA). Minimal essential medium containing Earle's balanced salt solution (MEM/EBSS) was purchased from Hyclone (Logan, UT). (Gentamicin (50 mg/ml) and fetal bovine serum (FBS) were obtained from Gibco (Carlsbad, CA). DMEM and trypsin-EDTA (0.05% trypsin, 0.53 mM EDTA) in Hanks' balanced salt solution was purchased from Mediatech (Manassas, VA). Heparin (1000 USP units/ml), isoflurane, and doxorubicin (DXR) were purchased from Baxter Healthcare (Deerfield, IL). Fisher 344 male rats were purchased from Harlan (Indianapolis, IN) and nu/nu mice were purchased from Charles River Laboratories International, Inc. (Wilmington, MA).

5.2.2 Cell Culture

9L glioma cell line was maintained in MEM/EBSS medium supplemented with 10% fetal bovine serum and 0.05 mg/ml gentamicin. Cells were passaged by trypsinization and washed with growth medium.

A 9L glioma cell line transfected with the bacterial β-galactosidase encoding gene, LacZ, was maintained in MEM/EBSS medium supplemented with 10% fetal bovine serum and 0.05 mg/mL gentamicin.

5.2.3 Liposome Preparation

Liposomal nanocarriers were formed as described earlier [4-5]. Briefly, a ratio of 54:3:30:3 of and DPPC:DMPC:Cholesterol:DSPE-PEG2000 to fabricate thermosensitive stealth liposomes (TSL). A non-thermosensitive stealth liposomal formulation (NTSL) of DPPC: cholesterol: DSPE-PEG2000 in the ratio 57:40:3 respectively was also formulated for plasma clearance studies. The lipid mixture was dissolved in 1mL of ethanol at 60^{o}C. Liposome size was determined by dynamic light scattering (Particle Size Analyzer, Brookhaven Instruments, Holtsville, NY). For dye loaded liposomes, a 12 mg/ml solution of ADSWS645 in 0.9% saline was used to hydrate the liposomes after dissolution in ethanol. Following extrusion, extra dye was removed from the external phase by dialysis. Liposomal nanocarriers were dialyzed against a phosphate-buffered saline (PBS) solution to establish an ammonium sulfate gradient for DXR loading for plasma clearance studies.

Liposomal nanocarriers were actively loaded with DXR via the ammonium sulfate gradient published previously [6]. Briefly, liposomal nanocarriers and 5 mg/ml DXR solution in 0.9% saline were mixed at a ratio of 0.1 mg DXR per 1 mg of

phospholipid in the liposomal nanocarriers. The liposome/DXR suspension was heated at 45 °C for 30 minutes. The liposomal nanocarriers were then cooled immediately on ice and dialyzed in 100 000 MWCO membrane against PBS to remove un-encapsulated DXR. The formulations were sterilized by passing through a 0.2 μm filter. The final DXR concentration after dialysis was determined by lysing liposomal nanocarriers with 5% Triton X-100 and measurement of absorbance at 480 nm.

5.2.4 Liposomal Leak Studies

Liposomal dye ADS645WS was diluted to a final concentration of 1 μg/ml in 50% FBS solution and heated in circulating water bath. Samples were analyzed for the amount of dye released. 100% release was the intensity after the addition of detergent Triton X-100, while 0% (no release) was the intensity measured for 50% FBS solution. ADS645WS intensity was measured at 645/670 excitation and emission wavelength in a spectrophotometer. For stability and triggered release studies, samples were heated in circulating water bath at 37°C for 24 hours. Samples were then placed in water bath at 43°C for 10 minutes in order to quantify drug release and then transferred back to the water bath at 37°C. 24 hours later all samples were analyzed for the amount of drug released.

$$\%\text{release} = \frac{(\text{Sample Intensity})_t - (\text{Sample Intensity})_0}{(\text{Max Intensity})_{\text{lysed}} - (\text{Sample Intensity})_0}$$

where t = time

5.2.5 Plasma Clearance

All animal work was done according to an approved animal protocol and in strict compliance with NIH Clinical Center Animal Care and Use Committee guidelines and

regulations. 10-11 weeks old female Fisher rats weighing ~200g were anesthetized and maintained using isoflurane and administered DXR-NTSL nanocarriers (n=4) or DXR-TSL nanocarriers (n=4) via tail vein at a dose of 8 mg/kg DXR. 500 µl of blood was collected from the orbital sinus before IV injection and at 0.5, 2, 9, 24, 48, and 72 hours after injection in heparinized gel tubes. Tubes were centrifuged at 3000 rpm for 20 minutes to separate the plasma. Liposomal nanocarriers were lysed according to an established protocol [7]. Briefly, a mixture of 0.75N acidified isopropanol, 10% Triton-X100, water, and plasma was prepared to analyze the DXR content. To quantify total DXR content, fluorescent readings were obtained using a fluorescence spectrometer at excitation/emission of 485/590 nm. Plasma samples obtained prior to injection were used to correct for background fluorescence.

5.2.6 Tumor Inoculation

A rat glioma model was established by orthotopic inoculation of 1 x 10^6 9L/LacZ glioma cells following modified version of established methods [8]. Briefly, a dental drill was used to create a 2 mm hole at a position 1mm lateral and 1mm anterior to the bregma, with a custom trephine. The bone plug was carefully removed. A 26 gauge needle was inserted into the frontal lobe at a depth of 3mm to inject 10µl of the glioma cell suspension (1 x 10^6 cells). The cells were slowly injected over a period of approximately 30 seconds. Following injection of the cell suspension, the needle was slowly retracted over a period of approximately one minute to prevent backflow. The wound was, then, closed with suture (4.0). Animals were administered buprenorphine 0.03 mg/kg SC to alleviate pain as needed.

5.2.7 Heating via Gold Nanorods

At day 7 after tumor implantation, animals were intravenously injected with gold nanorods (courtesy of Dr. El-Sayed) through the tail vein. At this time the tumors were large enough to be seen visually. 48 hours after the injection, the animals were anesthetized with 50, 10 and 1.67 mg/kg respectively of ketamine/ xylazine/ acepromazine. A 33 gauge hypodermic thermocouple (Omega) 10 mm long was inserted into the tumor to measure the temperature rise at the tumor. Animals were then irradiated with NIR radiation and the power of the laser was varied till desired heating was obtained. The concentration of GNRs injected was varied, in order to determine the optimal heating. A temperature profile was obtained as a function of time.

5.2.8 Flow Cytometric Studies

Animals were allowed to recover from surgery, and 10 days later, saline sham, Stealth non-thermosensitive, or thermosensitive liposomal ADS645WS (2 mg/kg ADS645WS; ~70 mg/kg lipid) treatments were administered with or without 2.25 pmol/kg GNR i.v. After 48 hours, animals were subjected to NIR for 10 minutes each as described above. Animals were anesthetized with 5% isoflurane 24 hours later and decapitated immediately. Tumors were dissected from explanted brains, mechanically fragmented, and treated for 60 minutes at 37°C with a solution of collagenase (0.1 U/ml PBS) and dispase (0.8 U/ml PBS) to dissociate cells. The cell solution was re-suspended in 4% fetal bovine serum in PBS and treated with a *FluoReporter*® lacZ flow cytometry kit. Tumor cells expressing the lacZ reporter gene product, beta-galactosidase, hydrolyzed the fluorogenic beta-galactosidase substrate allowing fluorescent detection of expression to distinguish tumor cells from non-tumor cells. Flow cytometry was

conducted using a Becton-Dickinson DLSR digital flow cytometer equipped with a 488 nm excitation laser using the APC channel for detection of liposomal ADS645WS and the FITC channel for tumor cell (lacZ) detection. Liposome uptake by lacZ+ (tumor) cells and lacZ- (non-tumor) cells were then quantified. Tumor cells obtained from saline treated animals served as a negative control for ADS645WS while untransfected 9L glioma cells stained with the *FluoReporter*® lacZ flow cytometry kit were utilized as a negative control for lacZ staining.

5.2.9 Statistical Analysis

Means were determined for each variable in this study and the resulting values from each experiment were subjected to a one way analysis of variance (ANOVA) with Tukey post-hoc pairwise comparisons. Significance was determined using a 95% confidence level. For plasma clearance, a biphasic curve was fitted to the experimental data and groups were compared by a two way ANOVA. Half lives were determined from the curve fits.

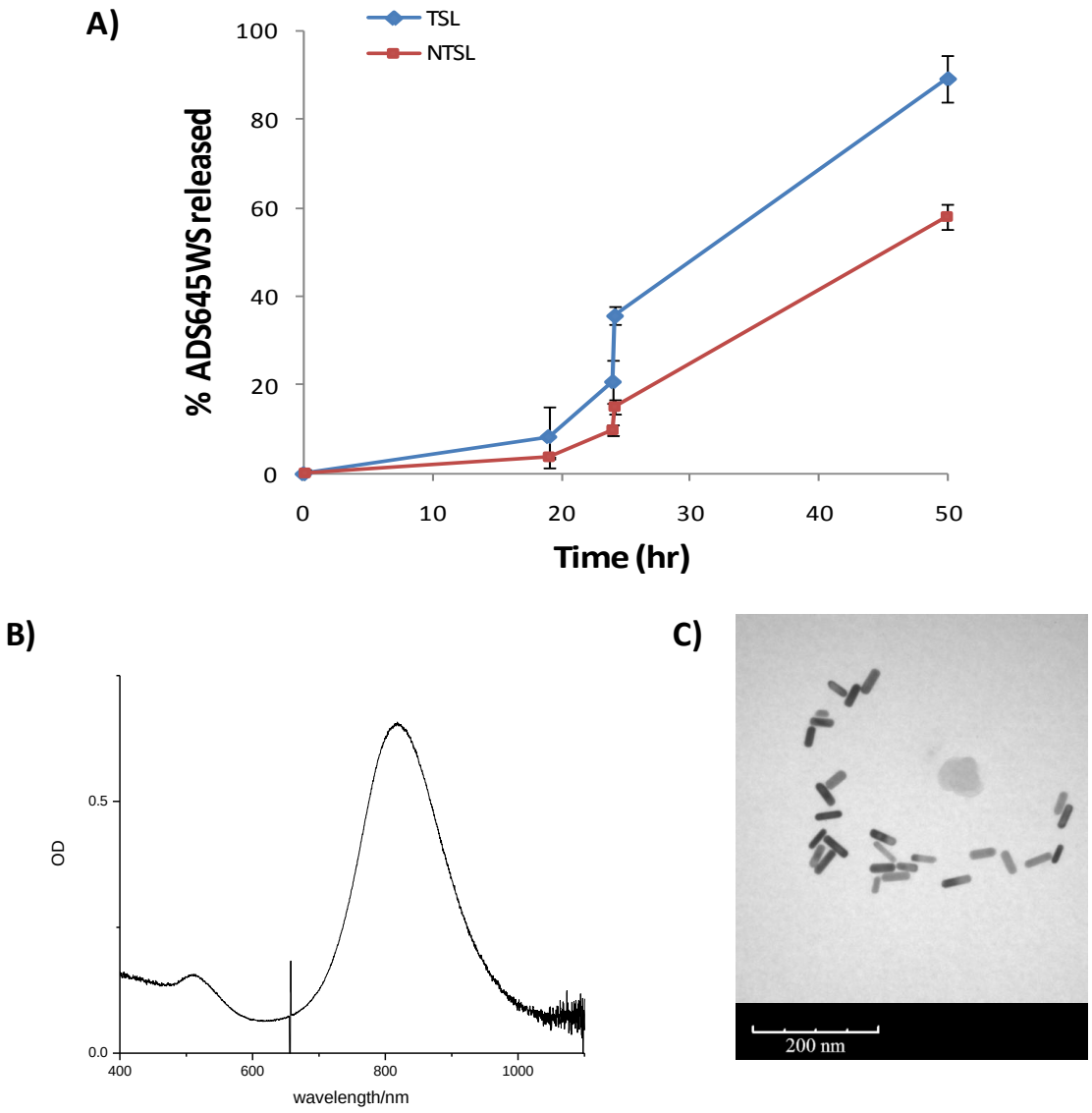

Figure 5.1. Characterization of liposomes and GNRs. A) ADS645WS dye release in 50:50 FBS:PBS. TSL and NTSL liposomes were diluted to 1 µg/ml of dye and incubated in a 37 °C circulating water bath. Samples were measured for released dye from the liposomes at indicated time points. At 24 hours, one sample for each liposomal formulation was transferred to a 43 °C water bath and incubated for 10 minutes. The liposomal dye released was measured and the sample was transferred back to the 37 °C water bath for another 24 hours, and dye released at this point was quantified. The release of the dye from TSL at 37 °C after 24 hours was slightly higher than NTSL. However, the release of the dye from TSL upon heating was significantly higher and continued to increase over the next 24 hours. B) Spectrum of GNRs used in this study. Peak wavelength was 818 nm. C) TEM image of PEG coated GNRs. Scale bars are 200 nm.

5.3 Results and Discussions

5.3.1 ADS645WS Release from Liposomes

TSL and NTSL were loaded with ADS645WS and compared for dye release at 37 °C and 43 °C. Liposomes were diluted at 1 µg/ml in 50:50 mixtures of FBS: PBS. Liposome aliquots were heated at various times and the fluorescence of ADS645WS released from the liposomes was quantified to assess % dye released. As shown in fig. 5.1, TSL exhibit similar stability to NTSL at 37 °C. However, when heated for 10 minutes at 43 °C, TSLs were able to release significantly higher amount of dye in comparison to NTSL. In addition, further incubation for another 24 hours at 37 °C of liposomes heated at 43 °C, resulted in almost complete loss of dye from TSLs. In contrast, NTSLs retained about 50% of the dye.

5.3.2 Controlled Heating of Tumors via Gold Nanorods

Orthotopic tumor bearing Fisher rats were administered different concentrations of GNRs via the tail vein (2.25 pmol/kg-11.25 pmol/kg). 2 days later, animals were irradiated with NIR-light (~0.5 W/cm^2, 808 nm) for a period of 10 minutes. Temperatures were recorded via a thermo-couple [9]. All animals receiving a dose of over 5 pmol/kg reached temperatures over 50 ˚C in less than 5 minutes of heating. The goal of this study was to determine a GNR dose that would limit the temperature rise to a maximum of 45 ˚C. We determined (fig 5.2B) that at a dose of 2.25 pmol/kg, desired temperature was attained and remained steady for 10 minutes of heating. 2.25 pmol/kg GNR dose was used for all further *in vivo* therapeutic studies.

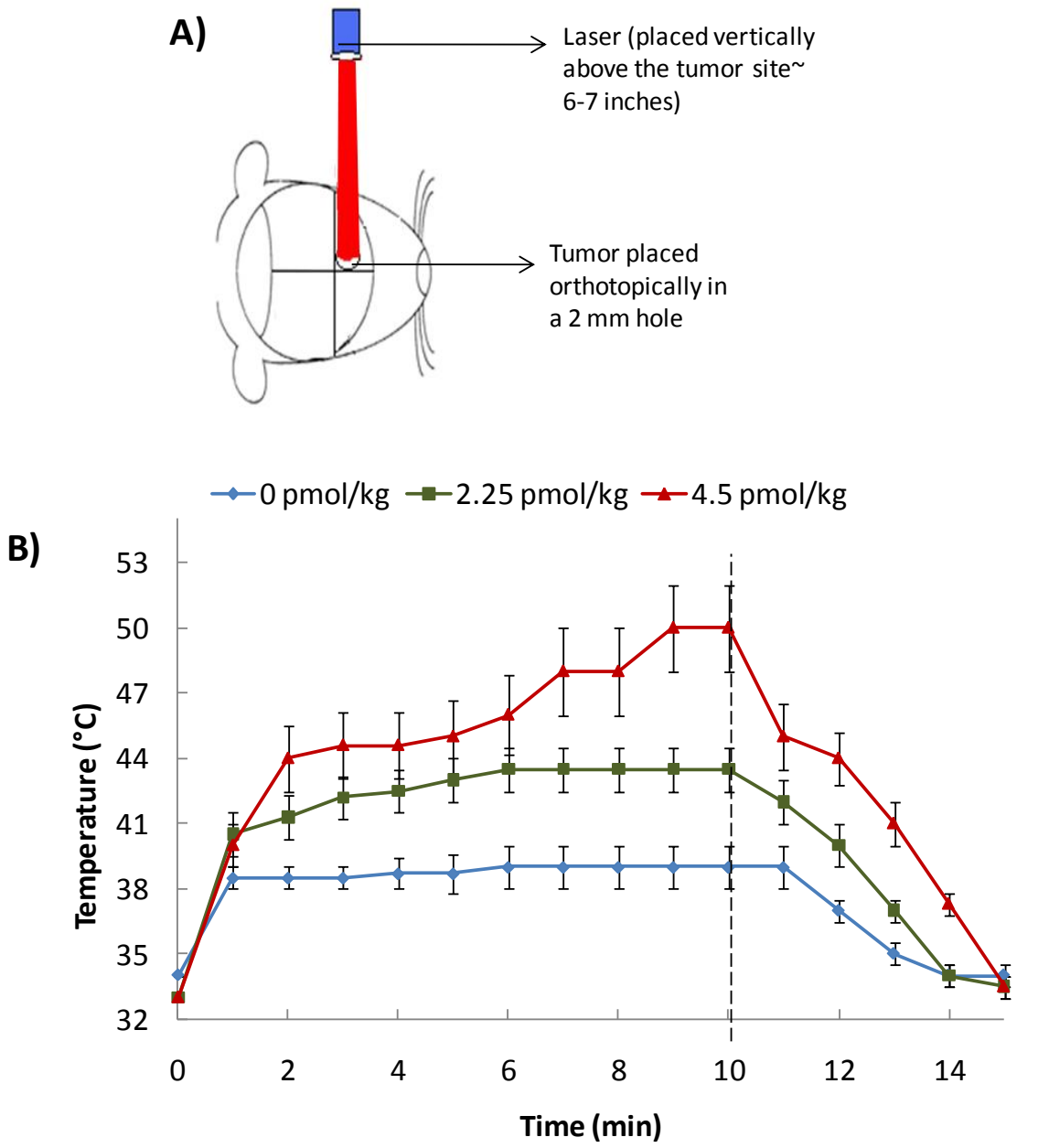

Figure 5.2. GNR mediated heating of brain tumors. A) Schematic representing the location of brain tumor implantation and the setup used for laser irradiation. B) Brain tumor bearing animals were either administered varying GNR concentrations and irradiated 48 hours later, as shown in A), with NIR. Animals that received 2.25 pmol/kg of GNR indicated a controlled and desired increase in temperature to 43 ± 1 °C. Control animals also showed slight increase in tumor temperature to 39 ± 1 °C. After NIR removal, tumor temperature quickly returned to normal.

5.3.3 In vivo ADS645WS Dye Distribution

To determine the ability to promote increased bioavailability and uptake of encapsulated contents delivered by TSL nanocarriers to tumor cells *in vivo*, we performed studies on brain tumor-bearing rats (9L/LacZ glioma model) receiving TSL encapsulating a fluorescent dye (ADS645WS) in combination with GNRs with or without NIR. Animal tumors were dissociated and stained for β-gal production, and analyzed through flow cytometry. Cultured 9L/LacZ cells and nontransfected 9L glioma cells were stained and served as positive and negative controls, respectively, for β-gal production. Cytometric detection of β-gal in the 9L/LacZ glioma tumors delineated two populations of cells, β-gal+ (tumor cells) and β-gal- (nontumor) cells. The β-gal- populations exhibited minimal ADS645WS staining intensity as percentage of the total population (TSL + GNR + NIR: 1.0984 ± 0.573%, TSL + NIR: 1.016 ± 0.852%, TSL + GNR: 0.67125 ± 0.3433%) indicating that the uptake of liposomes by non-tumor cells was nominal. The tumor population of cells obtained from animals receiving TSL + GNR followed up by NIR irradiation, demonstrated a significant increase in ADS645WS signal detected in the APC channel (Figure 5.3B). In contrast, tumor cells obtained from the other treatment groups (TSL + GNR, TSL + NIR) showed comparably low uptake of the dye. Frequency profiles of β-gal and dye signal intensity on two-dimensional graphs demonstrated an increase as well as a shift in the tumor cell population obtained from animals treated with TSL + GNR + NIR into the APC channel (Figure 5.4). The percentage of tumor cells from these animals that demonstrated dye uptake (APC+/FITC+) was significantly ($p<0.01$) greater than that of other treatment groups. Specific increased uptake of dye

ADS645WS *in vivo* delivered by TSLs heated via GNRs is indicative of increased release of the dye from the liposomes as a result of point specific heating.

Cytometric data allowed for quantitative analysis of the results obtained from treated animals (Table 5.1). The shift in fluorescent intensity representing liposomal uptake per cell observed in the group TSL + GNR + NIR was significant compared to the remaining treatment groups. Median ADS645WS fluorescence in tumor cells obtained from TSL + GNR + NIR was 1.9 times greater than that from other treatment groups.

Table 5.1. Tumor associated median fluorescence intensity for ADS645WS released from liposomes. Data represented is Mean ±S.D.

Treatment	Tumor ADS645WS Median Signal Intensity
TSL + GNR	1.245 ± 0.056
TSL + NIR	1.268 ± 0.053
TSL + GNR + NIR	1.912 ± 0.215 ***
	***p <0.0001

The above results verify that GNRs are successful in disrupting the tumor accumulated thermosensitive liposomes *in vivo*. The liberation of the dye from the liposomal nanocarriers significantly increased the number of cells stained by the dye as well as the intensity measured per tumor cells of the dye. The increase in dye uptake could be attributed to increased diffusion due to small size of the dye in contrast to the liposome. The relatively low level of dye uptake by host cells also shows that GNRs can be effectively heated remotely by NIR, and can successfully be used locally to disrupt the liposomes without unnecessary exposure of healthy tissue.

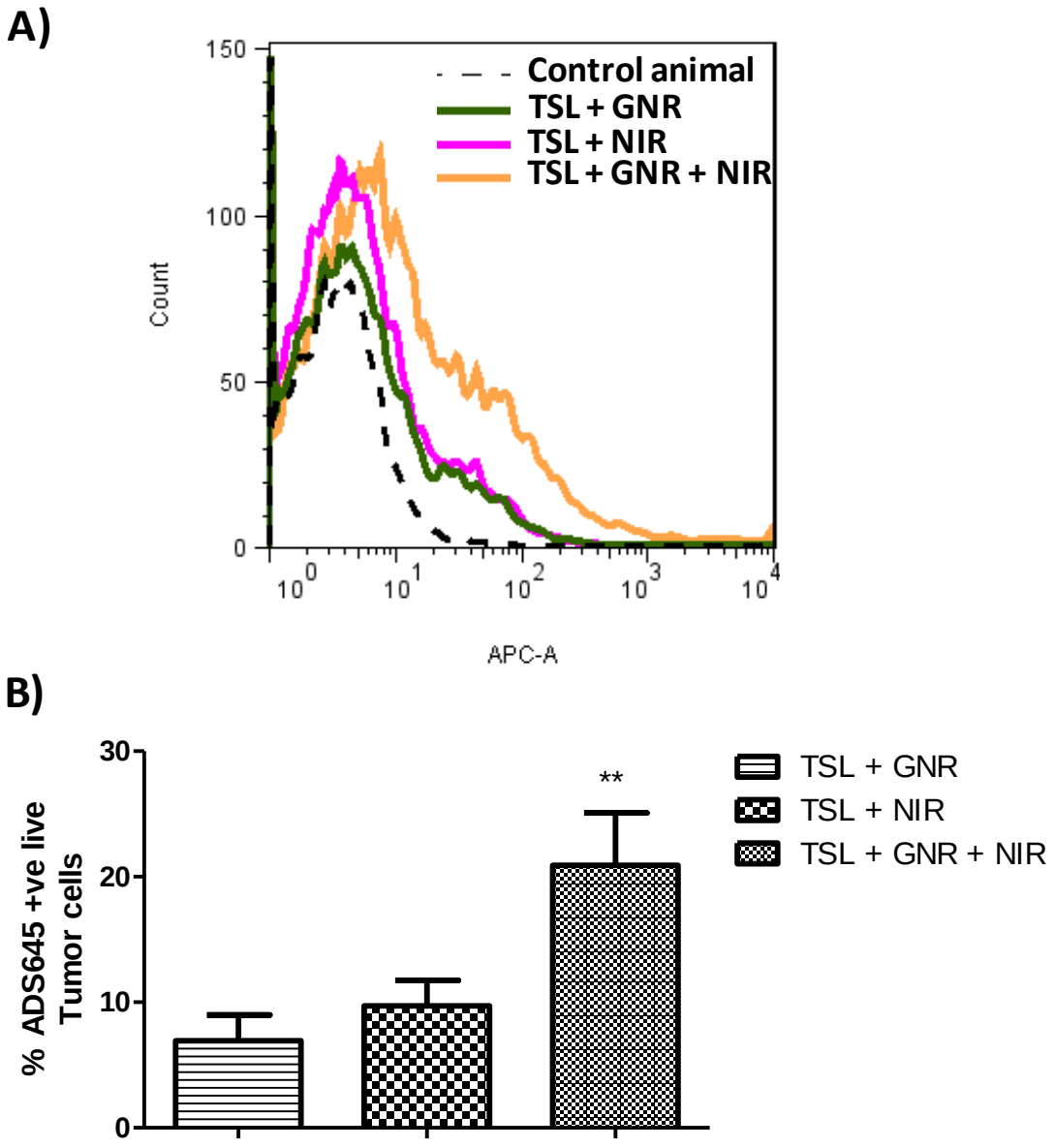

Figure 5.3. ***In vivo*** **dye distribution quantified by flow cytometry. A) Representative image showing the distribution of tumor cells (β-gal positive) in the APC channel indicative of ADS645WS dye staining. In contrast to TSL + GNR and TSL + NIR, TSL + GNR + NIR showed shift towards ADS645WS staining. Controls were β-gal positive tumors explanted from animals that did not receive any ADS645WS dye. B) ADS645WS stained cells normalized again unstained control cells were quantified for each group. For each animal, % of tumor cells that were positive for ADS645WS was determined (n = 6, for all groups). Animals that were treated with TSL + GNR + NIR showed significantly better staining of the tumor cells (**p <0.01) between all groups. Data represented in mean ± S.E.M.**

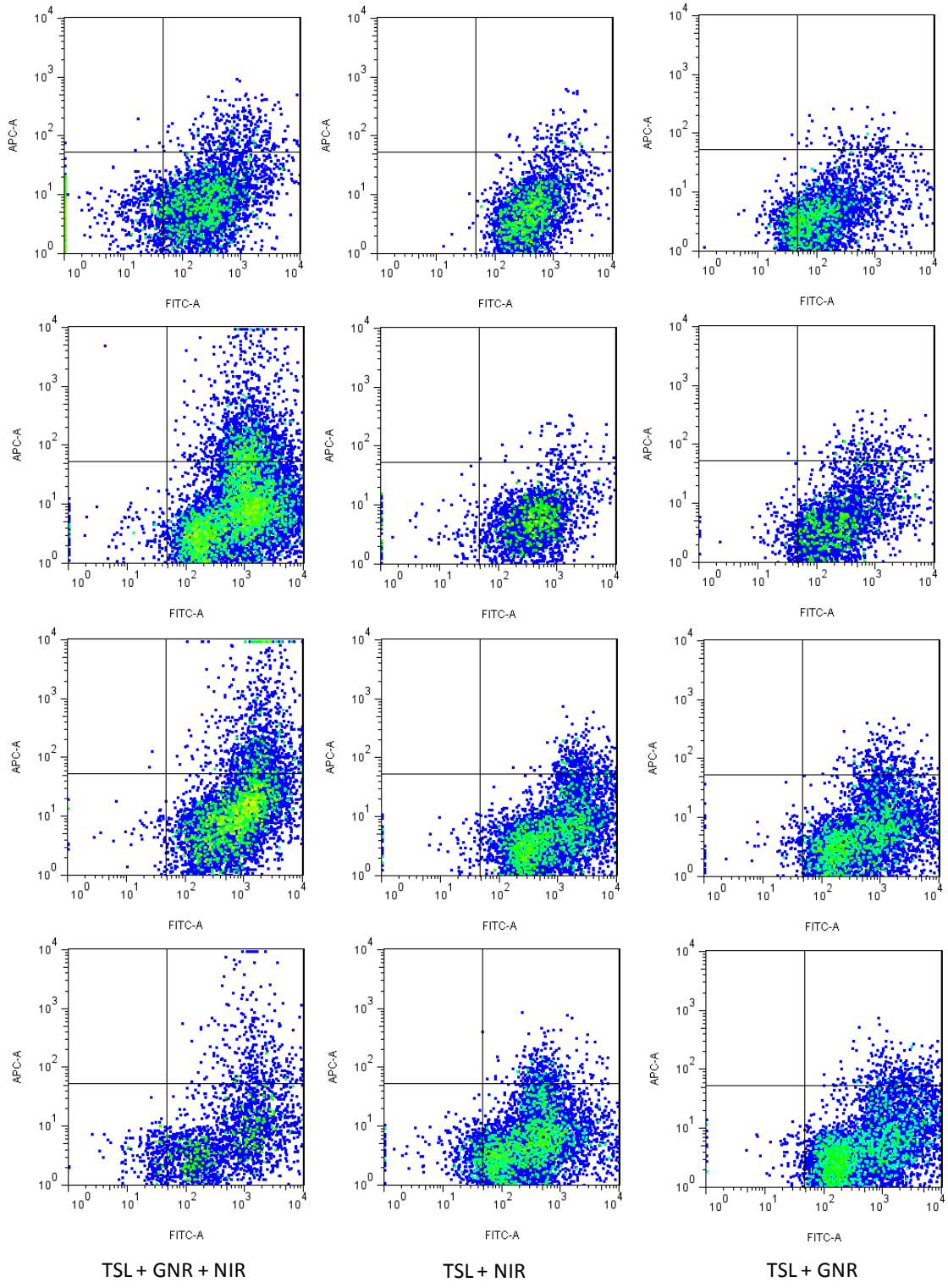

Figure 5.4. Flow cytometric distribution of cells in the APC (ADS645WS) versus the FITC (β-gal stained tumor cells) channel for different treatments.

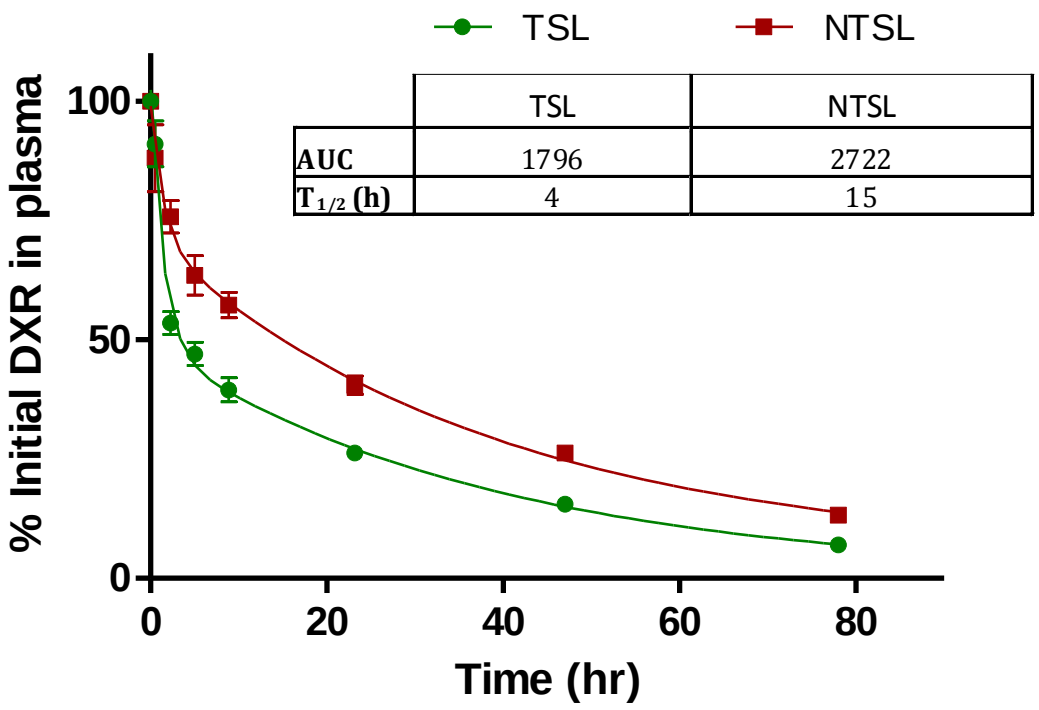

Figure 5.5. Plasma clearance profiles. TSLs were compared to NTSLs. 4 animals each were injected via the tail vein with 8 mg/kg of DXR. Blood was collected through the orbital's sinus at 0.5, 2, 9, 24, 48, and 72 hours. A) DXR concentrations in the blood were compared, plasma half lives, and the areas under the curves (AUCs) were evaluated. The AUCs of TSL and NTSL formulations were statistically different from each other (p <0.001). B) Lipid concentration in the plasma remaining in comparison to the initial injected dose was determined. Lipid clearance from the blood of TSL was similar to the DXR clearance. The AUC for lipid clearance in the case of TSL was also statistically different than NTSL (p <0.001).

5.3.4 Plasma Clearance of TSL

With favorable *in vitro* targeting established for RSI liposomal nanocarriers, we next addressed whether peptide coated liposomal nanocarriers demonstrated extended plasma half-life required for *in vivo* efficacy. Liposomal nanocarriers were formulated with 3% DSPE-PEG2000 to provide Stealth characteristics. The % initial dose of DXR, as well as the % initial dose of lipid administered was quantified for different time points. The area under the curves (AUCs) were computed and compared for statistical

significance. As shown in fig. 5.5, the AUC of TSL for the circulation of DXR was statistically significant from the NTSL nanocarriers. The half life of DXR and liposomes, in the case of TSL, were computed to be 4 hours. The lipid dose administered (80 mg/kg) for the pharmacokinetic study was kept significantly below the RES saturation dose of 280 mg/kg[10]. The reduction in the TSL content in plasma may significantly affect their passive accumulation in the tumor. In spite of 30% reduction in the total circulating levels of TSL compared to NTSL, if 20% of the encapsulated contents are being released upon heating (as seen from release studies), up to a 10 fold increase in tumor bioavailable drug levels can be expected. Further studies will need to be conducted to evaluate the effect of reduced plasma circulations on TSL accumulation in tumor.

In the present study, we show the differences between the distributions of a liposomally encapsulated particle upon, externally mediated, burst release from the liposomes versus slow self release in the tumor. In addition, the use of GNRs alongside liposomes allowed for remote and point specific tumor tissue heating. Animals treated with TSL + GNR + NIR demonstrated a significant increase in uptake of ADS645WS by tumor cells. The increase in uptake of ADS645WS is, therefore, a result of thermal disruption of liposomes mediated by GNRs. In addition, the percentage of tumor cells positive for ADS645WS was significantly greater in tumors explanted from animals treated with TSL + GNR + NIR compared to either TSL + GNR or TSL + NIR alone. Our outcomes indicate that a small molecule like ADS645WS upon release from the liposome has a higher opportunity to diffuse farther and reach more tumor cells. Since this was a short preliminary study with the objective to demonstrate the difference between triggered versus non-triggered release, non-thermosensitive liposomes controls

were not evaluated for tumor dye distribution. Further studies, with these controls included, will help us validate the outcomes of this study. Such efforts are currently underway.

The circulation half life of TSL was 4 times less than that of NTSL. However, as discussed in chapter 4, TSLs were effective in increasing the survival of xenograft model of U87-MG in mice over NTSLs. These results may indicate that the effect of fast release of the chemotherapeutic from the nanocarriers has significant benefits in spite of compromised circulation.

5.4 References

1. Kocer, A., *A remote controlled valve in liposomes for triggered liposomal release.* J Liposome Res, 2007. **17**(3-4): p. 219-25.
2. Gabizon, A., et al., *In vivo fate of folate-targeted polyethylene-glycol liposomes in tumor-bearing mice.* Clinical Cancer Research, 2003. **9**: p. 6551-6559.
3. Ponce, A.M., et al., *Hyperthermia mediated liposomal drug delivery.* Int J Hyperthermia, 2006. **22**(3): p. 205-13.
4. Saul, J.M., et al., *Controlled targeting of liposomal doxorubicin via the folate receptor in vitro.* J Control Release, 2003. **92**(1-2): p. 49-67.
5. Saul, J.M., A.V. Annapragada, and R.V. Bellamkonda, *A dual-ligand approach for enhancing targeting selectivity of therapeutic nanocarriers.* J Control Release, 2006. **114**(3): p. 277-87.
6. Bolotin, E.M., et al., *Ammonium sulfate gradients for efficient and stable remote loading of amphipathic weak bases into liposomes and ligandoliposomes.* J Liposome Res, 1994. **4**(1): p. 455-479.

7. Charrois, G.J. and T.M. Allen, *Drug release rate influences the pharmacokinetics, biodistribution, therapeutic activity, and toxicity of pegylated liposomal doxorubicin formulations in murine breast cancer.* Biochim Biophys Acta, 2004. **1663**(1-2): p. 167-77.

8. McNeeley, K., A. Annapragada, and R. Bellamkonda, *Decreased circulation time offsets increased efficacy of PEGylated nanocarriers targeting folate receptors of glioma.* Nanotechnology, 2007. **18**(385101): p. 1-11.

9. Dickerson, E.B., et al., *Gold nanorod assisted near-infrared plasmonic photothermal therapy (PPTT) of squamous cell carcinoma in mice.* Cancer Lett, 2008. **269**(1): p. 57-66.

10. Allen, T.M. and C. Hansen, *Pharmacokinetics of stealth versus conventional liposomes: effect of dose.* Biochim Biophys Acta, 1991. **1068**(2): p. 133-41.

CHAPTER 6

SUMMARY OF FINDINGS

The overall objective of the work presented in this thesis was to explore the possibility of increasing the therapeutic efficacy of existing long circulating liposomal nanocarriers. To further achieve this goal, the study was divided into two parts. To address the problem of increased plasma clearance of targeted liposomes, we identified small peptide ligands that would not suffer RES uptake and, thereby, would show benefits of active targeting. In addition, we explored the possibility of fabricating plasma stable thermosensitive liposomes that would enable rapid drug release at the tumor site, and hence, increase drug availability and therapeutic efficacy.

6.1 Rational Identification of Small Peptides for Targeting Liposomal Nanocarriers

We conducted a study to identify novel peptide sequences through phage display that bind to tumor cells but do not bind to blood cells. It has been shown that a negative impact on targeting ligand inclusion through demonstrated reductions in circulating levels of actively targeted formulations in the bloodstream [1-6]. Since passive accumulation to tumor is directly related to circulating levels in the bloodstream, accelerated clearance of actively targeted liposomal formulations reduces passive targeting to tumor. Decrease in passive targeting effectively offsets the benefits of active targeting to tumor. Therefore, we wanted ensure that the peptide carrying liposomes were able to evade the RES *in vivo*. One peptide sequence was chosen out of the 9 that were identified using phage display due to its maximal binding to 9L glioma cells and minimal binding to blood cells.

Consequentially, the RSI peptide, when presented on the surface of liposomal nanocarriers, enhanced specificity and uptake of chemotherapeutics by tumor cells. Initial FACS analysis demonstrated relatively reduced binding of the RSI peptide to blood cells with more rigorous *in vivo* confirmation through plasma clearance studies that confirmed the plasma half life for RSI liposomal nanocarriers was not compromised. In fact, the strength of this peptide selection technique was the ability to screen peptides that minimally bound to blood cells, which can thus evade the RES *in vivo* and have high selectivity towards the desired cell type.

RSI peptide was bound to liposomal nanocarriers by conjugating the peptide to the end of a long spacer lipid-PEG molecule (DSPE-PEG3400-mal). PEG is known to promote steric hindrance [7-8] for interaction of targeting moieties with the cell surface. Therefore, smaller PEG chains (2000) were used to impart stealth characteristic to the liposomes *in vivo*. DXR was the chosen as the preferred drug due to its fluorescent properties that enable both its detection intracellularly, and its ability to remotely load in the liposome [9-10] with high efficiency >95% [11].

The RSI peptide liposomal nanocarriers were successful in delivering high payload (up to a six fold increase compared to the conventional non-targeted liposomes) of the drug DXR to the 9L cells, in a fashion that increased with higher number of peptides on the surface of the liposomal nanocarriers. The number of peptides that could be tethered on the liposomal nanocarriers was limited as the method of post-insertion of lipid-peptide conjugates in numbers >1000 per liposome became highly inefficient. In addition, plasma half life was reduced when more than 500 peptides were used per nanocarrier. Nevertheless, as seen from the DXR uptake study, when 500 RSI peptides

were presented on the liposomal nanocarriers, significantly increased cellular DXR levels were observed as compared to liposomal nanocarriers with no peptides. It is likely that increased exposure of the RSI peptide to immune system is able to elicit a response against the peptide; however, 500 or less RSI peptides do not sensitize the immune system.

The requirement for the specific RSI peptide sequence is evident suggested by the significant reduction in DXR delivery when a scrambled version of the RSI peptide was used. Although, it can be argued that the effect of the scrambled peptide is larger than the non-targeted liposomes. This effect can be attributed to the preservation of the phage sequence (GPPVESC) on the RSI and the scrambled peptide. Therefore, one may conclude that the phage part of the peptide may have had a significant role in binding to the cells. In a competitive environment where RSI liposomes were presented to the cells in the presence of excess of free RSI peptides, RSI liposome-mediated DXR delivery was significantly reduced indicating increased uptake specifically due to the RSI peptide.

From the cytotoxicity experiments, it was observed 72 hours after treatment with DXR-RSI-liposomal nanocarriers that a large number of cells died. These data confirmed that DXR payload was cellular uptake and not merely surface binding. 9L cells were also treated with free RSI peptide to rule out any cytotoxic effects of the peptide. There were no differences found in the viability of the untreated cells and the cells treated with free RSI peptide. This result argues that cytotoxicity was medicated by DXR and RSI peptides.

In the survival studies, we failed to observe an improvement in survival of tumor bearing animals compared to non targeted formulations. We followed these animals with

a second dose. There was overall improvement in survival due to multiple doses. However, the presence of the 9L tumor binding peptide (RSI) did not have any effect on the survival of tumor bearing mice receiving liposomal doxorubicin. Such outcome could be attributed to a number of factors. It is likely that the 9L tumor cells may have changed *in vivo* compared to their phenotype *in vitro*. Therefore, the binding of the RSI peptide to the tumors would be affected and the peptide presenting liposomes would be then similar to non-targeted liposomes in their outcome. *In vivo* environment is significantly different than what can be replicated *in vitro*. Although, a BLAST search did not reveal any known or similar sequences, RSI peptide could have been competed out by other peptides and proteins in the microenvironment of the tumor cells, in turn, leading to less liposomal uptake of the RSI targeted liposomes.

In comparison to folate targeting liposomes that binds 9L cells about 18 times more than non-targeted liposomes, RSI-peptide presenting liposomes were about 3.5 times better than non-targeted liposomes *in vitro*. The gain seen *in vitro* may have been insignificant *in vivo*, and several doses needed to be administered before a therapeutic difference could be registered.

It is, also, likely that once extravasated, the liposomes do not penetrate far into the tumor tissue. Liposomes are big particles and interstitial diffusion is limited. In addition, it is known that long circulating liposomal particles that extravasate into the tumor interstitium exhibits very slow release of the encapsulated drug. Presence of targeting moieties, therefore, may not be useful in solid tumors due to limited diffusion of liposomal particle.

6.2 Remotely Triggerable Liposomes for Therapeutic Efficacy

In this study, we designed a thermally triggered synergistic system that stably carried its payload at physiological temperature and released the payload in the tumor interstitium upon heating with gold nanorods via near infrared laser. *In vivo* studies in chapter 3 and other recent studies in the lab have indicated that targeting alone may not be sufficient for therapeutic efficacy. Designing a liposome that is capable of delivering its payload to the tumor tissue, may present a more promising opportunity for improving chemotherapeutic efficacy. As described earlier, passively accumulating liposomes release the drug from their inner compartment very slowly and over time. The release rate of the drug has to be faster than the division cycle of the tumor cells and sufficient to overcome the cell multiplication. Traditional long circulating liposomes have failed to achieve therapeutic levels in systemically non-toxic levels. Rapid drug release, in this study, and elsewhere enables overcoming the tumor growth rate and hence was able to significantly improve therapeutic efficacy. The triggered release of liposomes was first proposed by Yatvin et al. The shortcoming of a triggered liposomal system is that when designing cannot stably hold its contents in circulation. In addition, the triggers that cause the liposomes to lose its contents are not specific and sophisticated, and cause systemic toxicity or injury to neighboring healthy tissue.

In this study we compared several liposomal formulations reported in literature for stability over a 24 hour period at physiological conditions. Most thermosensitive formulations lost over 50% of their doxorubicin content in contrast to long circulating FDA approved formulation composed of HSPC/39%Chol/3.1%PEG. One criterion for increased efficacy is passive accumulation due to the EPR effect. Loss of drug at

physiological temperature not only compromises passive drug accumulation in the tumor, but also increases systemic cytotoxicity.

To this end, we fabricated and tested several liposomal formulations for drug encapsulation stability at physiological temperature and release at 4-5 ˚C elevated temperature. We found that that DPPC liposomes that have exhibit gel-liquid state at 41 ˚C, lost ~50% of the encapsulated DXR. DSPC liposomes, on the other hand, do not release any DXR at 37 ˚C, which could be attributed to the fact that they have very high transition temperature of 55 ˚C preventing leakiness. Addition of varying amounts of DPPC to DSPC liposome did not affect their stability, but DXR was also not released from these formulations upon heating at 43 ˚C. In earlier reports, such liposomes were shown to release ~100% calcein a temperature of 37-45 ˚C [12]. These differences, in comparison, with our studies can be explained by the fact that upon heating, the liposomal bilayer is not closely packed and calcein, that is passively loaded, moves outwards driven by concentration gradient. Contrastingly, DXR loaded remotely and is trapped inside the liposomes as precipitates of the sulfate. This leads to extinction of concentration gradient from inside to outside of the liposomes. In addition, the slight increase in release of DXR upon heating to 43 ˚C, in the case of DPPC/DSPC liposomes, could be due to increase in DXR solubility in comparison to its solubility at 37 ˚C.

DPPC liposomes fabricated by inclusion of varying amounts of cholesterol showed found that 30% cholesterol in DPPC liposomes results in very small loss of DXR over a 24 hour period at 37 ˚C. However, these liposomes, also, do not exhibit any thermosensitivity at 43 ˚C [13]. We incorporated small amounts of very low transition temperature (23 °C) lipid DMPC to DPPC/30%cholesterol liposomes. The rationale

behind this approach was that DMPC being in liquid state at >23 °C will render the membrane permeable and allow some movement of DXR at increased temperature. In addition, cholesterol will help stabilize the membrane at physiological temperature. DPPC/30%Chol/3%DMPC/3%PEG (thermosensitive liposomes, TSL) had comparable stability to HSPC/39%Chol/3.1%PEG at physiological temperature and released DXR at 43 ˚C when heated for 10 minutes. The increase in DXR release at 43 ˚C can be attributed to increased DXR solubility that drove the chemical gradient of DXR to the outside of the liposomes.

Additionally, we found that after heating for 10 minutes and placing TSLs back in 37 ˚C for another 24 hours resulted in complete loss of DXR from these liposomes. Since this temperature is higher than the transition temperature of both DPPC and DMPC lipids, the additional loss of DXR could be a result of rearrangement of liposomal bilayer when heated at 43 ˚C. Increase to liquid state may have resulted in a loss of cholesterol from these lipid bilayers resulting in pure lipid liposomes. In such a case, the extended and complete release of DXR observed over the next 24 hours is expected. Further studies can be conducted to determine the molecular phenomenon of the complete release of DXR when incubated over an additional 24 hour period. The thermosensitive formulation developed here is specific to DXR. Extension of this formulation to other chemotherapeutic will require further investigation and testing. The mechanism of loading, the solubility of the drug, and the chemical structure of the drug are all important in determining the right thermosensitive formulation.

Next, we explored a remote trigger for TSLs. Traditional triggers for thermosensitive liposomes, like a water bath, can be inconvenient, require patient

compliance, and can be destructive to surrounding healthy tissue. To this effect, we used gold nanorods to heat the TSLs. GNRs can be effectively heated using NIR [14-19]. Sterically stabilized gold nanorods have a circulation half life of 17 hours and accumulate in the tumors due to EPR [20]. Light in the near infrared range (NIR 650–900 nm) can traverse tissue very efficiently as the absorption by water and hemoglobin is relatively low in this spectrum [21]. The low absorption coefficients (μ_a) prevent excessive tissue heating and allow for use of GNRs for heating.

We co-administered and used GNRs with TSL formulation and remotely heated them via NIR in an *in vivo* xenograft model. We waited for 48 hours to heat the TSLs to allow for passive accumulation. We recorded an average temperature increase of 43 ± 1˚C using a thermo-probe in all animal tumors heated via GNRs. All other animals recorded an average of 39 ± 1˚C showing that increase in tissue temperature was an effect of GNR heating and not the laser alone.

We found that GNR mediated heating of TSL was highly effective in suppressing tumor progression. All saline treated animals showed exponential increase in tumor size. Although, other liposomal treatments were able to suppress tumors to a degree, there was a significant difference in the ability to suppress tumors between TSL + GNR + NIR treatment and all other liposomal treatments. In addition, TSL + GNR + NIR treatment was successful in extending overall survival over all other treatments. These results indicate that GNRs were highly effective in releasing the DXR from TSLs. All liposomally treated animals received DXR at 2.5 mg/kg. In our studies, we tested 10 mg/kg and 5 mg/kg DXR doses as well; however, animals did not tolerate these doses very well and were not further investigated.

Increased animal survival, in this study, is suggestive of increased bioavailability of DXR trapped in TSLs due to GNR mediated heating. The incapability of NTSL heated via GNRs in reducing tumor progression shows that the drug is not able to escape the nanocarrier. Therefore, the cytotoxic effects of the drug are also suppressed. It can be concluded that GNRs can be effectively used to remotely and locally trigger the release of the drug from nanocarriers, thereby, promoting drug distribution and bioavailability.

We further demonstrated the immediate effect of drug release from the nanocarriers on cell viability *in vivo* by using Annexin-Vivo 750 and whole body fluorescence reflectance imaging. Annexin, injected 18 hours after NIR irradiation, was able to bind to apoptotic cells *in vivo*. Imaging was conducted at 2, 4 and 24 hours post annexin administration. The fluorescent signal from each animal normalized by their respective tumor volume determined via calipers indicated a signal enhancement for all time points for animal tumors that received TSLs and were heated via GNRs using NIR. Enhancement in signal intensity can be attributed to increase in annexin binding per apoptotic tumor cell. After blood clearance of annexin at 24 hours, all treatment groups showed reduction in annexin intensity. In comparison, TSL + GNR + NIR group showed the maximum fluorescent signal per cubic millimeter indicating retention of annexin indicative of higher apoptosis due to the combination treatment.

The synergistic effect of GNRs and TSL in this study proves the principle that liposomes can be disrupted remotely and can be, especially, useful in treating tumors without the toxic exposure of the chemotherapeutic to surrounding normal tissue. The combination can provide a strong tool in increasing the effects of a chemotherapeutic. In this study, we demonstrated that when same amount of liposomal drug accumulates

passively in a tumor, the effect of release of the chemotherapeutic from a nanocarrier is much more beneficial than the drug being slowly released from the nanocarrier over time.

Successful outcome of the above study encouraged us to perform a short study and evaluate the applicability of such a combination in an orthotopic brain tumor model. TSLs encapsulating a fluorochrome ADS645WS were fabricated. The release characteristics of the dye from TSLs were found to be similar to that of DXR. We evaluated and determined a dose of GNRs needed (2.25 pmol/kg rods) to achieve heating of brain tumors to 43 ± 1˚C. We did not observe any adverse effects of GNR mediated heating of the brain tumors. Tumor bearing animals received TSL +/- GNR/NIR i.v. Explanted tumors were dissociated and analyzed for liposomally delivered dye. Flow cytometry was utilized to distinguish between non-disrupted and disrupted liposomal outcome. Animals treated with TSL + GNR + NIR demonstrated a significant increase in uptake of ADS645WS by tumor cells. The increase in uptake of ADS645WS is, therefore, a result of thermal disruption of liposomes mediated by GNRs. In addition, the percentage of tumor cells positive for ADS645WS was significantly greater in tumors explanted from animals treated with TSL + GNR + NIR compared to either TSL + GNR or TSL + NIR alone. The increased number of tumor cells uptake indicates that release of contents from the liposomes presents an opportunity for higher diffusion of a small molecule into the tumor tissue. In this study, non-thermosensitive liposomes were not evaluated for tumor dye distribution. In a plasma clearance study for liposomal DXR, TSLs showed a significantly lower half life compared to non-thermosensitive liposomes. Further studies, with the inclusion of non-thermosensitive liposomes, will help elucidate if reduced circulation has imperative effects on passive accumulation of TSLs.

Nonetheless, the above study indicates that the combination therapy can be a real advantage for orthotopic tumors.

6.3 References

1. Pastorino, F., et al., *Vascular damage and anti-angiogenic effects of tumor vessel-targeted liposomal chemotherapy.* Cancer Res., 2003. **63**(21): p. 7400-7409.
2. Gabizon, A., et al., *In vivo fate of folate-targeted polyethylene-glycol liposomes in tumor-bearing mice.* Clinical Cancer Research, 2003. **9**: p. 6551-6559.
3. Pan, X.Q., H. Hang, and R.J. Lee, *Antitumor activity of folate receptor-targeted liposomal doxorubicin in a KB oral carcinoma murine xenograft model.* Pharmaceutical research, 2003. **20**(3): p. 417-422.
4. Gabizon, A., et al., *Tumor cell targeting of liposome-entrapped drugs with phospholipid-anchored folic acid-PEG conjugates.* Adv Drug Deliv Rev, 2004. **56**(8): p. 1177-92.
5. Wu, J., Q. Liu, and R.J. Lee, *A folate receptor-targeted liposomal formulation for paclitaxel.* Int J Pharm, 2006. **316**(1-2): p. 148-53.
6. Huwyler, J., D. Wu, and W.M. Pardridge, *Brain drug delivery of small molecules using immunoliposomes.* Proc Natl Acad Sci U S A, 1996. **93**(24): p. 14164-9.
7. Harris, J.M., N.E. Martin, and M. Modi, *Pegylation: a novel process for modifying pharmacokinetics.* Clin Pharmacokinet, 2001. **40**(7): p. 539-51.
8. Eto, Y., et al., *PEGylated adenovirus vectors containing RGD peptides on the tip of PEG show high transduction efficiency and antibody evasion ability.* J Gene Med, 2005. **7**(5): p. 604-12.

9. Haran, G., et al., *Transmembrane ammonium sulfate gradients in liposomes produce efficient and stable entrapment of amphipathic weak bases.* Biochim Biophys Acta, 1993. **1151**(2): p. 201-15.

10. Bolotin, E.M., et al., *Ammonium sulfate gradients for efficient and stable remote loading of amphipathic weak bases into liposomes and ligandoliposomes.* J Liposome Res, 1994. **4**(1): p. 455-479.

11. Fritze, A., et al., *Remote loading of doxorubicin into liposomes driven by a transmembrane phosphate gradient.* Biochim Biophys Acta, 2006. **1758**(10): p. 1633-40.

12. Paasonen, L., et al., *Gold nanoparticles enable selective light-induced contents release from liposomes.* J Control Release, 2007. **122**(1): p. 86-93.

13. Drummond, D.C., et al., *Pharmacokinetics and in vivo drug release rates in liposomal nanocarrier development.* J Pharm Sci, 2008. **97**(11): p. 4696-740.

14. El-Sayed, I.H., X. Huang, and M.A. El-Sayed, *Selective laser photo-thermal therapy of epithelial carcinoma using anti-EGFR antibody conjugated gold nanoparticles.* Cancer Lett, 2006. **239**(1): p. 129-35.

15. Huang, X., et al., *Cancer cell imaging and photothermal therapy in the near-infrared region by using gold nanorods.* J Am Chem Soc, 2006. **128**(6): p. 2115-20.

16. Lee, K.S. and M.A. El-Sayed, *Gold and silver nanoparticles in sensing and imaging: sensitivity of plasmon response to size, shape, and metal composition.* J Phys Chem B, 2006. **110**(39): p. 19220-5.

17. Huang, X., et al., *Gold nanoparticles: interesting optical properties and recent applications in cancer diagnostics and therapy.* Nanomedicine (Lond), 2007. **2**(5): p. 681-93.

18. Oyelere, A.K., et al., *Peptide-conjugated gold nanorods for nuclear targeting.* Bioconjug Chem, 2007. **18**(5): p. 1490-7.

19. Dickerson, E.B., et al., *Gold nanorod assisted near-infrared plasmonic photothermal therapy (PPTT) of squamous cell carcinoma in mice.* Cancer Lett, 2008. **269**(1): p. 57-66.

20. von Maltzahn, G., et al., *SERS-Coded Gold Nanorods as a Multifunctional Platform for Densely Multiplexed Near-Infrared Imaging and Photothermal Heating.* Adv Mater, 2009. 21(31): p. 3175-3180.

21. Bremer, C., V. Ntziachristos, and R. Weissleder, Optical-based molecular imaging: contrast agents and potential medical applications. Eur Radiol, 2003. 13(2): p. 231-43.

CHAPTER 7

FUTURE DIRECTIONS

Significant research has been conducted towards the improvement of liposomal therapy since their first FDA approval; however, very little has been translated to clinical practice. The ideal chemotherapeutic liposome should be able to retain the drug, evade the RES, target the tumor, and release the drug within the tumor. In the present work, we described a few novel methods to improving liposomal targeting and efficacies and enhanced bioavailability of the drug (DXR) as compared to traditional approach like Doxil. We demonstrated a novel technique of identifying RES evading targeting ligands for improved plasma circulation and active targeting. We, further address the need to release the drug from nanocarriers, after tumor extravasation, in order to increase the distribution of the drug and overcome heterogeneous nanocarrier distribution. To this effect, we described a novel technique using synergistic application of gold nanorods and thermosensitive liposomes for increasing therapeutic efficacy.

While it is important to maintain the integrity, and the longer circulation time of a chemotherapeutic loaded nanocarrier, our findings suggest that it is absolutely necessary to make the encapsulated chemotherapeutic bioavailable to the surrounding tumor tissue. Although, targeting can be used to achieve better tissue accumulation, tissue penetration remains a problem. Slow release from the current stearically stabilized nanocarriers is clearly not enough to achieve the cytotoxicity required to overcome tumor multiplication. In all future studies, while designing a nanocarrier, it would be extremely necessary to keep in mind how to make the encapsulated drug bioavailable at doses necessary to cause

a cytotoxic effect. In addition, comparison of treatments in an appropriate animal model can severely affect the interpretation of the overall outcomes. With respect to the above discoveries, this chapter will further shed light on the future directions to optimizing the proposed nanocarriers.

7.1 Tumor model selection and *In vivo* study evaluation

7.1.1 Tumor model

In chapter 3, we used an intracranial tumor model in an immune-competent animal model show the differences in survival and evaluate efficacy of a targeted liposomal formulation. In chapter 4, we used a xenograft glioma model, where the rate of tumor growth could be evaluated as a function of treatment. Evaluation of tumor size using an intracranial tumor model can be challenging. Therefore, survival times are typically utilized for determination of therapeutic efficacy. The drawback in doing so is that reductions in tumor volume due to treatment may not be realized if the tumor is aggressive and growth recovers rapidly resulting in no significant change in survival times. Using survival as the only measure of treatment efficacy, therefore, may not be the best method to evaluate treatment efficacy. Although, the intracranial model was more relevant for translational purposes, in the xenograft model the infinite amount of space available in the subcutaneous space was able to elucidate the differences between the treatments in time. In the case of the human brain, the gliomas can grow in the order of centimeters. The time frame for vascular recruitment does not change significantly from animals to humans. Therefore, it is only appropriate to evaluate treatments in similar sized tumors. With the information about relative tumor size and treatment efficacy, further studies may be designed with the aid of computational modeling, to

assess and achieve optimal dosing quantity and frequency for enhanced tumor retardation.

7.1.2 Bioavailability of the Chemotherapeutic

The major outcome of our study is that it is necessary to make the encapsulated drug bioavailable for increased therapeutic advantage. Solid tumors exhibit interstitial fluid pressure that is higher in the tumor center compared to the periphery and surrounding tissue [1-3]. This pressure differential along with heterogeneity in blood supply leads to lower fluid extravasation in the tumor core reducing drug delivery to this region. In addition, this condition makes it difficult for macromolecules like liposomes delivered to the periphery to diffuse into tumor since they have to overcome the outward convection of fluid from regions of high to low pressure [4]. Free drug, however, should not suffer from diffusion limitations due to its small size and should be able to penetrate more deeply into the tumor resulting in a more uniform intratumoral distribution. It is therefore, imperative, to design nanocarriers realizing the method to liberate the contents for enhanced spatial distribution. At the same time, studies directed towards understanding the effect of such enhanced spatial distribution can be designed to further evaluate treatment efficacy. Further studies should be conducted to understand at the distribution of the drug (doxorubicin) in the tumor upon nanocarrier destabilization. A window chamber in tumor and intravital microscopy could be utilized to monitor the release of fluorescent doxorubicin from liposomes. Doxorubicin should be quenched inside the liposomes; however, upon thermal destabilization, doxorubicin should be free to fluoresce. Tumors, 24h after thermal destabilization of liposomes, can be removed and sectioned frozen to analyze the extent of doxorubicin distribution spatially. However, the

fluorescence detection sensitivity may be limited and it may be difficult to distinguish the drug signal from disrupted versus undisrupted liposomes. An indirect evaluation of cell apoptosis may also help understand the spatial increase in drug bioavailability due to thermal destabilization. If more amount of the drug is available, it should be able to reach or kill more number of cells in contrast to the drug trapped inside the liposomes. Therefore, an evaluation of cell death using TUNEL staining may help establish the importance of rapid drug bioavailability for enhanced tumor cell death.

In this thesis, apoptosis imaging using annexin was useful in assessing short term advantage of rapid drug release. Fluorescent *in vivo* imaging, here, was possible due the small size and transparent skin of nude mice. In a rat model, however, *in vivo* fluorescent imaging would not be possible. However, MRI can be very useful here. Iron oxide is used an MRI contrast agent. Recently, iron oxide tagged annexin V analog has been fabricated and used for apoptosis imaging [5]. The high resolution that is available on MRI, compared to the low resolution in *in vivo* fluorescent imaging, can be beneficial in elucidating the spatial distribution of the released drug, indirectly, by changes in apoptotic areas. In addition, from a translational perspective, it would be beneficial to use detection technologies that are available and useful clinically. This would lead to wider adaptation.

7.1.3 Tumor Tracking with MRI

As discussed earlier in this chapter, therapeutic efficacy could be analyzed through evaluation of changes in tumor size at a predetermined time point following treatment administration. Future studies with the nanocarriers proposed in this thesis can be evaluated in an intracranial model with the use of *in vivo* imaging modalities like MRI

to estimate the changes in tumor size. When designing a study with MRI, it is important to delineate the right parameters needed. Since gliomas tend to be more fluidic, often times water surrounding the tumor tissue can be falsely interpreted as tumor. Conversely, tumor tissue can be assumed as surrounding water. As described in detail in Appendix A, using contrast agents can significantly improve our ability to delineate tumors. However, frequent contrast agent administration can also lead to a compromised RES by means of saturation and severe systemic toxicity. Therefore, time between contrast agent administrations would need to be optimized.

It has recently been shown in our laboratory that tumor vasculature is heterogeneous spatially within a tumor type (Appendix A). In addition, the vasculature permeability varies significantly from one subject to the other and affects the chemotherapeutic outcome [6-7]. With such differences in permeability, the end outcome of two treatments can often be similar. In future studies, MRI can also be employed to select subjects with similar vascular permeability to nanocarriers. These subjects can, then, be followed up with additional nanocarrier based chemotherapy. However, such an approach can lead to RES burden. Alternatively, MRI contrast agent and chemotherapeutic agents can be co-loaded within the same nanocarrier. The chemotherapeutic outcomes can then be grouped based on the extent of vascular permeability. Treatment of tumors exhibiting highly permeable vasculature should demonstrate greater success over tumors with vessels that are less “leaky” because it is the vascular permeability, in large part, which determines the extent of extravasation. This, in turn, should allow a better comparison of therapeutic efficacy of various nanocarrier treatments.

7.1.4 Treatment Regimen

Most studies investigating targeted chemotherapeutics have not demonstrated a positive impact on therapeutic efficacy unless an aggressive treatment regimen involving multiple administrations of treatment is followed. As discussed earlier in this chapter, if the tumor growth is aggressive, when comparing targeted carriers to non-targeted liposomal carriers, the effect of a single dose may not be realized due to sudden recovery in tumor size. In a clinical setting, often times multiple chemotherapeutic regimens are administered for therapeutic benefit. In essence, at any time, there should be enough amount of drug available to achieve the rate of cell destruction greater than the rate of cell division in the tumor. Multiple treatments delivered every other day for a week and if necessary for two weeks may further help achieve such drug concentrations. In addition, by administering multiple and frequent doses, we may be able to restrict the tumor growth and elucidate the benefits of gliomas targeted nanocarriers over non-targeted nanocarriers. Consequentially, this would enable the development of functionalized nanocarriers that can be tailored to individual patients and overall increase in the therapeutic efficacy of the drug.

7.1.5 Combining Targeting and Triggered Release

The ultimate goal of nanocarrier mediated drug delivery is to achieve higher drug accumulation in the tumor and higher bioavailability of this accumulated drug to tumor cell for increased cytotoxicity. As described earlier in this thesis, phage display can help identify peptides that can bind to tumor tissue in high affinity. Future studies could also be directed towards fabricating thermosensitive liposomes with phage identified, tumor surface binding, non-internalizing peptides. The selection criteria for such peptides are

discussed in further detail below. The potential advantage of a non-internalizing targeting ligand would be higher drug accumulation and retention at the tumor site. GNRs could then be applied to remotely disrupt such liposomes for increasing drug availability and diffusion and increase therapeutic efficacy. Such a multifactorial approach can provide a significant advantage over current clinical technologies and has the potential to improve survival in tumor patients.

7.2 Selection and Validation of Targeting Ligands

7.2.1 Phage Display for Tumor Over-expressed Receptors

As is discussed in chapter 3, the RSI peptide did enable higher drug uptake *in vitro*, however, the mechanism behind the uptake was unknown since the RSI peptide receptor was unknown. Determination of the receptor can enable further modulation of the binding strength of the nanocarriers on the cell surfaces. Many factors can govern the interaction of nanocarrier presented ligand and receptors on the surface of cell. It has been shown that the distance of separation between two curved surfaces (cell and liposome) plays a significant role in the binding of ligand on the liposomes to its respective receptor on the cell [8]. As the two surfaces approach each other, the overall free energy of the system starts decreasing as a result of binding between the receptors and ligands. At a certain critical distance the overall free energy of the system reaches a minimum, coincident with the onset of spontaneous contact. It was also shown that for a ligand–receptor pair having a high association constant, the vast majority of ligand–receptor bond formation will take place at this critical distance, also defined as the binding distance. At a binding distance separation between the nanocarrier and the cell surface, the number of bonds that can be formed will therefore depend on 1) number of

ligands on the surface of nanocarrier, 2) length of tether, 3) nanocarrier size, and 4) receptor density on the surface of cell. Thus, based on a given receptor density and distribution, carriers can be tailored (by altering the tether length and number of ligands) to achieve optimal binding to the cell [9].

In addition, when designing a targeted liposome, the mechanism of targeting can help understand whether the delivery is intracellular, mediated by endocytosis, or if the targeting ligand merely enhances surface binding on the cells. In the event of a ligand binding to the surface of the cell but not being internalized, it would again have the same fate as a non-targeted liposome. As the lipids hydrolyse over time, the drug would become bioavailable slowly over time, only in this case, will be right on top of a few cells close to the vasculature. However, endocytosing receptor ligand will ensure rapid drug availability once inside the cell. A possibility is to conduct future phage panning studies using the approach described in this thesis to identify small peptide sequences binding to specific endocytosisng receptors over expressed on the specific tumor cell type. In earlier studies in our lab, we found that folate ligand can increase liposomal uptake in 9L gliomas cell 18 times over non-targeted liposomes. Hence, identifying peptides capable of evading the RES and able to bind with high affinity to receptors that can endocytose liposomes carried by the peptides may significantly enhance therapeutic efficacy.

7.2.2 In vivo Tumor Binding Validation

As discussed in chapter 3, we were not able to identify the lack of survival improvement with peptide liposomes over non-targeted liposomes. *In vivo* environment is significantly different than what can be replicated *in vitro*. Peptides identified with our specific technique if checked for binding *in vivo*, would enhance our understanding of

specific differences between *in vivo* and *in vitro* environment. *Ex vivo* slices could be obtained from orthotopically grown tumors and peptide binding to the tumor could be determined. In doing so, one can identify if the tumor phenotype changes *in vitro* to *in vivo*, and whether this change affects the binding of the phage identified peptide *in vivo*.

7.2.3 In vivo Phage Display for Peptide Motif Identification

Recently, there has been advancement in *in vivo* phage selection techniques for bind and accumulate in tumors, synovium, and vascular tissues [10-11]. In fact, a recent study has shown the advantages of simultaneously using an *in vivo* and *in vitro* phage identification for increasing specificity and binding affinity [12]. Combing the *in vitro* phage identification technique we described in chapter 3 and applying it *in vivo* can help identify a sequence that is does not elicit an immune response. In doing so, the number of peptides that can be presented on the liposomal nanocarrier may not be limited and higher binding affinity can also be achieved. These techniques, however, were not available to us at that time.

Even though some of these technologies are in their infancy, they are powerful tools that will impact the development of future tumor drug therapies. The mechanistic insight that will be obtained from exploring the interactions between different short peptides and tumor cells will further help in development of targeted therapies.

7.3 Further Evaluation and Validation of Thermosensitive Liposomes

7.3.1 Biodistribution Studies with Thermosensitive Liposomes and Gold Nanorods

In chapter 4, we discussed the benefits of a new combination therapy with gold nanorods and thermosensitive liposomes. Although we showed increased survival in a

xenograft model, further studies will be required for clinical translation. The biodistribution of the thermosensitive liposomes and related toxicity to RES organs should be evaluated and compared to the gold standard DOXIL. Cardiotoxicity is one of the biggest problems with doxorubicin therapies. The altered uptake of TSLs by the heart, liver and spleen can verify the extent of systemic cytotoxicity. In addition, histological examination and analysis of apoptosis in the tumors 24 hours after NIR treatment can help confirm the results of the *in vivo* imaging study. With the validation of these results, *in vivo* fluorescent imaging can be reliably used as measure apoptosis in future preclinical studies. Such efforts are currently underway.

7.3.2 Gold Nanorod Mediated Heating Effects

In our studies, we show that gold nanorods can be effectively used for heating intracranial tumors. However, in our studies, we used a thermo-couple to measure the temperature. The conduction of heat by the thermo-couple and the rate at which it can produce a reading can affect the end recordings. If the thermo-couple does not read temperature accurately, the end-user interpretation is also affected. It is possible in our experiment that we were able to achieve higher temperatures than were recorded due to such limitations. Determining the response rate of the thermo-couple, and the simultaneous drop in the tissue temperature, will help accurately determine the temperature rise achieved due to GNR mediated heating. Further validation with an IR thermographic camera may also be useful.

If higher temperatures were achieved, we would have to re-evaluate dosing. In the case of the brain, temperature of 45 °C can trigger hyperthermic brain death. A point source of heat, such as the tumor with GNR, at temperatures >50 °C, will heat the

surrounding normal brain tissue to hyperthermic levels. In future studies, it would be important to examine the effect of local heating and determine any detrimental damage, as a consequence, to the surrounding tissue. It would also be important to understand if increasing the laser strength to access deeply seated tumors would heat any normal tissue en-route. Brain slices of intracranial tumor animal model, after GNR mediated heating, should be obtained and stained for histopathological analysis. H/E stain can inform about the overall change in the integrity of the surrounding tissue. In addition, TUNEL staining can elucidate the extent of apoptosis or necrosis, if any, in the normal tissue. The effects of NIR heating would give us valuable insight into the clinical applicability of the proposed treatment.

7.3.3 Therapeutic Studies with Thermosensitive liposomes in an Orthotopic Brain Tumor Model

In chapter 5, we did a preliminary study with dye loaded liposomes to show the benefits of triggered release and the possibility of using gold nanorods in an intracranial model. To establish the true clinical potential of this combination, the intracranial model should be used to evaluate therapeutic efficacy. For evaluating therapeutic efficacy, all the controls, as discussed in chapter 4, should be used. In doing so, the advantage of rapid drug release and increasing drug bioavailability over the traditional liposomal carrier (Doxil) can be established. Since we saw increased clearance of thermosensitive liposomes (chapter 5) over non-thermosensitive liposomes, therapeutic studies will help elucidate if reduced circulation has imperative effects on passive accumulation of TSLs, and thereby efficacy.

In addition, NIR has a maximum penetration depth of 10 cm. In theory, if the location of the tumor is identified through imaging, the shortest distance from the surface of the skull and tumor can be computed and a hole can be drilled to access the tumor. However, the human brain is larger than 20 cm and therefore, tumors deep seated (>10 cm from the skull) may be difficult to treat with the current approach. To address the applicability of the GNR mediated thermal destabilization of liposomes in a human glioma, further studies should be conducted in larger animal models with comparable skull size. In doing so, therapeutic efficacy for deep seated tumors can be evaluated. The extent of normal tissue heating resultant of alteration in laser power can also be evaluated. For larger animals, the amount of gold nanorods needed to achieve optimal heating may need readjustment.

7.4 Gold Nanorods

7.4.1 Gold Nanorods for Hyperthermia and Triggered Content Release

As demonstrated earlier by other groups, a combination of liposomes and GNR can also be used to increase the accumulation of the chemotherapeutic in the tumor region [13-14]. This approach again manifests the overall objective of increased drug accumulation at the tumor site. An addendum to our approach could be using GNRs for hyperthermia to cause higher drug accumulation at the tumor site and then using a second NIR pulse to disrupt the liposomes. Hyperthermia from GNRs will help more liposomes accumulate in the tumor [14]. A second NIR pulse will significantly enhance the bioavailability of the drug and the overall effects of chemotherapy. In addition, by causing a higher percentage of the nanocarrier transported drug to be bioavailable, we can achieve overall reduction in the amount of drug administered systemically.

7.4.2 Gold Nanorods for Tumor Imaging and Triggered Content Release

The combination of gold nanorods and thermosensitive liposomes can also be used to treat several other solid tumors. The major drawback of thermally induced triggered release therapy is that it requires the localization of the tumor [15]. In case of metastatic tumors, such a requirement would make the application of thermally triggered liposomal chemotherapy difficult. The advantages of tumor size and treatment monitoring through imaging have been stressed upon, and discussed at different times in this chapter. GNRs may, also, serve as additional tools for non invasive tracking of tumors using optical coherence tomography and photoacoustic tomography as has been demonstrated elsewhere [16]. In doing so, the exact location of the tumor can be identified. Since gold nanorods can serve both as heating antennas and imaging contrast agents, the need for an additional contrast agent administration, for using other modalities like MRI, can be eliminated. Further development of this multifaceted combinatorial approach of imaging and thermally destablizable liposomal therapy can really be useful clinically.

7.5 Iron oxide as an Alternative to Gold Nanorods

Another approach to remote triggered release from thermosensitive liposomes can be the use of iron oxide particles. Iron oxide nanoparticles have been demonstrated for inducing hyperthermia, in earlier reports, by use of low frequency <200k electromagnetic waves [17-18]. Iron oxide has also been shown to be a powerful MRI contrast agent for tumors [19-21]. For unreachable deep seated solid tumors, where hyperthermia is difficult to achieve with the use of traditional tools like a water bath or GNRs, combining iron oxide for disruption of thermosensitive liposomes can provide an alternative

synergistic tool for imaging and treatment. Since iron oxide particles are also cleared from the circulation by the components of the RES, using a whole body coil to achieve heating in the desired tissue could significantly heat the liver and kidney as well. Therefore, the design of the coil as well as the applicability of this technique will be limited by the location of the tumor (brain versus the abdomen). Further investigation is warranted to tailor such a setup for any clinical benefit.

7.6 Conclusions

Much work has been presented in this thesis to overcome the current challenges to nanochemotherapies. In conclusion, any cargo, be it protein, DNA, RNA, or drug, carried within the nanocarriers will show benefit if the bioavailability of such contents is ample to achieve the desired effect. Remotely triggered liposomes by gold nanorods offer a potential platform for advanced drug delivery. The possibility to control the time, place, and rate of drug release can provide better therapeutic response and less adverse effects by increasing the drug distribution to the target tissue. By selecting the liposomal formulation, triggering signal, and the mechanism of action to be suitable for a specific application, liposomes could be utilized in numerous medical treatments for enhanced efficacy. Future studies, as described in this chapter, can further help improve and optimize these approaches for potential translation into the clinic.

7.7 References

1. Jain, R.K. and L.T. Baxter, *Mechanisms of heterogeneous distribution of monoclonal antibodies and other macromolecules in tumors: significance of elevated interstitial pressure.* Cancer Res, 1988. **48**(24 Pt 1): p. 7022-32.

2. Baxter, L.T. and R.K. Jain, *Transport of fluid and macromolecules in tumors. I. Role of interstitial pressure and convection.* Microvasc Res, 1989. **37**(1): p. 77-104.

3. Boucher, Y., L.T. Baxter, and R.K. Jain, *Interstitial pressure gradients in tissue-isolated and subcutaneous tumors: implications for therapy.* Cancer Res, 1990. **50**(15): p. 4478-84.

4. Jain, R.K., *Delivery of molecular and cellular medicine to solid tumors.* Adv Drug Deliv Rev, 2001. **46**(1-3): p. 149-68.

5. Kenneth T. Cheng, Sam Gambhir, and Z. Cheng., *[18F]FB-(Ac-NIe-Asp-His-d-Phe-Arg-Trp-Gly-Lys-NH2). [18F]FB-NAPamide.* . In: Molecular Imaging and Contrast Agent Database (MICAD) [database online]. Bethesda (MD): National Library of Medicine (US), NCBI; Available from: http://micad.nih.gov., 2004-2009.

6. Karathanasis, E., et al., *Tumor vascular permeability to a nanoprobe correlates to tumor-specific expression levels of angiogenic markers.* PLoS One, 2009. **4**(6): p. e5843.

7. Karathanasis E, et al., *MRI mediated, non-invasive tracking of intratumoral distribution of nanocarriers in rat glioma.* Nanotechnology, 2008. **19**(31): p. 315101.

8. Jeppesen C, et al., *Impact of polymer tether length on multiple ligand–receptor bond formation.* Science, 2003. **2001**: p. 465-468.

9. Ghaghada, K.B., et al., *Folate targeting of drug carriers: A mathematical model.* J Control Release, 2005. **104**(1): p. 113-28.

10. Laakkonen, P., et al., *Antitumor activity of a homing peptide that targets tumor lymphatics and tumor cells.* Proc Natl Acad Sci U S A, 2004. **101**(25): p. 9381-6.

11. Mi, Z., et al., *Identification of a synovial fibroblast-specific protein transduction domain for delivery of apoptotic agents to hyperplastic synovium.* Mol Ther, 2003. **8**(2): p. 295-305.

12. Whitney, M., et al., *Parallel in vivo and in vitro selection using phage display identifies protease-dependent tumor-targeting peptides.* J Biol Chem, 2010. **285**(29): p. 22532-41.

13. Park, J.H., et al., *Cooperative nanoparticles for tumor detection and photothermally triggered drug delivery.* Adv Mater, 2010. **22**(8): p. 880-5.

14. Park, J.H., et al., *Cooperative nanomaterial system to sensitize, target, and treat tumors.* Proc Natl Acad Sci U S A, 2010. **107**(3): p. 981-6.

15. Kong, G. and M.W. Dewhirst, *Hyperthermia and liposomes.* Int J Hyperthermia, 1999. **15**(5): p. 345-70.

16. Wei, A., A.P. Leonov, and Q. Wei, *Gold nanorods: multifunctional agents for cancer imaging and therapy.* Methods Mol Biol, 2010. **624**: p. 119-30.

17. Mitsumori, M., et al., *Development of intra-arterial hyperthermia using a dextran-magnetite complex.* Int J Hyperthermia, 1994. **10**(6): p. 785-93.

18. Shinkai, M., et al., *Antibody-conjugated magnetoliposomes for targeting cancer cells and their application in hyperthermia.* Biotechnol Appl Biochem, 1995. **21 (Pt 2)**: p. 125-37.

19. Weissleder, R., et al., *Superparamagnetic iron oxide: enhanced detection of focal splenic tumors with MR imaging.* Radiology, 1988. **169**(2): p. 399-403.

20. Stark, D.D., et al., *Superparamagnetic iron oxide: clinical application as a contrast agent for MR imaging of the liver.* Radiology, 1988. **168**(2): p. 297-301.

21. Moffat, B.A., et al., *A novel polyacrylamide magnetic nanoparticle contrast agent for molecular imaging using MRI.* Mol Imaging, 2003. **2**(4): p. 324-32.

APPENDIX A

MRI MEDIATED, NON-INVASIVE TRACKING OF INTRATUMORAL DISTRIBUTION OF NANOCARRIERS IN RAT GLIOMA

As published with Karathanasis E, Park J, Patel V, Zhao F, Hu X, and Bellamkonda RV in Nanotechnology, 2008, 19:315101.

The following text, figures, and tables comprise a manuscript published in Nanotechnology related to the non-invasive tracking of contrast agents to tumors using liposomes. The manuscript is included for reference purposes in regards to the dissertational work provided in the main text.

Abstract

Nanocarrier mediated therapy of gliomas has shown promise. The success of systemic nanocarrier-based chemotherapy is critically dependent on the so-called leaky vasculature to permit drug extravasation across the blood-brain barrier. Yet, the extent of vascular permeability in individual tumors varies widely, resulting in a correspondingly wide range of responses to the therapy. However, there exist no tools currently to rationally determine whether tumor blood vessels are amenable to nanocarrier mediated therapy in an individualized, patient specific manner today. To address this need for brain tumor therapy, we have developed a multifunctional 100nm-scale liposomal agent encapsulating a gadolinium-based contrast agent for contrast enhanced Magnetic Resonance Imaging with prolonged blood circulation. Using a 9.4 Tesla MRI system, we

were able to track the intratumoral distribution of the gadolinium-loaded nanocarrier in rat glioma model for a period of three days due to improved magnetic properties of the contrast agent being packaged in a nanocarrier. Such a nanocarrier provides a tool to non-invasively assess the suitability of tumors to nanocarrier mediated therapy and then optimize the treatment protocol for each individual tumor. Additionally, the ability to image the tumor in high resolution can potentially constitute a surgical planning tool for tumor resection.

A.1. Introduction

Current approaches for the treatment of glioma are limited in their effectiveness because malignant brain tumors are characteristically diffuse, highly invasive, and non-localized (Black and Pikul, 1999). Complete surgical resection of malignant gliomas is a rarity, partly due to the inability to clearly map the tumor, and partly because of its invasive nature. Therefore, clinical standard of care includes radiation therapy and systemic and topical chemotherapy after surgical resection. Unfortunately, radiation and topical delivery of chemotherapeutics using polymer wafers have poor results and extend the median survival by 2-9 months and systemic chemotherapy has been minimally effective (Barker *et al.*, 1998; Fine *et al.*, 1993) . Given the diffuse and invasive nature of gliomas, the success of systemic chemotherapy is critically dependent on the so-called leaky vasculature to permit drug extravasation across the blood-brain barrier (BBB). Currently, systemic chemotherapy is not the primary treatment of choice for malignant brain tumors due to the exposure of non-target organs to chemotherapeutic resulting from systemic administration and due to the presence of the highly impermeable BBB, which limits transport to lipophilic or low molecular weight, uncharged compounds. Therefore,

new strategies improving systemic delivery of chemotherapeutics will be a potent tool for treatment of gliomas.

Nanocarrier mediated therapy of gliomas has shown promise because multifunctional nanocarriers can (i) carry large payloads of one or more types of drugs for therapy or contrast agents for imaging or combos of drugs and contrast agents, and (ii) manipulate pharmacokinetics and biodistribution of systemically administered agents to increase accumulation in tumor site. This multifunctionality of nanoscale systems is projected to enable personalized cancer therapy by diagnosing, treating, and monitoring the progress of treatment for each individual cancer (Service, 2005; van de Wiele *et al.*, 2002; Koning and Krijger, 2007; Torchilin, 2006; Mitra *et al.*, 2006). Such nanocarriers can theoretically be designed not only to carry a range of chemotherapeutic or anti-invasive agents (not just low molecular weight, uncharged lipophilic drugs), but also to both passively and actively target intracranial tumors such as gliomas. Passive targeting results from prolonged circulation of nanocarriers allowing for accumulation at sites with abnormal, leaky vasculature. In recent rodent studies of glioma, effective passive tumor dosing was achieved by intravenous (IV) injections of drug-loaded liposomal nanocarriers (R.D. Arnold *et al.*, 2005). It was demonstrated in patients with glioblastomas and metastatic brain tumors that long circulating liposomal nanocarriers overcome the BBB in the tumor lesions resulting in 13-19 times higher accumulation in the glioblastoma as compared to the normal brain (M.I. Koukourakis *et al.*, 2000). In addition, active targeting can be achieved by decorating nanocarriers with multiple ligands to increase targeting affinity and selectivity by binding to multiple receptors of the same or different type on cancer cells (Saul *et al.*, 2006; Hong *et al.*, 2007).

The success of passive (and subsequent active) targeting of nanoscale chemotherapeutic agent therapy for intracranial tumors is critically dependent on the access that these agents have to tumors via the leaky vasculature across the BBB (Jain, 1994, 2001; Maeda *et al.*, 2000). Unfortunately, it is well-known that the degree of tumor vascular leakiness differs not only among same type tumors but even spatially within the same tumor (Fukumura and Jain, 2007; Hobbs *et al.*, 1998; Yuan *et al.*, 1996). For instance, previous studies in our laboratory showed that the standard deviation of the intratumoral accumulation of liposomal doxorubicin in a rat brain tumor was 150% of the mean value (McNeeley *et al.*, 2007). However, there exist no tools currently to rationally determine whether tumor blood vessels are amenable to nanocarrier mediated therapy in an individualized, patient specific manner today. Such a determination would no doubt be of great benefit for the planning and assessment of multiple chemotherapeutic strategies. One recent example demonstrating the critical role that tumor vessels play in determining therapeutic outcomes comes from the work of Jain et al, where they demonstrate the modulation of tumor vessels by normalizing them leads to better chemotherapeutic outcomes (Jain, 2005).

Here, we report the development of a multifunctional long-circulating nanocarrier trackable by Magnetic Resonance Imaging (MRI). The nanocarrier consists of a 100nm-scale Pegylated liposomal carrier encapsulating Gadolinium (Gd) and/or a chemotherapeutics. Conventional MR contrast agents, such as Gd chelates, restrict the time window for image acquisition due to their rapid elimination from blood. In the recent past, we demonstrated that the prolonged blood circulation of the agent allowed enhanced signal for long scanning times resulting in high resolution MR images of rat

vasculature (Ayyagari *et al.*, 2006). Other groups have also utilized Gd-loaded liposomal formulations as a paramagnetic agent for angiography resulting in a positive signal enhancement associated with T_1-shortening (Ghaghada *et al.*, 2007; Erdogan *et al.*, 2008; Erdogan *et al.*, 2006; Torchilin, 1994; Krauze *et al.*, 2006; Weissing *et al.*, 2000). In this work, we have validated the utility of the Gd-nanocarrier for non-invasive determination of tumor vasculature permeability to nanoparticles in 9L glioma model rat using a 9.4 Tesla Bruker Biospin MR system. Interestingly, under this strength of the magnetic field, the Gd-containing nanocarrier produces negative signal enhancement due to significant T_2 shortening resulting in a more potent contrast agent. While more intricate nanoparticle systems are novel from a materials science perspective, their potential for translation to clinical use is limited by the dearth of knowledge about their toxicity, biodistribution and in vivo fate, while liposomal nanoparticles are relatively well characterized and thus provide the potential for rapid translation to the clinic. For instance, nanoscale liposomal doxorubicin formulations were the first nanotherapeutics to be approved for clinical use as the first line for treatment of AIDS-related Kaposi's Sarcoma and relapsed ovarian cancer (Lasic and Papahadjopoulos, 1995) and is under numerous clinical trials (128 active studies) for treatment of many types of cancer (www.ClinicalTrials.gov; accessed 12/12/2007). Besides liposomal doxorubicin, other liposomal formulations (Ferrari, 2005), polymeric micelles and polymer-based particles (Heath and Davis, 2007; Schiffelers *et al.*, 2004; Kim and Rossi, 2007) are under preclinical and clinical evaluation.

A.2. Materials and Methods

A.2.1. Materials

The phospholipids 1,2-dipalmitoyl-sn-glycero-3-phosphocholine (DPPC) and 1,2 disteroyl-sn-glycero-phosphoethanolamine poly(ethylene glycol)$_{2000}$ (DSPE-PEG$_{2000}$) were purchased from Genzyme Pharmaceuticals (Cambridge, MA). Cholesterol was purchased from Sigma (St. Louis, MO). Gadodiamide (Omniscan) was obtained from GE Healthcare (Milwaukee, WI). 1,2-Dipalmitoyl-sn-glycero-phosphoethanolamine-N-(lissamine rhodamine B sulfonyl) (DPPE-Lissamine-Rhodamine) was purchased from Avanti Lipids (Birmingham, AL). Mouse monoclonal anti-rat CD31 antibody was obtained from BD Biosciences Pharmingen (San Diego, CA). The mouse anti-rat RECA-1 monoclonal antibody (IgG1) was purchased from GeneTex (San Antonio, TX). The secondary antibodies, Alexa Fluor 594 goat anti-rabbit IgG and Alexa Fluor 488 goat anti-mouse, and 2-(3-(diphenylhexatrienyl)propanoyl)-1-hexadecanoyl-*sn*-glycero-3-phosphocholine (β-DPH-HPC) were purchased from Invitrogen (Carlsbad, CA). All animals were purchased from Harlan (Indianapolis, IN). A 9L glioma cell line was received as a generous donation from the Neurosurgery Tissue Bank at UCSF. Minimal essential medium containing Earle's balanced salt solution (MEM/EBSS) was purchased from Hyclone (Logan, UT). Gentamicin (50 mg/ml), fetal bovine serum (FBS), and Leibovitz's L-15 medium were obtained from Gibco (Carlsbad, CA). Trypsin-EDTA (0.05% trypsin, 0.53 mM EDTA) in Hanks' balanced salt solution was purchased from Mediatech (Herndon, VA). Heparin and isoflurane were obtained from Baxter Healthcare (Deerfield, IL). Ketamine was purchased from Fort Dodge Laboratories (Madison, NJ). Marcaine was obtained from Abbott Laboratories (Abbott Park, IL). Flunixin meglumine

was purchased from Phoenix Scientific (San Marcos, CA). Xylazine was purchased from The Butler Company (Dublin, OH). Acetylpromazine (10 mg/ml) was obtained from Boehringer Ingelheim (Ingelheim, Germany). The rest of the reagents were of analytical grade (Fisher Scientific, Atlanta, GA).

A.2.2. Fabrication and Characterization of the Gd-nanocarrier

A lipid composition of DPPC, cholesterol and DSPE-PEG_{2000} in the molar ratio of 55: 40: 5 was used. Fluorescent phospholipid (β-DPH-HPC) at 0.01 mol% was used to track phospholipid content. The formulations used in the *in vivo* imaging studies were tagged with DPPE-Lissamine-Rhodamine at 1 mol% of the total lipids (for fluorescent microscopy of tissue sections as described in section 2.8). The lipids were dissolved in ethanol and hydrated with 0.5 M gadodiamide (Gd) solution at 60°C followed by sequential extrusion in a Lipex Biomembranes Extruder (Northern Lipids, Vancouver, Canada), to size the liposomal nanocarrier to about 100 nm. Free, un-encapsulated gadodiamide was replaced by a saline solution (300 mM NaCl; 596 mOsm/kg water) with comparable osmolarity as the internal phase of the nanocarrier using a 2-day dialysis with a 100k molecular weight cutoff dialysis tubing. The size of the Gd-nanocarrier was determined by dynamic light scattering (90 Plus Particle Size Analyzer, Brookhaven Instruments, Holtsville, NY). The osmolality of the nanocarrier was determined using a vapor osmometer (Wescor, Logan, UT).

A.2.3. In vitro T_1 and T_2 Measurements

In vitro, the spin-lattice T_1 and spin-spin T_2 relaxation times of the Gd-nanocarrier suspension and gadodiamide solution were determined on a 0.47 T Bruker Minispec NMR system at 37°C. The longitudinal and transverse relaxation rates were determined

by an inversion recovery pulse sequence and a spin-echo sequence, respectively. To determine the effective Gd concentration, the liposomal nanocarrier was lysed with 20% SDS (sodium dodecyl sulfate). The effective relaxivity (per unit Gd concentration) in the nanocarrier was then determined from the equation: $r_1 = (T_{1Gd}^{-1} - T_{1noGd}^{-1})/[Gd]$; where T_{1Gd} (or T_{2Gd}) is the observed T_1 (or T_2) relaxation time for the Gd-containing formulations, T_{1noGd} (or T_{2noGd}) is the observed T_1 (or T_2) relaxation time for the buffer, and r_1 (or r_2) is the relaxivity of gadodiamide at 37°C. T_1 and T_2 relaxation times of the formulations were measured over a concentration range of 0.5–2.0 mM Gd. The r_1 (and r_2) relaxivity were then determined from the slope of the linear regression fits of $1/T_1$ (and $1/T_2$) against the Gd concentration.

Comparative T_1 and T_2 measurement at 9.4 T were performed on a Bruker Biospin MR system. A series of fast imaging in steady-state precession (TrueFISP) sequences was performed for T_1 measurements. The parameters for the TrueFISP were TR/TE = 3 msec/1.5msec, delay time = 8 sec. A total of 40 frames were acquired during one excitation with inversion time (TI) linearly ranged from 50 msec to 6 sec. The field of view (FOV) was 4 × 4 cm^2 with a matrix of 128 × 128. A series of Multiple Slices Multiple Echos (MSME) sequences was performed for T2 measurements. The pulse sequence parameters were TR = 4 sec, number of echoes = 8 with TE of 9, 18, 27, 36, 45, 54, 63, 72 msec; FOV=4 × 4 cm2 with a matrix of 128 × 128.

A.2.4. Ex vivo T1 and T2 Measurements

All of the animal experiments were carried out in compliance with the institutional animal use and care protocols of the Georgia Institute of Technology and Emory University. Under anesthesia with 2-3% inhalant isoflurane, 9–10 week old male

Fisher 344 rats were injected with 0.25 mmol Gd/kg body weight of either the Gd-nanocarrier (n=3) or gadodiamide (n=3) intravenously (IV) in the tail vein using a 24G catheter. Blood samples were withdrawn orbitally once before injection and at 5, 35, 60, 180, 240 and 300 min after injection and transferred to heparinized blood tubes. Plasma was collected by centrifugation at 2,000 rpm. The plasma T_1 and T_2 values were measured immediately as described above on the 9.4 Tesla Bruker Biospin MR system.

A.2.5. 9L glioma Cell Culture

9L glioma cell line was maintained in MEM/EBSS medium supplemented with 10% fetal bovine serum and 0.05 mg/mL gentamicin. Cells were passaged by trypsinization and washed with growth medium. Prior to implantation, cells were resuspended in serum-free Leibovitz's L-15 medium to a concentration of 2×10^8 cells/ml.

A.2.6. Tumor Inoculation

A rat glioma model was established by surgically implanting 2×10^6 9L glioma cells into the frontal lobe of 9–10 week old male Fisher 344 rats. All procedures were conducted under a protocol approved by the Institutional Animal Care and Use Committee (IACUC) at Georgia Institute of Technology. During surgery, anesthesia was maintained through the administration of 2-3% inhalant isoflurane. The incision site was shaved and the animal mounted in a stereotaxic frame. The scalp was opened to expose the skull, and a burr hole was drilled 2 mm anterior and 2 mm lateral to the bregma. 2×10^6 9L glioma cells in 10 μl of Leibovitz's L-15 medium were slowly injected into the frontal lobe through a 21-gauge needle at a depth of 3 mm below the brain surface. The burr hole was then sealed with bone wax, and the scalp was sutured closed. Animals

received 5 ml Lactated Ringer's solution through intraperitoneal (IP) injection and a subcutaneous injection of 0.5% marcaine at the wound site. Flunixin meglumine (2.5 mg/kg) was administered through an intramuscular injection to alleviate pain as needed.

A.2.7. In vivo Images

All MRI image data were acquired on the 9.4 T Bruker system. A volume coil (72-mm inner diameter) and an inductively coupled surface coil (20-mm diameter) for signal built saddle volume coil was employed. High resolution angiograms of the rat brain (n=1) were obtained before and 15 min after IV injection of the Gd-nanocarrier (at a dose of 0.25 mmol Gd/kg b.w.) using a T_2*-weighted 3D FLASH sequence with the following parameters: TR/TE=50/15 msec, flip angle=30°, matrix=512 x 384 x 32, FOV=4 x 3 x 0.5 cm^3, and 8 averages (scan time = 81 min) for high resolution brain angiography. This resulted in an in-plane spatial resolution of 78 μm and a slice thickness of 156 μm.

The intratumoral extravascular accumulation of the nanocarrier was monitored by employing a 3D FLASH sequence with shorter scan time (and lower spatial resolution) than the high resolution angiograms with the following parameters: TR/TE=50/15 msec, flip angle=30°, matrix=256 x 256 x 32, FOV=4 x 3 x 0.75 cm^3, and 2 averages (scan time = 13 min). This resulted in a spatial resolution of 156 x 117 x 234 μm. Two groups of animals were monitored for a period of 3 days after injection of 0.25 mmol Gd/kg b.w. of the nanocarrier (group A; n=3) and injection of a saline solution at equal volume to the nanocarrier (group B; n=3). Imaging was performed pre-injection and 5 min, 1 day and 3 days post-injection. Care was taken to maintain similar positioning of the animal for pre- and post-contrast images. After each 3D imaging session, a T_2*-weighted 2D map was

obtained using a multi-gradient echo (MGE) sequence with the following parameters: TR/TE=500/3 msec, number of echoes = 12, matrix=128 x 128, FOV=3.4 x 3.4 cm^3, and 8 averages (scan time = 9 min). At day 3 post-injection, the animals were euthanized immediately after completion of the last imaging session and histological analysis was performed as described below.

A.2.8. Immunohistochemistry and Histological Evaluation of Explanted Tumors

Upon completion of the imaging study, the animals were anesthetized with ketamine (1 mg/kg) and xylazine (0.17 mg/kg), transcardially perfused with 4% paraformaldehyde, the tumors were retrieved, and stored in 4% paraformaldehyde. The tumors were transferred from 4% paraformaldehyde to 30% sucrose and allowed to incubate for 48-72 h. Serial coronal cryostat (Leica CM 300, Leica, Bannockburn, IL) sections of 16 μm thickness were made and mounted onto glass slides. Care was taken to obtain brain sections with the same orientation as that of the MR images. To visualize the tumor microvasculature, the tissue slices were immunohistochemically stained with RECA-1, a cell surface antigen which is expressed by all rat endothelial cells. After three washes in PBS for 10 min each, the sections were incubated in 4% goat serum and 0.5% Triton X-100 for 1 hr. Upon adding the primary antibody (1:250 dilution) in 4% goat serum and 0.5% Triton X-100, the sections were incubated at 4 °C overnight. After washing the sections three times with PBS, the secondary antibody (1:220 dilution), Alexa Fluor 488 goat anti-mouse IgG, was added and allowed to incubate for 1 hr. The sections were washed three times with PBS, incubated with DAPI (nuclear stain) for 15 min followed by three washes with PBS and covered with glass coverslips. The tumor sections were imaged at 20x on the Nikon Eclipse 80i upright microscope using a

Microfire CCD camera (Optronics, Golate, CA) that interfaced with the Neurolucida software (MicroBrightField Bioscience, Williston, VT) to obtain a 2D montage of the entire brain tissue section.

A.2.9. Data and Statistical Analysis

The plasma T_1 and T_2 values measured *ex vivo* (Fig. A.2) and the T_2* values obtained from *in vivo* 2D mapping (Fig. A.5) are expressed as mean ± standard deviation. To determine the significance of the relaxation times among the various animal groups at different time points, an unpaired t test analysis was performed. A p-value less than 0.05 was used to confirm significant differences at the 95% confidence level. The analysis was performed using the Minitab software.

A.3. Results and Discussion

A.3.1. In vitro Characterization of the Gd-nanocarrier

The liposomal Gd-nanocarrier contained 150 mM lipids and 87 mM Gd, 100% of Gd being encapsulated within the liposomes. The average diameter of the Gd-nanocarrier was 98 nm (standard deviation = 9 nm) as determined by dynamic light scattering, a size known to prevent renal clearance while allowing extravasation. The 600 mOsm/kg water osmolality of the formulation allowed intravenous injection, since the liposomal walls can sustain the osmotic pressures expected to occur in isotonic environments. Indeed, in vitro leakage experiment against isotonic phosphate buffered saline exhibited very low leakage of the encapsulated Gd (less than 6% of the initial payload) over a period of 3 days.

The r_1 and r_2 relaxivities of the Gd-nanocarrier at 25 °C and 9.4 T were 0.65 and 20.7 s^{-1} mM^{-1}, respectively (Figure 1). At the high magnetic field of 9.4 T, the r_2/r_1 ratio of the Gd- nanocarrier substantially increased, which is expected since the r_2/r_1 ratio usually increases with increasing resonance frequencies (Strijkers *et al.*, 2005). Previous studies have measured the r2 relaxivity of liposomal Gd to be around 1 s^{-1} mM^{-1}on 0.47 T magnets, a value significantly smaller than the one measured on the 9.4 T system. This high r_2 value allowed us to use the Gd- nanocarrier in the *in vivo* imaging studies as a T_2-shortening agent.

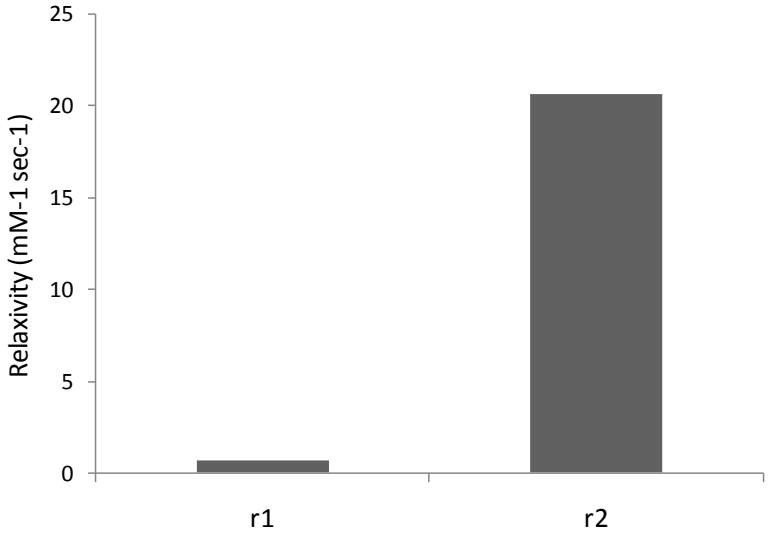

Figure A.1. In vitro r1 and r2 relaxivities of the Gd-nanocarrier measured on 9.4 T and 25 °C.

A.3.2. Ex vivo Plasma T_1 and T_2 Measurements

Figure 2.a shows the changes in plasma T_1 relaxation time measured at 9.4 T following administration of Gd- nanocarrier and gadodiamide. At t=5 min after administration of the nanocarrier, a sharp decrease of the T_1 value from the pre-injection value of 2500 msec to the post-injection value of 570 msec was observed. Due to the prolonged blood residence time of the nanocarrier (Lasic and Martin, 1995), the plasma

T_1 value remained at low values of about 650 msec for the rest of the duration of the experiment. While we did not attempt to measure the blood half life ($t_{1/2}$) in this study, we have shown that liposomes of similar size and lipid composition as the Gd-nanocarrier have a $t_{1/2}$ of about 18 h in Fisher rats (McNeeley *et al.*, 2007). In a previous study (Ayyagari *et al.*, 2006), we observed that the post-injection T_1 values were about 180 msec measured at 0.47 T upon administration of the Gd-nanocarrier at a dose similar to the one used in the current study. This difference is expected since higher resonance frequencies (or magnetic strength such as that used in the current study) produce longer T_1 values. Following administration of (non-liposomal) gadodiamide, the plasma T_1 value decreased to about 450 msec at 5 min post-injection. The rapid clearance of the agent from blood circulation resulted in a rapid increase of the T_1 value reaching the pre-injection value within 2 h after administration. Similarly, administration of the Gd-nanocarrier resulted in a rapid drop of the plasma T_2 value from the pre-injected value of 113 msec to the post-injection value of about 16 msec which remained at these low values for the rest of the duration of the experiment (Figure 2.b). Such low plasma T_2 values suggest that the gadolinium-based contrast agent being packaged in the nanocarrier displays improved magnetic properties when used as a T_2-shortening agent at the high magnetic field of 9.4 T. Upon injection of (non-liposomal) gadodiamide, the plasma T_2 value dropped to 59 msec at 5 min post-injection and then rapidly returned to the pre-injection value.

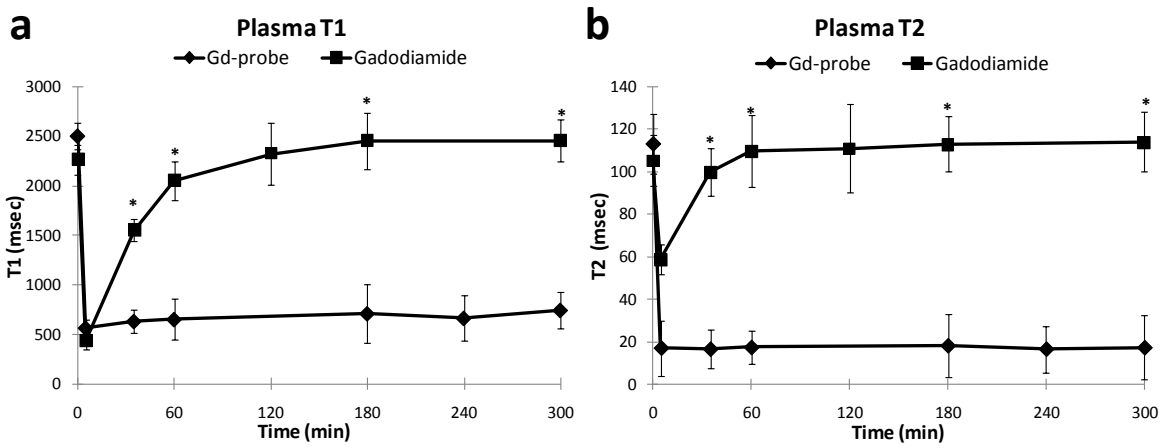

Figure A.2. Plasma relaxation time (a) T1 and (b) T2 measured ex vivo on 9.4 T after administration of the liposomal Gd-nanocarrier (n=3) and gadodiamide (n=3) at a dose of 0.25 mmol Gd/kg. The * indicates significant statistical difference ($p<0.05$) between the Gd- nanocarrier and gadodiamide.

A.3.3. MR Angiograms

Figure 3 shows high resolution coronal T_2*-weighted images obtained using the 9.4 T MRI before and after administration of the Gd-nanocarrier. It should be noted that the scanning parameters in the pre-and post-contrast images were identical. In the pre-contrast image (Figure 3.a), few blood vessels (appear as black dots) of the vasculature of the cerebral cortex can be seen in the healthy tissue or in the cancerous lesion located in the front of the right hemisphere (as indicated by the arrow). The prolonged blood circulation of the Gd-nanocarrier allowed negatively enhanced signal for long time increasing scanning times and the time window for image acquisition (subsequently lowering the signal to noise ratio). Administration of the nanoscale agent allowed clear visualization of the cerebral vasculature (Figure 3.b). Importantly, details of the glioma vasculature were revealed in the post-contrast image. The tumor lesion

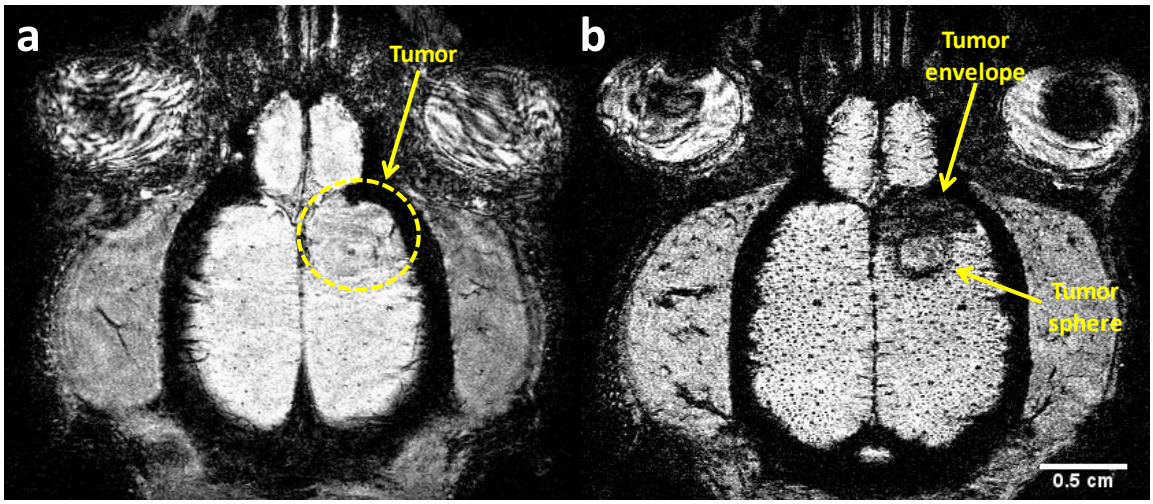

Figure A.3. High resolution (78 µm in-plane resolution) coronal T2*-weighted images of rat brain on a 9.4 T MRI. (a) In the pre-contrast image, minor vasculature enhancement was seen in the normal cerebral tissue and tumor (arrow). (b) Administration of 0.25 mmol Gd/kg of the nanocarrier allowed clear visualization of the vasculature of the normal cerebral tissue. The post-contrast image revealed a spherical part of the tumor lesion with highly vascularized rim and a less vascularized inner core and a very well-vascularized envelope-shaped part of the lesion (scale bar is 0.5 cm).

consisted of a spherical and an envelope-shaped part (as indicated in Figure 3.b). The sphere part (where originally inoculation of the cancer cells occurred) was characterized by a highly vascularized peripheral rim which is usually associated with high levels of angiogenic and permeability factors resulting in neoangiogenesis (Damert *et al.*, 1997; Takano *et al.*, 1996) and an inner core with less vascularization. The entire envelope (the other portion of the tumor) appeared highly vascularized. In previous studies (McNeeley *et al.*, 2007), we have observed in many cases a similar pattern where the glioma grows initially as a sphere and then grows towards the front of the lobe most likely due to less restriction (e.g. pressure).

A.3.4. Intratumoral Visualization of the Nanocarrier

The Gd-nanocarrier was tested in adult male rats using an orthotopic brain tumor model developed by inoculation of 9L glioma cells. By utilizing a fast imaging protocol (with a duration of 13 min), we were able to obtain images of the brain with a spatial resolution

of 156 x 117 x 234 μm. Figure 4 shows brain images of the same animal before and 5 min, 1 day and 3

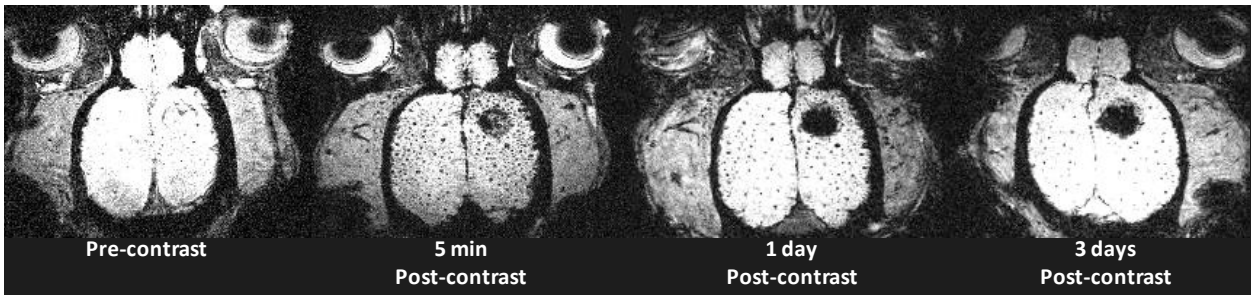

Figure A.4. Coronal T_2*-weighted images of rat brain with spatial resolution of 156 x 117 x 234 μm obtained before and 5 min, 1 day and 3 days after administration of the Gd-nanocarrier at a dose of 0.25 mmol Gd/kg on a 9.4 T MRI.

days after injection of the Gd- nanocarrier. High density vasculature in normal and tumor tissue can be visualized immediately after injection. Over the time course of three days, the tumor exhibited increasing negative enhancement whereas the negative enhancement of the blood vessels in normal tissue was disappearing. This is consistent with clearance of the nanocarrier from circulation while accumulation of the agent within the intratumoral extravascular space via extravasation through the tumor's leaky vasculature was increasing. It should be noted that the vasculature of normal brain with intact BBB is impermeable to the nanocarrier. In previous reports from our lab (McNeeley *et al.*, 2007), we have shown that the half life ($t_{1/2}$) of liposomes in rat blood circulation is about 18 h and that less than 10% of the nanocarrier remained in circulation at three days post-injection. To verify the low levels of the nanocarrier in blood, a blood sample was obtained and measured *ex vivo* using the 9.4 T MRI (similar to the measurements in section 3.2). The plasma T_2 value at 3 days post-contrast was 108 msec which is close to the pre-contrast values. A comparison of the enhancement of normal brain vasculature in the pre-contrast and in the 3-day post-contrast image (Figure 4) also supports the fact that

low levels of the nanocarrier remained in circulation 3 days after administration. This allowed clear visualization of the extravascular accumulation of the nanocarrier since minor interfering signal was obtained from the blood side. The time course of the increase of tumor enhancement is consistent with previous reports in which biodistribution studies showed that the liposome intratumoral accumulation in rat brain tumors (McNeeley *et al.*, 2007) and mouse breast tumors (Kirpotin *et al.*, 2006) peaks at 24-48 h after injection.

Gadodiamide chelates have been extensively employed to perform dynamic contrast-enhanced MRI to evaluate tumor vasculature leakiness in animals and patients (Brix *et al.*, 2004; Furman-Haran and Degani, 2002; Leach, 2001; Oshida *et al.*, 2005; Sardanelli *et al.*, 2005); (Teifke *et al.*, 2006). These studies show that the temporal intratumoral uptake of the contrast agent displays a fast wash-in-wash-out profile indicating that the agent leaks out of the blood vessel into the tumor extravascular space and returns back to the blood in short times. This is not surprising since the transport of molecules (such as gadodiamide) is governed by passive diffusion, whereas extravasation of nanoparticles is governed by convective terms and therefore once a liposome extravasates it is generally difficult to return back to blood stream (Jain, 1999). While it's difficult to directly determine whether the Gd chelate was intra-liposomal when the nanocarrier was deposited in the tumor extravascular space, it is reasonable to assume that the chelate would quickly return to the blood if it were not encapsulated within the liposome.

To better realize the intratumoral accumulation of the nanocarrier, we performed T_2* mapping and subsequently quantified the T_2* values of the normal and the tumor

tissue. Figure 5 summarizes these findings. Even before administration of the nanocarrier, the tumor tissue displayed significantly lower T_2* values than normal brain consistent with cancer-related neovascularization resulting in higher density of vasculature in the tumor comparing to normal brain. Immediately after administration of the nanocarrier, the T_2* values of both normal and tumor tissue dropped significantly. While the values of normal brain reached its pre-contrast values in 3 days after injection, the T_2* values remained low displaying a statistically significant difference when compared to the pre-contrast values of the tumor tissue ($p<0.001$). This suggests that the nanocarrier was cleared from blood circulation while accumulated in the extravascular space of the tumor.

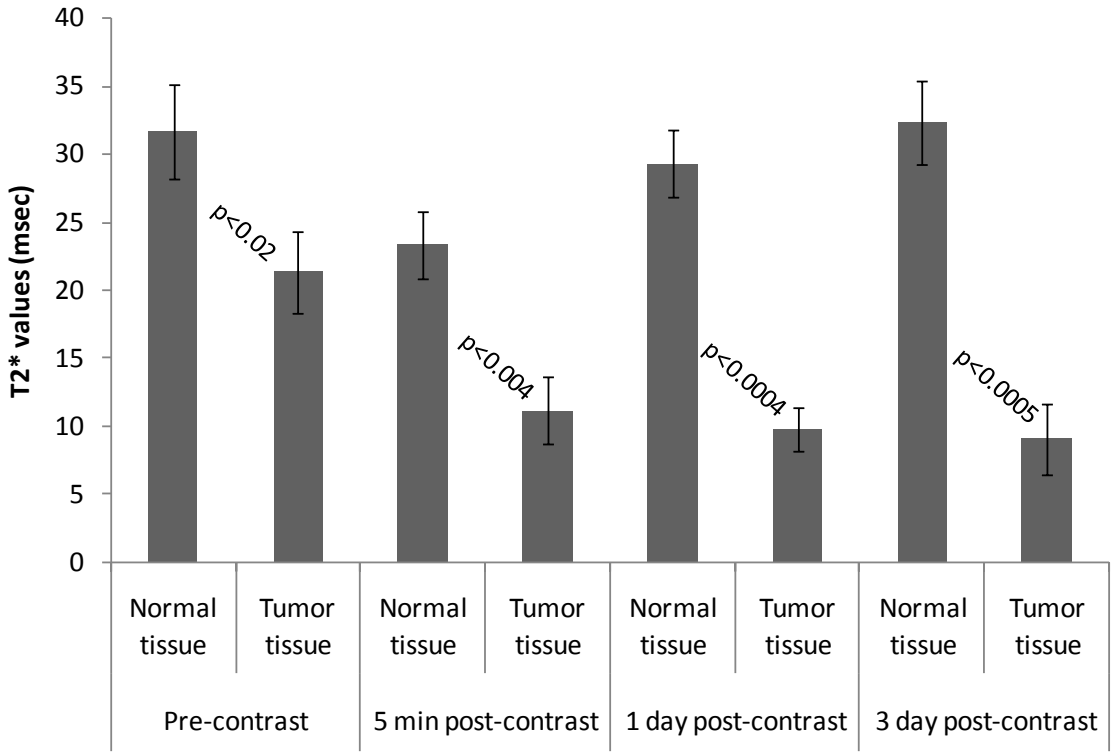

Figure A.5. Comparison of T_2* values of normal brain and tumor obtained via T_2*-weighted 2D maps over the period of 3 days before and after administration of 0.25 mmol Gd/kg of the nanocarrier in rats (n=3).

In the past, nanoscale liposomal contrast agents encapsulating Gd with prolonged blood circulation were used for blood pool imaging (Ghaghada *et al.*, 2007; Erdogan *et*

al., 2008; Erdogan *et al.*, 2006; Torchilin, 1994; Krauze *et al.*, 2006; Weissing *et al.*, 2000) but not for detecting extravascular deposition in tumors. Other macromolecular gadolinium-based agents (Daldrup *et al.*, 1998) and iron oxide nanoparticles (USIOP) (Turetschek *et al.*, 2001b; Turetschek *et al.*, 2001a) have been employed to evaluate tumor vascular permeability. These agents and method of use however, failed to transparently characterize the tumor vascular permeability to nanoparticles due to persistent intravascular signal and/or inadequate extravascular signal. The primary explanation for these results is that the short duration of the imaging sessions (less than 1 hr) used in those studies did not allow enough time for extravasation of large quantities of the nanoscale contrast agents to yield adequate signal. Indeed it has been established that the intratumoral, extravascular accumulation of long-circulating nanoscale agents peaks at about 48 h (Kirpotin *et al.*, 2006). Though a liposomal based nanocarrier enabled evaluation of vascular permeability in this study, we hypothesize that such evaluation would be possible with other long-circulating nanoscale contrast agents as well. However, liposomal nanocarriers can serve as multifunctional agents since they can carry combinations of drugs and contrast agents and can conveniently be modified for active targeting (Zalipsky, 1993).

A.3.5. Histological Analysis

Histological analysis of tumors was performed on animals euthanized 3 days after administration of the rhodamine-tagged Gd- nanocarrier (immediately after completion of the last imaging session). Fluorescent microscopy of brain tissue section verified the intratumoral extravascular deposition of the nanocarrier. The tumor was characterized by a highly vascularized peripheral rim and an internal core with a lower vascularization

(Figure 6.a), consistent with earlier reports (Marzola *et al.*, 2005; McNeeley *et al.*, 2007). In the same histolological slice (Figure 6.b) the extravasated nanocarrier was observed to localize within the lesion (not in normal brain) exhibiting a patchy distribution. The typical intratumoral microdistribution of PEGylated liposomes is predominantly at the tumor (Kirpotin *et al.*, 2006; Huang *et al.*, 1992; Yuan *et al.*, 1994), which is usually associated with high levels of angiogenic and permeability factors resulting in neoangiogenesis (Damert *et al.*, 1997; Takano *et al.*, 1996). This is consistent with our histological observations.

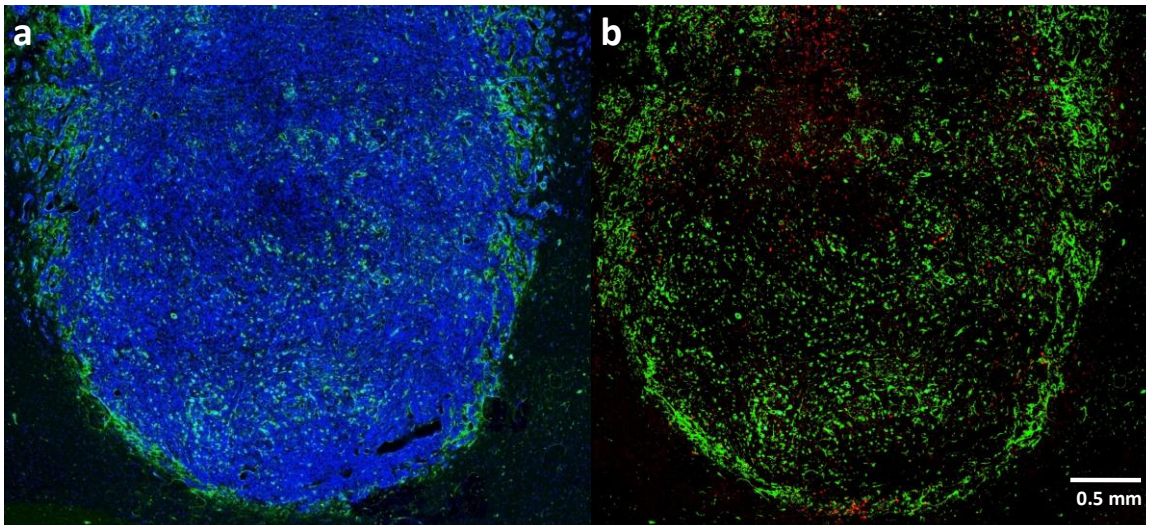

Figure A.6. Microdistribution of the nanocarrier in the brain tumor lesion (the MR images of the same animal are shown in Fig. A.4) 72 h after IV injection of rhodamine-tagged Gd-nanocarrier using fluorescent microscopy at 20x magnification. (a) Immuhistochemical microvascular staining was achieved by staining with RECA-1, a cell surface antigen which is expressed by all rat endothelial cells (appeared as green) revealing a highly vascularized peripheral rim and a less vascularized inner core (DAPI was used as a nuclear stain; appeared as blue); (b) In the same histological slice, the liposomes (appeared as red) displayed a patchy distribution (scale bar is 0.5 mm).

A.4. Conclusions

In this work, we demonstrated the ability to track non-invasively the fate of a systemically-administered nanocarrier. The nanocarrier consists of a 100nm-scale long-circulating liposomal agent encapsulating gadolinium of similar composition and particle

size as the clinically used liposomal chemotherapy (Lasic and Papahadjopoulos, 1995). While gadolinium is traditionally used as a T_1-shortening contrast agent under the currently used magnetic fields in the clinic (1.5-3 Tesla), the Gd-containing nanocarrier behaved as a potent T_2-shortening agent on a 9.4 T MRI system. The significant T_2 shortening effect of the nanocarrier and the method of use allowed detection of the intratumoral, extravascular accumulation of the nanocarrier in a rat brain tumor model using a 9.4 T MRI system. It would be expected that a long-circulating agent would produce undistinguishable extravascular and intravascular signal making determination of the degree of vascular permeability unfeasible. This is the case for the first 24 h after injection since the intravascular levels of the agent are still high. As the concentration of the nanocarrier in the blood decreased, its extravascular accumulation in the tumor increased resulting in adequate negative enhancement without interference from the blood for detection. This allowed the evaluation of the nanocarrier uptake by a brain tumor 3 days post-injection. The visualization of the extravascular accumulation of the nanocarrier and at the same time invisibility of the vasculature makes MR imaging an attractive non-invasive method. Such an a priori determination of the extent of tumor susceptibility to nanocarrier-based chemotherapy would therefore facilitate personalized therapy, and spare potential non-responders from the rigors of a chemotherapy regimen. However, human cancer as a disease is much more heterogeneous than experimental tumor models in terms of both tumors and hosts. The current study demonstrated the feasibility of tracking the intratumoral deposition of the Gd-loaded nanocarrier on a single tumor model, and further testing of imaging followed by treatment in more tumor models is required to fully assess the clinical value of this approach. Recently, we have

fabricated a liposomal nanocarrier co-encapsulating Gd and doxorubicin (data not shown). Future studies will be performed with the nanocarrier co-encapsulating the contrast agent and the drug, and determine that indeed a rationally determined treatment regime would significantly enhance therapeutic efficacy of the chemotherapeutic nanocarriers. In addition, surgical units are increasingly co-locating MRI units to assist in surgical planning. Imaging of tumor border and location using MRI could also serve as a useful surgical planning tool for tumor border mapping and resection.

Acknowledgments

This work was funded by the National Science Foundation (NSF), Bioengineering and Environmental Systems (0401627) and the Georgia Cancer Coalition (to RVB). The authors would like to acknowledge Ketan Ghaghada and Kathleen McNeeley for useful discussions. We also thank Dr. Gang Bao for helping us with measurements using the NMR Minispec.

A.5. References

Ayyagari A L, Zhang X, Ghaghada K B, Annapragada A, Hu X and Bellamkonda R V 2006 Long-circulating liposomal contrast agents for magnetic resonance imaging *Magn Reson Med* **55** 1023-9

Barker F G, 2nd, Chang S M, Gutin P H, Malec M K, McDermott M W, Prados M D and Wilson C B 1998 Survival and functional status after resection of recurrent glioblastoma multiforme *Neurosurgery* **42** 709-20; discussion 20-3

Black K L and Pikul B K 1999 Gliomas--past, present, and future *Clin Neurosurg* **45** 160-3

Brix G, Kiessling F, Lucht R, Darai S, Wasser K, Delorme S and Griebel J 2004 Microcirculation and microvasculature in breast tumors: pharmacokinetic analysis of dynamic MR image series *Magn Reson Med* **52** 420-9

Daldrup H, Shames D M, Wendland M, Okuhata Y, Link T M, Rosenau W, Lu Y and Brasch R C 1998 Correlation of dynamic contrast-enhanced MR imaging with histologic tumor grade: comparison of macromolecular and small-molecular contrast media *AJR Am J Roentgenol* **171** 941-9

Damert A, Machein M, Breier G, Fujita M Q, Hanahan D, Risau W and Plate K H 1997 Up-regulation of vascular endothelial growth factor expression in a rat glioma is conferred by two distinct hypoxia-driven mechanisms *Cancer Res* **57** 3860-4

Erdogan S, Medarova Z O, Roby A, Moore A and Torchilin V P 2008 Enhanced tumor MR imaging with gadolinium-loaded polychelating polymer-containing tumor-targeted liposomes *J Magn Reson Imaging*

Erdogan S, Roby A, Sawant R, Hurley J and Torchilin V P 2006 Gadolinium-loaded polychelating polymer-containing cancer cell-specific immunoliposomes *J Liposome Res* **16** 45-55

Ferrari M 2005 Cancer nanotechnology: opportunities and challenges *Nat Rev Cancer* **5** 161-71

Fine H A, Dear K B, Loeffler J S, Black P M and Canellos G P 1993 Meta-analysis of radiation therapy with and without adjuvant chemotherapy for malignant gliomas in adults *Cancer* **71** 2585-97

Fukumura D and Jain R K 2007 Tumor microenvironment abnormalities: causes, consequences, and strategies to normalize *Journal of cellular biochemistry* **101** 937-49

Furman-Haran E and Degani H 2002 Parametric analysis of breast MRI *J Comput Assist Tomogr* **26** 376–86

Ghaghada K B, Bockhorst K H, Mukundan S, Jr., Annapragada A V and Narayana P A 2007 High-resolution vascular imaging of the rat spine using liposomal blood pool MR agent *AJNR Am J Neuroradiol* **28** 48-53

Heath J R and Davis M E 2007 Nanotechnology and Cancer *Annu Rev Med*

Hobbs S K, Monsky W L, Yuan F, Roberts W G, Griffith L, Torchilin V P and Jain R K 1998 Regulation of transport pathways in tumor vessels: role of tumor type and microenvironment *Proc Natl Acad Sci U S A* **95** 4607-12

Hong S, Leroueil P R, Majoros I J, Orr B G, Baker J R, Jr. and Banaszak Holl M M 2007 The binding avidity of a nanoparticle-based multivalent targeted drug delivery platform *Chem Biol* **14** 107-15

Huang S K, Lee K D, Hong K, Friend D S and Papahadjopoulos D 1992 Microscopic localization of sterically stabilized liposomes in colon carcinoma-bearing mice *Cancer Res* **52** 5135-43

Jain R K 1994 Barriers to drug delivery in solid tumors *Sci Am* **271** 58-65

Jain R K 1999 Transport of molecules, particles, and cells in solid tumors *Annu Rev Biomed Eng* **1** 241-63

Jain R K 2001 Delivery of molecular and cellular medicine to solid tumors *Adv Drug Deliv Rev* **46** 149-68

Jain R K 2005 Normalization of Tumor Vasculature: An Emerging Concept in Antiangiogenic Therapy *Science* **307** 58-62

Kim D H and Rossi J J 2007 Strategies for silencing human disease using RNA interference *Nat Rev Genet* **8** 173-84

Kirpotin D B, Drummond D C, Shao Y, Shalaby M R, Hong K, Nielsen U B, Marks J D, Benz C C and Park J W 2006 Antibody targeting of long-circulating lipidic nanoparticles does not increase tumor localization but does increase internalization in animal models *Cancer Res* **66** 6732-40

Koning G A and Krijger G C 2007 Targeted multifunctional lipid-based nanocarriers for image-guided drug delivery *Anticancer Agents Med Chem* **7** 425-40

Krauze M T, Forsayeth J, Park J W and Bankiewicz K S 2006 Real-time imaging and quantification of brain delivery of liposomes *Pharm Res* **23** 2493-504

Lasic D and Martin F 1995 *Stealth Liposomes*: CRC Press Inc)

Lasic D D and Papahadjopoulos D 1995 Liposomes revisited *Science* **267** 1275-6

Leach M O 2001 Application of magnetic resonance imaging to angiogenesis in breast cancer *Breast Cancer Res Treat* **3** 22–7

M.I. Koukourakis, S. Koukouraki I F, N. Kelekis, G. Kyrias S A and N. Karkavitsas 2000 High intratumoural accumulation of stealth liposomal doxorubicin (Caelyx) in glioblastomas and in metastatic brain tumours *Br J Cancer* **83** 1281-6

Maeda H, Wu J, Sawa T, Matsumura Y and Hori K 2000 Tumor vascular permeability and the EPR effect in macromolecular therapeutics: a review *J Control Release* **65** 271-84

Marzola P, Ramponi S, Nicolato E, Lovati E, Sandri M, Calderan L, Crescimanno C, Merigo F, Sbarbati A, Grotti A, Vultaggio S, Cavagna F, Lorusso V and Osculati F 2005 Effect of tamoxifen in an experimental model of breast tumor studied by dynamic contrast-enhanced magnetic resonance imaging and different contrast agents *Investigative radiology* **40** 421-9

McNeeley K M, Annapragada A and Bellamkonda R V 2007 Decreased circulation time offsets increased efficacy of PEGylated nanocarriers targeting folate receptors of glioma *Nanotechnology* **18** 385101

Mitra A, Nan A, Line B R and Ghandehari H 2006 Nanocarriers for nuclear imaging and radiotherapy of cancer *Curr Pharm Des* **12** 4729-49

Oshida K, Nagashima T, Ueda T, Yagata H, Tanabe N, Nakano S, Nikaidou T, Funatsu H, Hashimoto H and Miyazaki M 2005 Pharmacokinetic analysis of ductal carcinoma in situ of the breast using dynamic MR mammography *European radiology* **15** 1353-60

R.D. Arnold, D.E.Mager, J.E. Slack and R.M. Straubinger 2005 Effect of Repetitive Administration of Doxorubicin-Containing Liposomes on Plasma Pharmacokinetics and Drug Biodistribution in a Rat Brain Tumor Model *Clin Cancer Res* **11** 8856-65

Sardanelli F, Iozzelli A, Fausto A, Carriero A and Kirchin M A 2005 Gadobenate dimeglumine-enhanced MR imaging breast vascular maps: association between invasive cancer and ipsilateral increased vascularity *Radiology* **235** 791-7

Saul J M, Annapragada A V and Bellamkonda R V 2006 A dual-ligand approach for enhancing targeting selectivity of therapeutic nanocarriers *J Control Release* **114** 277-87

Schiffelers R M, Ansari A, Xu J, Zhou Q, Tang Q, Storm G, Molema G, Lu P Y, Scaria P V and Woodle M C 2004 Cancer siRNA therapy by tumor selective delivery with ligand-targeted sterically stabilized nanoparticle *Nucleic Acids Res* **32** e149

Service R F 2005 Materials and biology. Nanotechnology takes aim at cancer *Science* **310** 1132-4

Strijkers G J, Mulder W J, van Heeswijk R B, Frederik P M, Bomans P, Magusin P C and Nicolay K 2005 Relaxivity of liposomal paramagnetic MRI contrast agents *MAGMA* **18** 186-92

Takano S, Yoshii Y, Kondo S, Suzuki H, Maruno T, Shirai S and Nose T 1996 Concentration of vascular endothelial growth factor in the serum and tumor tissue of brain tumor patients *Cancer Res* **56** 2185-90

Teifke A, Behr O, Schmidt M, Victor A, Vomweg T W, Thelen M and Lehr H A 2006 Dynamic MR imaging of breast lesions: correlation with microvessel distribution pattern and histologic characteristics of prognosis *Radiology* **239** 351-60

Torchilin V P 1994 Immunoliposomes and PEGylated immunoliposomes: possible use for targeted delivery of imaging agents *Immunomethods* **4** 244-58

Torchilin V P 2006 Multifunctional nanocarriers *Adv Drug Deliv Rev* **58** 1532-55

Turetschek K, Huber S, Floyd E, Helbich T, Roberts T P, Shames D M, Tarlo K S, Wendland M F and Brasch R C 2001a MR imaging characterization of

microvessels in experimental breast tumors by using a particulate contrast agent with histopathologic correlation *Radiology* **218** 562-9

Turetschek K, Roberts T P, Floyd E, Preda A, Novikov V, Shames D M, Carter W O and Brasch R C 2001b Tumor microvascular characterization using ultrasmall superparamagnetic iron oxide particles (USPIO) in an experimental breast cancer model *J Magn Reson Imaging* **13** 882-8

van de Wiele P, Dierckx R, Scopinaro F, Waterhouse R, Annovazzi A, Kolindou A and Signore A 2002 Nuclear medicine imaging for prediction or early assessment of response to chemotherapy in patients suffering from breast carcinoma *Breast Cancer Res Treat* **72** 279-86

Weissing V, Babich J and Torchilin V 2000 Long-circulating gadolinium loaded liposomes: potential use for mangetic resonance imaging of the blood pool *Colloids and Surfaces B: Biointerfaces* **18** 293-9

Yuan F, Chen Y, Dellian M, Safabakhsh N, Ferrara N and Jain R K 1996 Time-dependent vascular regression and permeability changes in established human tumor xenografts induced by an anti-vascular endothelial growth factor/vascular permeability factor antibody *Proc Natl Acad Sci U S A* **93** 14765-70

Yuan F, Leunig M, Huang S K, Berk D A, Papahadjopoulos D and Jain R K 1994 Microvascular permeability and interstitial penetration of sterically stabilized (stealth) liposomes in a human tumor xenograft *Cancer Res* **54** 3352-6

Zalipsky S 1993 Synthesis of an end-group functionalized polyethylene glycol-lipid conjugate for preparation of polymer-grafted liposomes *Bioconjug Chem* **4** 296-9

BIBLIOGRAPHY

Allen, T. M. and C. Hansen (1991). "Pharmacokinetics of stealth versus conventional liposomes: effect of dose." Biochim Biophys Acta **1068**(2): 133-141.

Allen, T. M., C. Hansen, et al. (1991). "Liposomes containing synthetic lipid derivatives of poly(ethylene glycol) show prolonged circulation half-lives in vivo." Biochim Biophys Acta **1066**(1): 29-36.

Andresen, T. L., S. S. Jensen, et al. (2005). "Advanced strategies in liposomal cancer therapy: problems and prospects of active and tumor specific drug release." Prog Lipid Res **44**(1): 68-97.

Arap, W., R. Pasqualini, et al. (1998). "Cancer treatment by targeted drug delivery to tumor vasculature in a mouse model." Science **279**: 377-380.

Ayyagari, A. L., X. Zhang, et al. (2006). "Long-circulating liposomal contrast agents for magnetic resonance imaging." Magn Reson Med **55**(5): 1023-1029.

Barker, F. G., 2nd, S. M. Chang, et al. (1998). "Survival and functional status after resection of recurrent glioblastoma multiforme." Neurosurgery **42**(4): 709-720; discussion 720-703.

Bisby, R. H., C. Mead, et al. (2000). "Active uptake of drugs into photosensitive liposomes and rapid release on UV photolysis." Photochem Photobiol **72**(1): 57-61.

Bisby, R. H., C. Mead, et al. (2000). "Wavelength-programmed solute release from photosensitive liposomes." Biochem Biophys Res Commun **276**(1): 169-173.

Black, K. L. and B. K. Pikul (1999). "Gliomas--past, present, and future." Clin Neurosurg **45**: 160-163.

Bolotin, E. M., R. Cohen, et al. (1994). "Ammonium sulfate gradients for efficient and stable remote loading of amphipathic weak bases into liposomes and ligandoliposomes." J Liposome Res **4**(1): 455-479.

Bondurant, B., A. Mueller, et al. (2001). "Photoinitiated destabilization of sterically stabilized liposomes." Biochim Biophys Acta **1511**(1): 113-122.

Bremer, C., V. Ntziachristos, et al. (2003). "Optical-based molecular imaging: contrast agents and potential medical applications." Eur Radiol **13**(2): 231-243.

Brigger, I., C. Dubernet, et al. (2002). "Nanoparticles in cancer therapy and diagnosis." Adv Drug Deliv Rev **54**(5): 631-651.

Brignole, C., D. Marimpietri, et al. (2005). "Neuroblastoma targeting by c-myb-selective antisense oligonucleotides entrapped in anti-GD2 immunoliposome: immune cell-mediated anti-tumor activities." Cancer Lett **228**(1-2): 181-186.

Brix, G., F. Kiessling, et al. (2004). "Microcirculation and microvasculature in breast tumors: pharmacokinetic analysis of dynamic MR image series." Magn Reson Med **52**(2): 420-429.

Buckner, J. C., P. D. Brown, et al. (2007). "Central nervous system tumors." Mayo Clin Proc **82**(10): 1271-1286.

Calvo, P., C. RemunanLopez, et al. (1997). "Chitosan and chitosan ethylene oxide propylene oxide block copolymer nanoparticles as novel carriers for proteins and vaccines." Pharm. Res. **14**: 1431-1436.

Cerletti, A., J. Drewe, et al. (2000). "Endocytosis and transcytosis of an immunoliposome-based brain drug delivery system." J Drug Target **8**(6): 435-446.

Cevc, G. and H. Richardsen (1999). "Lipid vesicles and membrane fusion." Adv Drug Deliv Rev **38**(3): 207-232.

Chang, S. M., N. A. Butowski, et al. (2006). "Standard treatment and experimental targeted drug therapy for recurrent glioblastoma multiforme." Neurosurg Focus **20**(4): E4.

Charrois, G. J. and T. M. Allen (2004). "Drug release rate influences the pharmacokinetics, biodistribution, therapeutic activity, and toxicity of pegylated liposomal doxorubicin formulations in murine breast cancer." Biochim Biophys Acta **1663**(1-2): 167-177.

Chen, Q. D., L. M. Dai, et al. (2001). "Plasma activation of carbon nanotubes for chemical modification." Journal of Physical Chemistry B **105**(3): 618-622.

Chernomordik, L. (1996). "Non-bilayer lipids and biological fusion intermediates." Chem Phys Lipids **81**(2): 203-213.

Collins, D., D. C. Litzinger, et al. (1990). "Structural and functional comparisons of pH-sensitive liposomes composed of phosphatidylethanolamine and three different diacylsuccinylglycerols." Biochim Biophys Acta **1025**(2): 234-242.

Connor, J., M. B. Yatvin, et al. (1984). "pH-sensitive liposomes: acid-induced liposome fusion." Proc Natl Acad Sci U S A **81**(6): 1715-1718.

Couvreur, P. (1980). "Tissue distribution of anti-tumor drugs associated with polyalkylcyanoacrylate nanoparticles." J. Pharm. Sci. **69**: 199-202.

Couvreur, P., B. Kante, et al. (1979). "Adsorption of anti-neoplastic drugs to polyalkylcyanoacrylate nanoparticles and their release in calf serum." J. Pharm. Sci. **68**: 1521-1524.

D.S. Mohan, J.H. Suh, et al. (1998). "Outcome in elderly patients undergoing definitive surgery and radiation therapy for supratentorial glioblastoma multiforme at a tertiary institution." Int. J. Radiat. Biol. Phys. **42**: 981–987.

Daldrup, H., D. M. Shames, et al. (1998). "Correlation of dynamic contrast-enhanced MR imaging with histologic tumor grade: comparison of macromolecular and small-molecular contrast media." AJR Am J Roentgenol **171**(4): 941-949.

Daleke, D. L., K. Hong, et al. (1990). "Endocytosis of liposomes by macrophages: binding, acidification and leakage of liposomes monitored by a new fluorescence assay." Biochim Biophys Acta **1024**(2): 352-366.

Damert, A., M. Machein, et al. (1997). "Up-regulation of vascular endothelial growth factor expression in a rat glioma is conferred by two distinct hypoxia-driven mechanisms." Cancer Res **57**(17): 3860-3864.

Davidsen, J., K. Jorgensen, et al. (2003). "Secreted phospholipase A(2) as a new enzymatic trigger mechanism for localised liposomal drug release and absorption in diseased tissue." Biochim Biophys Acta **1609**(1): 95-101.

Davis, S. C. and F. C. Szoka, Jr. (1998). "Cholesterol phosphate derivatives: synthesis and incorporation into a phosphatase and calcium-sensitive triggered release liposome." Bioconjug Chem **9**(6): 783-792.

Dewhirst, M. W., L. Prosnitz, et al. (1997). "Hyperthermic treatment of malignant diseases: current status and a view toward the future." Semin Oncol **24**(6): 616-625.

Dickerson, E. B., E. C. Dreaden, et al. (2008). "Gold nanorod assisted near-infrared plasmonic photothermal therapy (PPTT) of squamous cell carcinoma in mice." Cancer Lett **269**(1): 57-66.

Drummond, D. C., C. O. Noble, et al. (2008). "Pharmacokinetics and in vivo drug release rates in liposomal nanocarrier development." J Pharm Sci **97**(11): 4696-4740.

Drummond, D. C., M. Zignani, et al. (2000). "Current status of pH-sensitive liposomes in drug delivery." Prog Lipid Res **39**(5): 409-460.

Dugan, L. L., D. M. Turetsky, et al. (1997). "Carboxyfullerenes as neuroprotective agents." Proc Natl Acad Sci U S A **94**(17): 9434-9439.

Duncan, R. (1999). "Polymer conjugates for tumour targeting and intracytoplasmic delivery. The EPR effect as a common gateway?" Pharm Sci Technolo Today **11**(2): 441-449.

Duncan, R. (2006). "Polymer conjugates as anticancer nanomedicines." Nat. Rev. Cancer **6**: 688-701.

Duzgunes, N., R. M. Straubinger, et al. (1985). "Proton-induced fusion of oleic acid-phosphatidylethanolamine liposomes." Biochemistry **24**(13): 3091-3098.

Eavarone, D. A., X. Yu, et al. (2000). "Targeted drug delivery to C6 glioma by transferrin-coupled liposomes." J Biomed Mater Res **51**(1): 10-14.

Ebrahim, S., G. A. Peyman, et al. (2005). "Applications of liposomes in ophthalmology." Surv Ophthalmol **50**(2): 167-182.

El-Sayed, I., X. Huang, et al. (2007). "Effect of plasmonic gold nanoparticles on benign and malignant cellular autofluorescence: a novel probe for fluorescence based detection of cancer." Technol Cancer Res Treat **6**(5): 403-412.

El-Sayed, I. H., X. Huang, et al. (2005). "Surface plasmon resonance scattering and absorption of anti-EGFR antibody conjugated gold nanoparticles in cancer diagnostics: applications in oral cancer." Nano Lett **5**(5): 829-834.

El-Sayed, I. H., X. Huang, et al. (2006). "Selective laser photo-thermal therapy of epithelial carcinoma using anti-EGFR antibody conjugated gold nanoparticles." Cancer Lett **239**(1): 129-135.

Ellens, H., J. Bentz, et al. (1984). "pH-induced destabilization of phosphatidylethanolamine-containing liposomes: role of bilayer contact." Biochemistry **23**(7): 1532-1538.

Elsamaligy, M. S. and P. Rohdewald (1983). "Reconstituted collagen nanoparticles, a novel drug carrier delivery system." J. Pharm. Pharmacol. **35**: 537-539.

Erdogan, S., Z. O. Medarova, et al. (2008). "Enhanced tumor MR imaging with gadolinium-loaded polychelating polymer-containing tumor-targeted liposomes." J Magn Reson Imaging.

Erdogan, S., A. Roby, et al. (2006). "Gadolinium-loaded polychelating polymer-containing cancer cell-specific immunoliposomes." J Liposome Res **16**(1): 45-55.

Eto, Y., J. Q. Gao, et al. (2005). "PEGylated adenovirus vectors containing RGD peptides on the tip of PEG show high transduction efficiency and antibody evasion ability." J Gene Med **7**(5): 604-612.

Euhus, D. M., C. Hudd, et al. (1986). "Tumor measurement in the nude mouse." J Surg Oncol **31**(4): 229-234.

F.G. Barker, S.M. Chang, et al. (1998). "Survival and functional status after resection of recurrent glioblastoma multiforme." Neurosurgery **42**: 709–720.

Farokhzad, O. C. and R. Langer (2006). "Nanomedicine: Developing smarter therapeutic and diagnostic modalities." Adv. Drug Deliv. Rev. **58**: 1456-1459.

Feil, H., Y. H. Bae, et al. (1993). "Effect of comonomer hydrophilicity and ionization on the lower critical solution temperature of N-isopropylacrylamide copolymers." Macromolecules **26**(10): 2496-2500.

Ferrari, M. (2005). "Cancer nanotechnology: Opportunities and challenges." Nature Reviews Cancer **5**(3): 161-171.

Fine, H. A., K. B. Dear, et al. (1993). "Meta-analysis of radiation therapy with and without adjuvant chemotherapy for malignant gliomas in adults." Cancer **71**(8): 2585-2597.

Finlay, J. L. and S. Zacharoulis (2005). "The treatment of high grade gliomas and diffuse intrinsic pontine tumors of childhood and adolescence: a historical - and futuristic - perspective." J Neurooncol **75**(3): 253-266.

Fritze, A., F. Hens, et al. (2006). "Remote loading of doxorubicin into liposomes driven by a transmembrane phosphate gradient." Biochim Biophys Acta **1758**(10): 1633-1640.

Fukumura, D. and R. K. Jain (2007). "Tumor microenvironment abnormalities: causes, consequences, and strategies to normalize." J Cell Biochem **101**(4): 937-949.

Furman-Haran, E. and H. Degani (2002). "Parametric analysis of breast MRI." J Comput Assist Tomogr **26**: 376–386.

Gaber, M. H. (2002). "Modulation of doxorubicin resistance in multidrug-resistance cells by targeted liposomes combined with hyperthermia." J Biochem Mol Biol Biophys **6**(5): 309-314.

Gaber, M. H., K. Hong, et al. (1995). "Thermosensitive sterically stabilized liposomes: formulation and in vitro studies on mechanism of doxorubicin release by bovine serum and human plasma." Pharm Res **12**(10): 1407-1416.

Gaber, M. H., N. Z. Wu, et al. (1996). "Thermosensitive liposomes: extravasation and release of contents in tumor microvascular networks." Int J Radiat Oncol Biol Phys **36**(5): 1177-1187.

Gabizon, A., A. T. Horowitz, et al. (1999). "Targeting folate receptor with folate linked to extremities of poly(ethylene glycol)-grafted liposomes: in vitro studies." Bioconjug Chem **10**(2): 289-298.

Gabizon, A., A. T. Horowitz, et al. (2003). "In vivo fate of folate-targeted polyethylene-glycol liposomes in tumor-bearing mice." Clin Cancer Res **9**(17): 6551-6559.

Gabizon, A. and F. Martin (1997). "Polyethylene glycol-coated (pegylated) liposomal doxorubicin. Rationale for use in solid tumours." Drugs **54 Suppl 4**: 15-21.

Gabizon, A., H. Shmeeda, et al. (2003). "Pharmacokinetics of pegylated liposomal Doxorubicin: review of animal and human studies." Clin Pharmacokinet **42**(5): 419-436.

Gabizon, A., H. Shmeeda, et al. (2004). "Tumor cell targeting of liposome-entrapped drugs with phospholipid-anchored folic acid-PEG conjugates." Adv Drug Deliv Rev **56**(8): 1177-1192.

Gabizon, A. A., H. Shmeeda, et al. (2006). "Pros and cons of the liposome platform in cancer drug targeting." J Liposome Res **16**(3): 175-183.

Garin-Chesa, P., I. Campbell, et al. (1993). "Trophoblast and ovarian cancer antigen LK26. Sensitivity and specificity in immunopathology and molecular identification as a folate-binding protein." Am J Pathol **142**(2): 557-567.

Gerasimov, M., D. Marona-Lewicka, et al. (1999). "Further studies on oxygenated tryptamines with LSD-like activity incorporating a chiral pyrrolidine moiety into the side chain." Journal of Medicinal Chemistry **42**(20): 4257-4263.

Ghaghada, K. B., K. H. Bockhorst, et al. (2007). "High-resolution vascular imaging of the rat spine using liposomal blood pool MR agent." AJNR Am J Neuroradiol **28**(1): 48-53.

Ghoroghchian, P. P., M. J. Therien, et al. (2009). "In vivo fluorescence imaging: a personal perspective." Wiley Interdiscip Rev Nanomed Nanobiotechnol **1**(2): 156-167.

Goni, F. M. and A. Alonso (2000). "Membrane fusion induced by phospholipase C and sphingomyelinases." Biosci Rep **20**(6): 443-463.

Gosk, S., C. Vermehren, et al. (2004). "Targeting anti-transferrin receptor antibody (OX26) and OX26-conjugated liposomes to brain capillary endothelial cells using in situ perfusion." J Cereb Blood Flow Metab **24**(11): 1193-1204.

Graves, E. E., R. Weissleder, et al. (2004). "Fluorescence molecular imaging of small animal tumor models." Curr Mol Med **4**(4): 419-430.

Greish, K., J. Fang, et al. (2003). "Macromolecular therapeutics: advantages and prospects with special emphasis on solid tumour targeting." Clin Pharmacokinet **42**(13): 1089-1105.

Guo, R. (2007). "Synthesis of alginic acid-poly[2-(diethylamino)ethyl methacrylate] monodispersed nanoparticles by a polymer-monomer pair reaction system." Biomacromolecules **8**: 843-850.

Gupta, B. and V. P. Torchilin (2007). "Monoclonal antibody 2C5-modified doxorubicin-loaded liposomes with significantly enhanced therapeutic activity against intracranial human brain U-87 MG tumor xenografts in nude mice." Cancer Immunol Immunother.

Gupta, U., H. B. Agashe, et al. (2006). "Dendrimers: novel polymeric nanoarchitectures for solubility enhancement." Biomacromolecules **7**(3): 649-658.

H. Brem, M.G. Ewend, et al. (1995). "The safety of interstitial chemotherapy with BCNU-loaded polymer followed by radiation therapy in the treatment of newly diagnosed malignant gliomas: phase I trial." J. Neurooncol. **26**: 111-123.

Hafez, I. M. and P. R. Cullis (2001). "Roles of lipid polymorphism in intracellular delivery." Adv Drug Deliv Rev **47**(2-3): 139-148.

Haley, B. and E. Frenkel (2008). "Nanoparticles for drug delivery in cancer treatment." Urol Oncol **26**(1): 57-64.

Halin, C. (2002). "Enhancement of the antitumor activity of interleukin-12 by targeted delivery to neovasculature." Nat. Biotechnol. **20**: 264-269.

Haran, G., R. Cohen, et al. (1993). "Transmembrane ammonium sulfate gradients in liposomes produce efficient and stable entrapment of amphipathic weak bases." Biochim Biophys Acta **1151**(2): 201-215.

Harasym, T. O., P. R. Cullis, et al. (1997). "Intratumor distribution of doxorubicin following i.v. administration of drug encapsulated in egg phosphatidylcholine/cholesterol liposomes." Cancer Chemother Pharmacol **40**(4): 309-317.

Harasym, T. O., P. Tardi, et al. (1995). "Poly(ethylene glycol)-modified phospholipids prevent aggregation during covalent conjugation of proteins to liposomes." Bioconjug Chem **6**(2): 187-194.

Harris, J. M., N. E. Martin, et al. (2001). "Pegylation: a novel process for modifying pharmacokinetics." Clin Pharmacokinet **40**(7): 539-551.

Hauck, M. L., S. M. LaRue, et al. (2006). "Phase I trial of doxorubicin-containing low temperature sensitive liposomes in spontaneous canine tumors." Clin Cancer Res **12**(13): 4004-4010.

Heath, J. R. and M. E. Davis (2007). "Nanotechnology and Cancer." Annu Rev Med.

Helmlinger, G., A. Sckell, et al. (2002). "Acid production in glycolysis-impaired tumors provides new insights into tumor metabolism." Clin Cancer Res **8**(4): 1284-1291.

Ho, I. A., P. Y. Lam, et al. (2004). "Identification and characterization of novel human glioma-specific peptides to potentiate tumor-specific gene delivery." Hum Gene Ther **15**(8): 719-732.

Hobbs, S. K., W. L. Monsky, et al. (1998). "Regulation of transport pathways in tumor vessels: role of tumor type and microenvironment." Proc Natl Acad Sci U S A **95**(8): 4607-4612.

Holliger, P. and P. J. Hudson (2005). "Engineered antibody fragments and the rise of single domains." Nat Biotechnol **23**(9): 1126-1136.

Hong, S., P. R. Leroueil, et al. (2007). "The binding avidity of a nanoparticle-based multivalent targeted drug delivery platform." Chem Biol **14**(1): 107-115.

Huang, S. K., K. D. Lee, et al. (1992). "Microscopic localization of sterically stabilized liposomes in colon carcinoma-bearing mice." Cancer Res **52**(19): 5135-5143.

Huang, S. K., E. Mayhew, et al. (1992). "Pharmacokinetics and therapeutics of sterically stabilized liposomes in mice bearing C-26 colon carcinoma." Cancer Res **52**(24): 6774-6781.

Huang, S. L. and R. C. MacDonald (2004). "Acoustically active liposomes for drug encapsulation and ultrasound-triggered release." Biochim Biophys Acta **1665**(1-2): 134-141.

Huang, X., I. H. El-Sayed, et al. (2006). "Cancer cell imaging and photothermal therapy in the near-infrared region by using gold nanorods." J Am Chem Soc **128**(6): 2115-2120.

Huang, X., P. K. Jain, et al. (2006). "Determination of the minimum temperature required for selective photothermal destruction of cancer cells with the use of immunotargeted gold nanoparticles." Photochem Photobiol **82**(2): 412-417.

Huang, X., P. K. Jain, et al. (2007). "Gold nanoparticles: interesting optical properties and recent applications in cancer diagnostics and therapy." Nanomed **2**(5): 681-693.

Huang, X., P. K. Jain, et al. (2008). "Plasmonic photothermal therapy (PPTT) using gold nanoparticles." Lasers Med Sci **23**(3): 217-228.

Huang, X., W. Qian, et al. (2007). "The potential use of the enhanced nonlinear properties of gold nanospheres in photothermal cancer therapy." Lasers Surg Med **39**(9): 747-753.

Hunt, C. A. (1982). "Liposomes disposition in vivo. V. Liposome stability in plasma and implications for drug carrier function." Biochim Biophys Acta **719**(3): 450-463.

Huwyler, J., D. Wu, et al. (1996). "Brain drug delivery of small molecules using immunoliposomes." Proc Natl Acad Sci U S A **93**(24): 14164-14169.

Ikegami, S., T. Tadakuma, et al. (2005). "Selective gene therapy for prostate cancer cells using liposomes conjugated with IgM type monoclonal antibody against prostate-specific membrane antigen." Hum Cell **18**(1): 17-23.

Ikegami, S., K. Yamakami, et al. (2006). "Targeting gene therapy for prostate cancer cells by liposomes complexed with anti-prostate-specific membrane antigen monoclonal antibody." Hum Gene Ther **17**(10): 997-1005.

Jain, P. K., X. Huang, et al. (2008). "Noble metals on the nanoscale: optical and photothermal properties and some applications in imaging, sensing, biology, and medicine." Acc Chem Res **41**(12): 1578-1586.

Jain, R. K. (1994). "Barriers to drug delivery in solid tumors." Sci Am **271**(1): 58-65.

Jain, R. K. (1999). "Transport of molecules, particles, and cells in solid tumors." Annu Rev Biomed Eng **1**: 241-263.

Jain, R. K. (2001). "Delivery of molecular and cellular medicine to solid tumors." Adv Drug Deliv Rev **46**(1-3): 149-168.

Jain, R. K. (2002). "Tumor angiogenesis and accessibility: role of vascular endothelial growth factor." Semin Oncol **29**(6 Suppl 16): 3-9.

Jain, R. K. (2005). "Normalization of Tumor Vasculature: An Emerging Concept in Antiangiogenic Therapy." Science **307**(5706): 58-62.

Jaye, D. L., H. A. Edens, et al. (2001). "Novel G protein-coupled responses in leukocytes elicited by a chemotactic bacteriophage displaying a cell type-selective binding peptide." J Immunol **166**(12): 7250-7259.

Jaye, D. L., C. M. Geigerman, et al. (2004). "Direct fluorochrome labeling of phage display library clones for studying binding specificities: applications in flow cytometry and fluorescence microscopy." J Immunol Methods **295**(1-2): 119-127.

Jaye, D. L., F. S. Nolte, et al. (2003). "Use of real-time polymerase chain reaction to identify cell- and tissue-type-selective peptides by phage display." Am J Pathol **162**(5): 1419-1429.

K.L. Black and B.K. Pikul (1999). "Gliomas--past, present, and future." Clin Neurosurg **45**: 160-163.

Kam, N. W. S., T. C. Jessop, et al. (2004). "Nanotube molecular transporters: Internalization of carbon nanotube-protein conjugates into mammalian cells." Journal of the American Chemical Society **126**(22): 6850-6851.

Karathanasis E, Park J, et al. (2008). "MRI mediated, non-invasive tracking of intratumoral distribution of nanocarriers in rat glioma." Nanotechnology **19**(31): 315101.

Karathanasis, E., L. Chan, et al. (2009). "Tumor vascular permeability to a nanoprobe correlates to tumor-specific expression levels of angiogenic markers." PLoS One **4**(6): e5843.

Kenneth T. Cheng, Sam Gambhir, and Z. Cheng (2004-2009). *[18F]FB-(Ac-NIe-Asp-His-d-Phe-Arg-Trp-Gly-Lys-NH2). [18F]FB-NAPamide.* . In: Molecular Imaging and Contrast Agent Database (MICAD) [database online]. Bethesda (MD): National Library of Medicine (US), NCBI; Available from: http://micad.nih.gov.,.

Kim, D. H. and J. J. Rossi (2007). "Strategies for silencing human disease using RNA interference." Nat Rev Genet **8**(3): 173-184.

Kirpotin, D., J. W. Park, et al. (1997). "Sterically stabilized anti-HER2 immunoliposomes: design and targeting to human breast cancer cells in vitro." Biochemistry **36**(1): 66-75.

Kirpotin, D. B., D. C. Drummond, et al. (2006). "Antibody targeting of long-circulating lipidic nanoparticles does not increase tumor localization but does increase internalization in animal models." Cancer Res **66**(13): 6732-6740.

Kocer, A. (2007). "A remote controlled valve in liposomes for triggered liposomal release." J Liposome Res **17**(3-4): 219-225.

Kolonin, M. G., J. Sun, et al. (2006). "Synchronous selection of homing peptides for multiple tissues by in vivo phage display." Faseb J **20**(7): 979-981.

Kong, G., G. Anyarambhatla, et al. (2000). "Efficacy of liposomes and hyperthermia in a human tumor xenograft model: importance of triggered drug release." Cancer Res **60**(24): 6950-6957.

Kong, G. and M. W. Dewhirst (1999). "Hyperthermia and liposomes." Int J Hyperthermia **15**(5): 345-370.

Koning, G. A. and G. C. Krijger (2007). "Targeted multifunctional lipid-based nanocarriers for image-guided drug delivery." Anticancer Agents Med Chem **7**(4): 425-440.

Kono, K. (2001). "Thermosensitive polymer-modified liposomes." Adv Drug Deliv Rev **53**(3): 307-319.

Kono, K., A. Henmi, et al. (1999). "Temperature-controlled interaction of thermosensitive polymer-modified cationic liposomes with negatively charged phospholipid membranes." Biochim Biophys Acta **1421**(1): 183-197.

Kono, K., K. Yoshino, et al. (2002). "Effect of poly(ethylene glycol) grafts on temperature-sensitivity of thermosensitive polymer-modified liposomes." J Control Release **80**(1-3): 321-332.

Koukourakis, M. I., S. Koukouraki, et al. (2000). "High intratumoural accumulation of stealth liposomal doxorubicin (Caelyx) in glioblastomas and in metastatic brain tumours." Br J Cancer **83**(10): 1281-1286.

Krauze, M. T., J. Forsayeth, et al. (2006). "Real-time imaging and quantification of brain delivery of liposomes." Pharm Res **23**(11): 2493-2504.

Laakkonen, P., M. E. Akerman, et al. (2004). "Antitumor activity of a homing peptide that targets tumor lymphatics and tumor cells." Proc Natl Acad Sci U S A **101**(25): 9381-9386.

Landon, L. A. and S. L. Deutscher (2003). "Combinatorial discovery of tumor targeting peptides using phage display." J Cell Biochem **90**(3): 509-517.

Lasic, D. and F. Martin (1995). Stealth Liposomes, CRC Press Inc.

Lasic, D. D. and D. Papahadjopoulos (1995). "Liposomes revisited." Science **267**(5202): 1275-1276.

Lasic, D. D. and D. Papahadjopoulos (1998). Medical applications of liposomes. Amsterdam ; New York, Elsevier.

LaVan, D. A., T. McGuire, et al. (2003). "Small-scale systems for in vivo drug delivery." Nat. Biotechnol. **21**: 1184-1191.

Leach, M. O. (2001). "Application of magnetic resonance imaging to angiogenesis in breast cancer." Breast Cancer Res Treat **3**: 22–27.

Lee, K. S. and M. A. El-Sayed (2006). "Gold and silver nanoparticles in sensing and imaging: sensitivity of plasmon response to size, shape, and metal composition." J Phys Chem B **110**(39): 19220-19225.

Lee, R. J. and P. S. Low (1994). "Delivery of liposomes into cultured KB cells via folate receptor-mediated endocytosis." J Biol Chem **269**(5): 3198-3204.

Lee, R. J. and P. S. Low (1995). "Folate-mediated tumor cell targeting of liposome-entrapped doxorubicin in vitro." Biochim Biophys Acta **1233**(2): 134-144.

Lee, T. Y., H. C. Wu, et al. (2004). "A novel peptide specifically binding to nasopharyngeal carcinoma for targeted drug delivery." Cancer Res **64**(21): 8002-8008.

Lestini, B. J., S. M. Sagnella, et al. (2002). "Surface modification of liposomes for selective cell targeting in cardiovascular drug delivery." J Control Release **78**(1-3): 235-247.

Li, X. B., H. J. Schluesener, et al. (2006). "Molecular addresses of tumors: selection by in vivo phage display." Arch Immunol Ther Exp (Warsz) **54**(3): 177-181.

Lindner, L. H., M. E. Eichhorn, et al. (2004). "Novel temperature-sensitive liposomes with prolonged circulation time." Clin Cancer Res **10**(6): 2168-2178.

Lockman, P. R., R. J. Mumper, et al. (2002). "Nanoparticle technology for drug delivery across the blood-brain barrier." Drug Dev Ind Pharm **28**(1): 1-13.

Lopes de Menezes, D. E., M. J. Kirchmeier, et al. (1999). "Cellular trafficking and cytotoxicity of anti-cd19-targeted liposomal doxorubicin in B lymphoma cells." Journal of Liposome Research **9**(2): 199-228.

M.D. Walker, S.B. Green, et al. (1980). "Randomized comparisons of radiotherapy and nitrosoureas for the treatment of malignant glioma after surgery." N. Engl. J. Med. **303**: 1323-1329.

M.I. Koukourakis, I. F. S. Koukouraki, et al. (2000). "High intratumoural accumulation of stealth liposomal doxorubicin (Caelyx) in glioblastomas and in metastatic brain tumours." Br J Cancer **83**: 1281-1286.

Maeda, H. (2001). "The enhanced permeability and retention (EPR) effect in tumor vasculature: the key role of tumor-selective macromolecular drug targeting." Adv Enzyme Regul **41**: 189-207.

Maeda, H., J. Wu, et al. (2000). "Tumor vascular permeability and the EPR effect in macromolecular therapeutics: a review." J Control Release **65**(1-2): 271-284.

Mamot, C., D. C. Drummond, et al. (2003). "Epidermal growth factor receptor (EGFR)-targeted immunoliposomes mediate specific and efficient drug delivery to EGFR- and EGFRvIII-overexpressing tumor cells." Cancer Res **63**(12): 3154-3161.

Maruyama, K., N. Takahashi, et al. (1997). "Immunoliposomes bearing polyethyleneglycol-coupled Fab' fragment show prolonged circulation time and high extravasation into targeted solid tumors in vivo." FEBS Lett **413**(1): 177-180.

Maruyama, K., S. Unezaki, et al. (1993). "Enhanced delivery of doxorubicin to tumor by long-circulating thermosensitive liposomes and local hyperthermia." Biochim Biophys Acta **1149**(2): 209-216.

Marzola, P., S. Ramponi, et al. (2005). "Effect of tamoxifen in an experimental model of breast tumor studied by dynamic contrast-enhanced magnetic resonance imaging and different contrast agents." Invest Radiol **40**(7): 421-429.

Mazzucchelli, L., J. B. Burritt, et al. (1999). "Cell-specific peptide binding by human neutrophils." Blood **93**(5): 1738-1748.

McNeeley, K., A. Annapragada, et al. (2007). "Decreased circulation time offsets increased efficacy of PEGylated nanocarriers targeting folate receptors of glioma." Nanotechnology **18**(385101): 1-11.

McNeeley, K. M., A. Annapragada, et al. (2007). "Decreased circulation time offsets increased efficacy of PEGylated nanocarriers targeting folate receptors of glioma." Nanotechnology **18**(38): 11.

Medina, O. P., K. Kairemo, et al. (2005). "Radionuclide imaging of tumor xenografts in mice using a gelatinase-targeting peptide." Anticancer Res **25**(1A): 33-42.

Meers, P. (2001). "Enzyme-activated targeting of liposomes." Adv Drug Deliv Rev **53**(3): 265-272.

Merlin, J. L. (1991). "Encapsulation of doxorubicin in thermosensitive small unilamellar vesicle liposomes." Eur J Cancer **27**(8): 1026-1030.

Mi, Z., X. Lu, et al. (2003). "Identification of a synovial fibroblast-specific protein transduction domain for delivery of apoptotic agents to hyperplastic synovium." Mol Ther **8**(2): 295-305.

Mitra, A., A. Nan, et al. (2006). "Nanocarriers for nuclear imaging and radiotherapy of cancer." Curr Pharm Des **12**(36): 4729-4749.

Mitsumori, M., M. Hiraoka, et al. (1994). "Development of intra-arterial hyperthermia using a dextran-magnetite complex." Int J Hyperthermia **10**(6): 785-793.

Moffat, B. A., G. R. Reddy, et al. (2003). "A novel polyacrylamide magnetic nanoparticle contrast agent for molecular imaging using MRI." Mol Imaging **2**(4): 324-332.

Moghimi, S. M., A. C. Hunter, et al. (2005). "Nanomedicine: current status and future prospects." Faseb Journal **19**(3): 311-330.

Moses, M. A., H. Brem, et al. (2003). "Advancing the field of drug delivery: taking aim at cancer." Cancer Cell **4**: 337-341.

Mueller, A., B. Bondurant, et al. (2000). "Visible-Light-Stimulated Destabilization of PEG-Liposomes." Macromolecules **33**(13): 4799-4804.

Mueller, A., Bondurant, B., O'Brien, D.F. (2000). "Visible-light-stimulated destabilization of PEG-liposomes." Macromolecules **33**(13): 4799-4804.

Muralkami, T., K. Ajima, et al. (2004). "Drug-loaded carbon nanohorns: Adsorption and release of dexamethasone in vitro." Molecular Pharmaceutics **1**(6): 399-405.

Nahrendorf, M., F. A. Jaffer, et al. (2006). "Noninvasive vascular cell adhesion molecule-1 imaging identifies inflammatory activation of cells in atherosclerosis." Circulation **114**(14): 1504-1511.

Needham, D., G. Anyarambhatla, et al. (2000). "A new temperature-sensitive liposome for use with mild hyperthermia: characterization and testing in a human tumor xenograft model." Cancer Res **60**(5): 1197-1201.

Needham, D. and M. W. Dewhirst (2001). "The development and testing of a new temperature-sensitive drug delivery system for the treatment of solid tumors." Adv Drug Deliv Rev **53**(3): 285-305.

Ni, S., S. M. Stephenson, et al. (2002). "Folate receptor targeted delivery of liposomal daunorubicin into tumor cells." Anticancer Res **22**(4): 2131-2135.

Nomura, K., T. Hoshino, et al. (1978). "Perturbed cell kinetics of 9L rat brain tumor cells following dianhydrogalactitol." Cancer Treat Rep **62**(12): 2055-2061.

Oshida, K., T. Nagashima, et al. (2005). "Pharmacokinetic analysis of ductal carcinoma in situ of the breast using dynamic MR mammography." Eur Radiol **15**(7): 1353-1360.

Oyelere, A. K., P. C. Chen, et al. (2007). "Peptide-conjugated gold nanorods for nuclear targeting." Bioconjug Chem **18**(5): 1490-1497.

P.L. Kornblith and M. Walker (1988). "Chemotherapy for malignant gliomas." J. Neurosurg. **68**: 1-17.

P.P. Wang, J. Frazier, et al. (2002). "Local drug delivery to the brain." Advanced Drug Delivery Reviews **54**: 987–1013

Paasonen, L., T. Laaksonen, et al. (2007). "Gold nanoparticles enable selective light-induced contents release from liposomes." J Control Release **122**(1): 86-93.

Pan, X. Q., H. Hang, et al. (2003). "Antitumor activity of folate receptor-targeted liposomal doxorubicin in a KB oral carcinoma murine xenograft model." Pharm Res **20**(3): 417-422.

Pan, X. Q. and R. J. Lee (2005). "In vivo antitumor activity of folate receptor-targeted liposomal daunorubicin in a murine leukemia model." Anticancer Res **25**(1A): 343-346.

Pan, X. Q., H. Wang, et al. (2003). "Antitumor activity of folate receptor-targeted liposomal doxorubicin in a KB oral carcinoma murine xenograft model." Pharm Res **20**(3): 417-422.

Pantarotto, D., J. P. Briand, et al. (2004). "Translocation of bioactive peptides across cell membranes by carbon nanotubes." Chem Commun (Camb)(1): 16-17.

Papahadjopoulos, D., T. M. Allen, et al. (1991). "Sterically stabilized liposomes: improvements in pharmacokinetics and antitumor therapeutic efficacy." Proc Natl Acad Sci U S A **88**(24): 11460-11464.

Papahadjopoulos, D., K. Jacobson, et al. (1973). "Phase transitions in phospholipid vesicles. Fluorescence polarization and permeability measurements concerning the effect of temperature and cholesterol." Biochim Biophys Acta **311**(3): 330-348.

Park, J. H., G. von Maltzahn, et al. (2010). "Cooperative nanoparticles for tumor detection and photothermally triggered drug delivery." Adv Mater **22**(8): 880-885.

Park, J. H., G. von Maltzahn, et al. (2010). "Cooperative nanomaterial system to sensitize, target, and treat tumors." Proc Natl Acad Sci U S A **107**(3): 981-986.

Park, J. W., K. Hong, et al. (1995). "Development of anti-p185HER2 immunoliposomes for cancer therapy." Proc Natl Acad Sci U S A **92**(5): 1327-1331.

Park, J. W., K. Hong, et al. (2002). "Anti-HER2 immunoliposomes: enhanced efficacy attributable to targeted delivery." Clin Cancer Res **8**(4): 1172-1181.

Park, J. W., K. Hong, et al. (1997). "Anti-HER2 immunoliposomes for targeted therapy of human tumors." Cancer Lett **118**(2): 153-160.

Pastorino, F., C. Brignole, et al. (2006). "Targeting liposomal chemotherapy via both tumor cell-specific and tumor vasculature-specific ligands potentiates therapeutic efficacy." Cancer Res **66**(20): 10073-10082.

Pastorino, F., C. Brignole, et al. (2003). "Vascular damage and anti-angiogenic effects of tumor vessel-targeted liposomal chemotherapy." Cancer Res. **63**(21): 7400-7409.

Peer, D., J. M. Karp, et al. (2007). "Nanocarriers as an emerging platform for cancer therapy." Nat Nanotechnol **2**(12): 751-760.

Perry, A. and R. E. Schmidt (2006). "Cancer therapy-associated CNS neuropathology: an update and review of the literature." Acta Neuropathol (Berl) **111**(3): 197-212.

Pluen, A., Y. Boucher, et al. (2001). "Role of tumor-host interactions in interstitial diffusion of macromolecules: cranial vs. subcutaneous tumors." Proc Natl Acad Sci U S A **98**(8): 4628-4633.

Ponce, A. M., Z. Vujaskovic, et al. (2006). "Hyperthermia mediated liposomal drug delivery." Int J Hyperthermia **22**(3): 205-213.

R.D. Arnold, D.E.Mager, et al. (2005). "Effect of Repetitive Administration of Doxorubicin-Containing Liposomes on Plasma Pharmacokinetics and Drug Biodistribution in a Rat Brain Tumor Model." Clin Cancer Res **11**(24): 8856-8865.

Ringsdorf, H., E. Sackmann, et al. (1993). "Interactions of liposomes and hydrophobically-modified poly-(N-isopropylacrylamides): an attempt to model the cytoskeleton." Biochim Biophys Acta **1153**(2): 335-344.

Ruiz-Arguello, M. B., F. M. Goni, et al. (1998). "Vesicle membrane fusion induced by the concerted activities of sphingomyelinase and phospholipase C." J Biol Chem **273**(36): 22977-22982.

S. I. Jeona, J. H. Leea, et al. (1991). "Protein—surface interactions in the presence of polyethylene oxide: I. Simplified theory." Journal of Colloid and Interface Science **142**(1): 149-158

S. Valtonen, U. Timonen, et al. (1997). "Interstitial chemotherapy with carmustine-loaded polymers for high-grade gliomas: a randomized double-blind study." Neurosurgery **41**: 44-48.

Samoylova, T. I., V. A. Petrenko, et al. (2003). "Phage probes for malignant glial cells." Mol Cancer Ther **2**(11): 1129-1137.

Sapra, P. and T. M. Allen (2004). "Improved outcome when B-cell lymphoma is treated with combinations of immunoliposomal anticancer drugs targeted to both the CD19 and CD20 epitopes." Clin Cancer Res **10**(7): 2530-2537.

Sardanelli, F., A. Iozzelli, et al. (2005). "Gadobenate dimeglumine-enhanced MR imaging breast vascular maps: association between invasive cancer and ipsilateral increased vascularity." Radiology **235**(3): 791-797.

Satchi-Fainaro, R. (2004). "Targeting angiogenesis with a conjugate of HPMA copolymer and TNP-470." Nat. Med. **10**: 255-261.

Satchi-Fainaro, R., R. Duncan, et al. (2006). Polymer Therapeutics II: Polymers as Drugs, Conjugates and Gene Delivery Systems, Nature Publishing Group**:** 1-65.

Sathornsumetee, S. and J. N. Rich (2006). "New approaches to primary brain tumor treatment." Anticancer Drugs **17**(9): 1003-1016.

Saul, J. M., A. Annapragada, et al. (2003). "Controlled targeting of liposomal doxorubicin via the folate receptor in vitro." J Control Release **92**(1-2): 49-67.

Saul, J. M., A. V. Annapragada, et al. (2006). "A dual-ligand approach for enhancing targeting selectivity of therapeutic nanocarriers." J Control Release **114**(3): 277-287.

Schiffelers, R. M., A. Ansari, et al. (2004). "Cancer siRNA therapy by tumor selective delivery with ligand-targeted sterically stabilized nanoparticle." Nucleic Acids Res **32**(19): e149.

Schiffelers, R. M., G. A. Koning, et al. (2003). "Anti-tumor efficacy of tumor vasculature-targeted liposomal doxorubicin." J Control Release **91**(1-2): 115-122.

Schild, H. G. (1992). "Poly(N-isopropylacrylamide): experiment, theory and application." Progress in Polymer Science **17**(2): 163-249.

Schinazi, R. F., R. Sijbesma, et al. (1993). "Synthesis and Virucidal Activity of a Water-Soluble, Configurationally Stable, Derivatized C60 Fullerene." Antimicrobial Agents and Chemotherapy **37**(8): 1707-1710.

Schluesener, H. J. and T. Xianglin (2004). "Selection of recombinant phages binding to pathological endothelial and tumor cells of rat glioblastoma by in-vivo display." J Neurol Sci **224**(1-2): 77-82.

Schraa, A. J. (2002). "Targeting of RGD-modified proteins to tumor vasculature: A pharmacokinetic and cellular distribution study." Int. J. Cancer **102**: 469-475.

Service, R. F. (2005). "Materials and biology. Nanotechnology takes aim at cancer." Science **310**(5751): 1132-1134.

Sharma, U. S., A. Sharma, et al. (1997). "Liposome-mediated therapy of intracranial brain tumors in a rat model." Pharm Res **14**(8): 992-998.

Shinkai, M., M. Suzuki, et al. (1995). "Antibody-conjugated magnetoliposomes for targeting cancer cells and their application in hyperthermia." Biotechnol Appl Biochem **21 (Pt 2)**: 125-137.

Shum, P., J. M. Kim, et al. (2001). "Phototriggering of liposomal drug delivery systems." Adv Drug Deliv Rev **53**(3): 273-284.

Siegel, M. J., J. L. Finlay, et al. (2006). "State of the art chemotherapeutic management of pediatric brain tumors." Expert Rev Neurother **6**(5): 765-779.

Siwak, D. R., A. M. Tari, et al. (2002). "The potential of drug-carrying immunoliposomes as anticancer agents. Commentary re: J. W. Park et al., Anti-HER2 immunoliposomes: enhanced efficacy due to targeted delivery. Clin. Cancer Res., 8: 1172-1181, 2002." Clin Cancer Res **8**(4): 955-956.

Slepushkin, V. A., S. Simoes, et al. (1997). "Sterically stabilized pH-sensitive liposomes. Intracellular delivery of aqueous contents and prolonged circulation in vivo." J Biol Chem **272**(4): 2382-2388.

Song, C. W. (1984). "Effect of local hyperthermia on blood flow and microenvironment: a review." Cancer Res **44**(10 Suppl): 4721s-4730s.

Spear, M. A., X. O. Breakefield, et al. (2001). "Isolation, characterization, and recovery of small peptide phage display epitopes selected against viable malignant glioma cells." Cancer Gene Ther **8**(7): 506-511.

Spratt, T., B. Bondurant, et al. (2003). "Rapid release of liposomal contents upon photoinitiated destabilization with UV exposure." Biochim Biophys Acta **1611**(1-2): 35-43.

Stark, D. D., R. Weissleder, et al. (1988). "Superparamagnetic iron oxide: clinical application as a contrast agent for MR imaging of the liver." Radiology **168**(2): 297-301.

Strijkers, G. J., W. J. Mulder, et al. (2005). "Relaxivity of liposomal paramagnetic MRI contrast agents." MAGMA **18**(4): 186-192.

Svenson, S. and D. A. Tomalia (2005). "Dendrimers in biomedical applications--reflections on the field." Adv Drug Deliv Rev **57**(15): 2106-2129.

Tabata, Y., Y. Murakami, et al. (1997). "Antitumor effect of poly(ethylene glycol)modified fullerene." Fullerene Science and Technology **5**(5): 989-1007.

Takano, S., Y. Yoshii, et al. (1996). "Concentration of vascular endothelial growth factor in the serum and tumor tissue of brain tumor patients." Cancer Res **56**(9): 2185-2190.

Takeuchi, H., H. Kojima, et al. (2001). "Passive targeting of doxorubicin with polymer coated liposomes in tumor bearing rats." Biol Pharm Bull **24**(7): 795-799.

Teifke, A., O. Behr, et al. (2006). "Dynamic MR imaging of breast lesions: correlation with microvessel distribution pattern and histologic characteristics of prognosis." Radiology **239**(2): 351-360.

Thompson, D. H., O. V. Gerasimov, et al. (1996). "Triggerable plasmalogen liposomes: improvement of system efficiency." Biochim Biophys Acta **1279**(1): 25-34.

Tiwari, S. B. and M. M. Amiji (2006). "A review of nanocarrier-based CNS delivery systems." Curr Drug Deliv **3**(2): 219-232.

Tomayko, M. M. and C. P. Reynolds (1989). "Determination of subcutaneous tumor size in athymic (nude) mice." Cancer Chemother Pharmacol **24**(3): 148-154.

Torchilin, V. P. (1994). "Immunoliposomes and PEGylated immunoliposomes: possible use for targeted delivery of imaging agents." Immunomethods **4**(3): 244-258.

Torchilin, V. P. (1998). Self-assembling complexes for gene delivery: from laboratory to clinical trial. New York, Wiley.

Torchilin, V. P. (2006). "Multifunctional nanocarriers." Adv Drug Deliv Rev **58**(14): 1532-1555.

Torchilin, V. P. (2007). "Targeted pharmaceutical nanocarriers for cancer therapy and imaging." AAPS J **9**(2): E128-147.

Troy, T., D. Jekic-McMullen, et al. (2004). "Quantitative comparison of the sensitivity of detection of fluorescent and bioluminescent reporters in animal models." Mol Imaging **3**(1): 9-23.

Tsao, N., T. Y. Luh, et al. (2001). "Inhibition of group A streptococcus infection by carboxyfullerene." Antimicrobial Agents and Chemotherapy **45**(6): 1788-1793.

Turetschek, K., S. Huber, et al. (2001). "MR imaging characterization of microvessels in experimental breast tumors by using a particulate contrast agent with histopathologic correlation." Radiology **218**(2): 562-569.

Turetschek, K., T. P. Roberts, et al. (2001). "Tumor microvascular characterization using ultrasmall superparamagnetic iron oxide particles (USPIO) in an experimental breast cancer model." J Magn Reson Imaging **13**(6): 882-888.

Tycko, B. and F. R. Maxfield (1982). "Rapid acidification of endocytic vesicles containing alpha 2-macroglobulin." Cell **28**(3): 643-651.

van de Wiele, P., R. Dierckx, et al. (2002). "Nuclear medicine imaging for prediction or early assessment of response to chemotherapy in patients suffering from breast carcinoma." Breast Cancer Res Treat **72**(3): 279-286.

Venugopalan, P., S. Jain, et al. (2002). "pH-sensitive liposomes: mechanism of triggered release to drug and gene delivery prospects." Pharmazie **57**(10): 659-671.

Villar, A. V., A. Alonso, et al. (2000). "Leaky vesicle fusion induced by phosphatidylinositol-specific phospholipase C: observation of mixing of vesicular inner monolayers." Biochemistry **39**(46): 14012-14018.

Villar, A. V., F. M. Goni, et al. (2001). "Diacylglycerol effects on phosphatidylinositol-specific phospholipase C activity and vesicle fusion." FEBS Lett **494**(1-2): 117-120.

von Maltzahn, G., A. Centrone, et al. (2009). "SERS-Coded Gold Nanorods as a Multifunctional Platform for Densely Multiplexed Near-Infrared Imaging and Photothermal Heating." Adv Mater **21**(31): 3175-3180.

Wei, A., A. P. Leonov, et al. (2010). "Gold nanorods: multifunctional agents for cancer imaging and therapy." Methods Mol Biol **624**: 119-130.

Weinstein, J. N., R. L. Magin, et al. (1979). "Liposomes and local hyperthermia: selective delivery of methotrexate to heated tumors." Science **204**(4389): 188-191.

Weissing, V., J. Babich, et al. (2000). "Long-circulating gadolinium loaded liposomes: potential use for mangetic resonance imaging of the blood pool." Colloids and Surfaces B: Biointerfaces **18**: 293-299.

Weissleder, R. (2001). "A clearer vision for in vivo imaging." Nat Biotechnol **19**(4): 316-317.

Weissleder, R., P. F. Hahn, et al. (1988). "Superparamagnetic iron oxide: enhanced detection of focal splenic tumors with MR imaging." Radiology **169**(2): 399-403.

Whitney, M., J. L. Crisp, et al. (2010). "Parallel in vivo and in vitro selection using phage display identifies protease-dependent tumor-targeting peptides." J Biol Chem **285**(29): 22532-22541.

Wong, J. Y., T. L. Kuhl, et al. (1997). "Direct measurement of a tethered ligand-receptor interaction potential." Science **275**(5301): 820-822.

Woodle, M. C. and D. D. Lasic (1992). "Sterically stabilized liposomes." Biochim Biophys Acta **1113**(2): 171-199.

Wu, J., Q. Liu, et al. (2006). "A folate receptor-targeted liposomal formulation for paclitaxel." Int J Pharm **316**(1-2): 148-153.

Wymer, N. J., O. V. Gerasimov, et al. (1998). "Cascade liposomal triggering: light-induced Ca2+ release from diplasmenylcholine liposomes triggers PLA2-catalyzed hydrolysis and contents leakage from DPPC liposomes." Bioconjug Chem **9**(3): 305-308.

Yan, H., C. Cheng, et al. (2008). "Distribution of free and liposomal doxorubicin after isolated lung perfusion in a sarcoma model." Ann Thorac Surg **85**(4): 1225-1232.

Yatvin, M. B., W. Kreutz, et al. (1980). "pH-sensitive liposomes: possible clinical implications." Science **210**(4475): 1253-1255.

Yatvin, M. B., J. N. Weinstein, et al. (1978). "Design of liposomes for enhanced local release of drugs by hyperthermia." Science **202**(4374): 1290-1293.

Yinghuai, Z., A. T. Peng, et al. (2005). "Substituted carborane-appended water-soluble single-wall carbon nanotubes: New approach to boron neutron capture therapy drug delivery." Journal of the American Chemical Society **127**(27): 9875-9880.

Yuan, F., Y. Chen, et al. (1996). "Time-dependent vascular regression and permeability changes in established human tumor xenografts induced by an anti-vascular endothelial growth factor/vascular permeability factor antibody." Proc Natl Acad Sci U S A **93**(25): 14765-14770.

Yuan, F., M. Leunig, et al. (1994). "Microvascular permeability and interstitial penetration of sterically stabilized (stealth) liposomes in a human tumor xenograft." Cancer Res **54**(13): 3352-3356.

Zalipsky, S. (1993). "Synthesis of an end-group functionalized polyethylene glycol-lipid conjugate for preparation of polymer-grafted liposomes." Bioconjug Chem **4**(4): 296-299.

Zalipsky, S., E. Brandeis, et al. (1994). "Long circulating, cationic liposomes containing amino-PEG-phosphatidylethanolamine." FEBS Lett **353**(1): 71-74.

Zhang, Z. Y., P. Shum, et al. (2002). "Formation of fibrinogen-based hydrogels using phototriggerable diplasmalogen liposomes." Bioconjug Chem **13**(3): 640-646.

Zhang, Z. Y. and B. D. Smith (2000). "High-generation polycationic dendrimers are unusually effective at disrupting anionic vesicles: membrane bending model." Bioconjug Chem **11**(6): 805-814.

Jai Shri Krishna